NASA
Technical
Paper
2176

October 1983

Low-Speed Aerodynamic Characteristics of a Highly Swept, Untwisted, Uncambered Arrow Wing

Paul L. Coe, Jr.,
Scott O. Kjelgaard,
and Garl L. Gentry, Jr.

NASA

25th Anniversary
1958-1983

NASA
Technical
Paper
2176

1983

Low-Speed Aerodynamic Characteristics of a Highly Swept, Untwisted, Uncambered Arrow Wing

Paul L. Coe, Jr.,
Scott O. Kjelgaard,
and Garl L. Gentry, Jr.
Langley Research Center
Hampton, Virginia

NASA
National Aeronautics
and Space Administration

Scientific and Technical
Information Branch

SUMMARY

An investigation was conducted in the Langley 4- by 7-Meter Tunnel to provide a detailed study of wing pressure distributions and forces and moments acting on a highly swept arrow-wing model at low Mach numbers (0.25). A limited investigation of the effect of spoilers at several locations was also conducted.

Analysis of the pressure data shows that for the configuration with undeflected leading edges, vortex separation occurs on the outboard wing panel for angles of attack on the order of only 3°, whereas conventional leading-edge separation occurs at a nondimensional semispan station of 0.654 for the same incidence angle. The pressure data further show that vortex separation exists at wing stations more inboard for angles of attack on the order of 7° and that these vortices move inboard and forward with increasing angle of attack. The force and moment data show the expected nonlinear increments in lift and pitching moment and the increased drag associated with the vortex separation.

The pressure data confirm that deflecting the entire wing leading edge uniformly to 30° is effective in forestalling the onset of flow separation to angles of attack greater than 8.6°. The corresponding force and moment data show that deflecting the leading edge yields improvements in lift and pitching-moment linearity with marked improvements in drag characteristics. Previous investigations have indicated that in this deflected condition, the inboard portion of the leading edge is overdeflected and results in a lift decrement and a drag increment. The pressure data confirm that with 30° deflection, the inboard portion of the leading edge is overdeflected. The investigation further identifies the contribution of the trailing-edge flap deflection to the leading-edge upwash field.

Spoilers located ahead of the trailing-edge flap system produce substantial reductions in lift and positive increments in pitching moment which accompany the increase in drag. However, a spoiler located outboard of the trailing-edge flap system was effective in producing equivalent increases in drag with only a minimal effect on lift and pitching moment.

INTRODUCTION

This investigation is part of an overall research effort by the National Aeronautics and Space Administration (NASA) to investigate the aerodynamic characteristics of advanced aircraft concepts designed for sustained cruise at supersonic speeds. To achieve high levels of supersonic-cruise efficiency, many of these conceptual designs employ highly swept, twisted, and cambered arrow wings. (See refs. 1 and 2.) Such designs typically incorporate a reduced sweep on the outer wing panel, which is intended to alleviate deficiencies in subsonic aerodynamic performance, stability, and control. However, experimental results indicate that these subsonic aerodynamic deficiencies are the result of flow separation along the entire leading edge and that reducing the outboard-panel sweep is only partially effective. Previous experiments with highly swept wings have demonstrated partial success in developing leading-edge treatments which are effective for inhibiting leading-edge flow separation. (See refs. 3 to 8.) These experiments were conducted with models of supersonic-cruise configurations which had wings with representative thickness,

twist, and camber distributions, in addition to deflectable leading-edge devices. For this reason, the separate effects of these geometric variables on leading-edge flow separation are not well understood.

The primary objective of the investigation reported herein was to provide a detailed study of wing pressure distributions and forces and moments acting on a highly swept arrow-wing model. The data were obtained to aid in understanding the effects of leading-edge deflection. To provide a more fundamental experiment than those previously conducted, the wing used in this investigation had a representative thickness distribution and neither twist nor camber were incorporated. The results of this study are intended to provide a base line for future assessments of various leading-edge geometries and for determinations of the detailed effects of twist and camber.

In addition to the primary concern with leading-edge flow separation, the investigation also included a limited study of the effects of spoiler location. Spoiler locations which result in increased drag with minimum change in lift and pitching moment are of interest. Deployment of spoilers in these locations would be useful for obtaining steeper landing-approach angles (and thereby potential reductions in community-noise exposure).

SYMBOLS

The longitudinal data are referred to the stability system of axes illustrated in figure 1. The moment reference center for the tests was located at 59.16 percent of the reference mean aerodynamic chord. The reference wing area and chord are based on the wing planform which results from extending the inboard (74°) leading-edge sweep angle and the outboard (41.46°) trailing-edge sweep angle to the model center line. (See fig. 2.)

The dimensional quantities are given in both the International System of Units (SI) and the U.S. Customary Units. The computer symbols enclosed in parentheses are used in a tabular listing of data in the appendix.

A		aspect ratio
b		wing span, m (ft)
C_D	(CD)	drag coefficient, Drag/qS_{ref}
$C_{D,o}$		drag coefficient at zero-lift condition
C_L	(CL)	lift coefficient, Lift/qS_{ref}
C_{L_α}		$= \partial C_L/\partial \alpha$
C_m	(CPM)	pitching-moment coefficient, $\text{Pitching moment}/qS_{ref}\bar{c}$
C_p		pressure coefficient, $(p - p_\infty)/q$
c		chord length at wing span station y, m (ft)
$\bar{c}$		mean aerodynamic chord, m (ft)

p static pressure, Pa (lbf/ft^2)

p_∞ free-stream static pressure, Pa (lbf/ft^2)

q free-stream dynamic pressure, Pa (lbf/ft^2)

S leading-edge suction parameter

S_{ref} reference wing area, m^2 (ft^2)

s_1,s_2,s_3,s_4 spoiler elements (see fig. 3)

t_1,t_3 trailing-edge flap elements (see fig. 3)

X,Y,Z body-axis system

x,y,z coordinates in body-axis system, m (ft)

α (ALPHA) angle of attack, deg

γ spanwise distance from center line nondimensionalized by local wing semispan

Δ increment

δ_f angular deflection of wing trailing-edge flap segments t_1 and t_3, measured perpendicular to hinge line, positive downward, deg (see fig. 3)

δ_{le} angular deflection of wing leading edge, measured perpendicular to hinge line, positive downward, deg (see fig. 3)

δ_s angular deflection of spoiler segment, measured perpendicular to segment hinge line, positive upward, deg (see fig. 3)

η distance aft of leading edge, nondimensionalized by local chord length

ξ distance aft of wing apex, nondimensionalized by wing root chord

Abbreviations:

L.E. leading edge

T.E. trailing edge

MODEL

The principal dimensional characteristics of the model used in the present study are listed in table I and shown in figures 2 and 3. In addition, a listing of the computer cards required for a numerical model is given in table II. The format for the listing provided in table II is described in reference 9. A photograph of the model in the Langley 4- by 7-Meter Tunnel is presented in figure 4.

The model incorporated a high-lift system comprised of plain leading- and trailing-edge flaps (see fig. 2); however, the model did not incorporate either nacelles or an aft fuselage. Spoilers were simulated by using sheet metal as sketched in figure 3.

TEST AND CORRECTIONS

The investigation was conducted in the Langley 4- by 7-Meter Tunnel at subsonic speeds. Forces and moments were measured with a standard six-component strain-gage balance mounted internal to the model. Wing-surface static pressures were measured by using 48-port scanning valves also mounted internal to the model. The tests were conducted at a dynamic pressure of 4309.2 Pa (90 lbf/ft^2). This value of dynamic pressure resulted in a Reynolds number (based on the wing mean aerodynamic chord) of 4.8×10^6 at a corresponding Mach number of 0.25. The angle of attack ranged from about -4° to 16°.

Jet-boundary corrections to the angle of attack and drag were applied in accordance with reference 10. Blockage corrections were applied to the data by the method of reference 11. Balance chamber pressure and model base pressure were measured and the drag measurements were adjusted to correspond to conditions of free-stream static pressure acting over the base of the model.

In accordance with the method of reference 12, 0.16-cm-wide (0.0625-in.) transition strips of No. 70 carborundum grains were placed 3.81 cm (1.5 in.) aft of the leading edges of the wing and outboard vertical tails. Similarly, No. 80 carborundum grains were placed 3.81 cm (1.5 in.) aft of the model nose.

RESULTS AND DISCUSSION

The present investigation was intended to examine the wing flow field and the detailed effects of leading-edge deflection for a highly swept arrow-wing configuration. In addition, a limited investigation of the effect of spoiler placement was conducted. Experimentally measured force and pressure data were also compared with theoretical predictions for some cases. A run schedule and a tabular listing of data (see tables AI and AII, respectively) are provided in the appendix.

Configuration With Undeflected Leading Edge

The experimental longitudinal aerodynamic characteristics of the basic configuration with undeflected leading and trailing edges are presented in figure 5. Also presented for purposes of comparison are theoretical lift and pitching-moment characteristics computed by using a planar vortex-lattice theoretical model. Reference 13 presents a discussion of the particular vortex-lattice mathematical model and computer code used for the theoretical prediction. Previous studies (ref. 7) have used a vortex-lattice model in an attempt to predict the aerodynamic characteristics for conditions with separated vortex flows. However, the underlying intent of the present work is toward the attainment of attached flow and, therefore, the theoretical results presented are representative of the attached-flow condition. As expected, the experimental lift data at low-angle-of-attack attached-flow conditions agree well

with the theoretical predictions $\left(\text{e.g., } C_{L_\alpha} = 0.036\right)$. However, as in previous studies (ref. 6), the theoretical prediction of the pitching-moment characteristics is not quite as accurate. Analysis of the experimental data indicates that the configuration neutral point is at $0.548\bar{c}$, whereas the theoretically predicted location is at $0.534\bar{c}$. This lack of agreement between theoretical and experimental pitching-moment coefficients arises because of the inability of the vortex-lattice models to predict detailed load distributions accurately for highly swept wings. Since the model is symmetrical, the small nonzero values of C_L and C_m at $\alpha = 0°$ are attributed to experimental inaccuracies. The nonlinear increase in the experimental values of C_L and C_m with increasing α, which occurs for $\alpha > 2°$, is caused by the formation of wing vortices and the stall of the outboard wing panel, as has been discussed in references 4, 5, and 7. Two theoretical bounding drag polars are also presented which correspond to the following conditions: (1) minimum induced drag (100-percent leading-edge suction) and (2) full leading-edge separation (0-percent leading-edge suction). These drag polars are defined for condition (1) as

$$C_D = C_{D,o} + C_L^2/\pi A \tag{1}$$

and for condition (2) as

$$C_D = C_{D,o} + C_L \tan\left(C_L/C_{L_\alpha}\right) \tag{2}$$

Equations (1) and (2) are presented herein to permit the aerodynamic performance to be quantified. The leading-edge suction parameter S can be written as (see ref. 14 for a comprehensive discussion of leading-edge suction)

$$S = \frac{C_D - \left[C_{D,o} + C_L \tan\left(C_L/C_{L_\alpha}\right)\right]}{C_L^2/\pi A - C_L \tan\left(C_L/C_{L_\alpha}\right)} \tag{3}$$

where C_{L_α} is the theoretical value determined to be 0.036, and the zero lift-drag coefficient $C_{D,o}$ is experimentally determined for the present tests to be 0.0090. The quantity $C_L \tan\left(C_L/C_{L_\alpha}\right)$ has been used in place of the more customary $C_L \tan \alpha$. This was done to provide a common basis for comparison. Use of the quantity $C_L \tan \alpha$ is often misleading when vortex separation occurs. For the type of vortex separation occurring with the present model, the angle of attack at which a particular value of C_L is achieved is dependent on the intensity of the separated vortices. Therefore, when considering leading-edge devices which are partially effective in reducing vortex separation, differing values of $C_L \tan \alpha$ are obtained. Thus, if this quantity is used to define S, a common basis for comparison does not exist.

Figure 6 presents a comparison of data from figure 5 for the untwisted, uncambered wing with data from reference 7 for a geometrically similar wing which is

twisted and cambered and also employs geometric anhedral. The increment in C_L at $\alpha = 0°$ is found experimentally to be 0.082, and the increment in C_m at zero lift is 0.012. The corresponding values obtained for the vortex-lattice theoretical model are 0.0835 and 0.0167, respectively. For the limited range of α over which fully attached flow exists on the twisted and cambered wing (i.e., $-2° \leqslant \alpha \leqslant 2°$), the static longitudinal stability parameter $\partial C_m/\partial C_L$ is, as expected, unaffected by twist and camber. Comparison of the experimental drag polars shows that the effect of twist and camber is quite favorable.

Figure 7 presents the measured and predicted chordwise pressure distributions along the four semispan stations illustrated in figure 2. These pressure distributions are presented for eight angles of attack (fig. 7) and are compared with theoretical estimates calculated by using a potential-flow surface-panel representation of the configuration. (See ref. 15 for a description of the surface-panel computer code.) As shown at the lowest angle of attack ($\alpha = 0.87°$), the agreement between theory and experiment is good. However, as the angle of attack is increased to only $\alpha = 2.96°$, the measured pressure distributions indicate flow separation at the nondimensional wing semispan stations of 0.654 and 0.862. As α is further increased, it becomes apparent that the separation at $y/(b/2) = 0.862$ is typical of a vortex separation; whereas inboard at $y/(b/2) = 0.654$, plain separation is in evidence. As α is still further increased to $\alpha \geqslant 6.99°$, vortex separation is evidenced at $y/(b/2) = 0.425$. This vortex-separation phenomenon is also observed at $y/(b/2) = 0.174$ for $\alpha \geqslant 9.05°$. To aid in the interpretation of these data, figure 8 presents corresponding experimental spanwise pressure distributions measured along the wing-body stations indicated in figure 2. Based on the data of figures 7 and 8, the spanwise and chordwise locations of the vortex cores can be approximated. These results are presented as a function of α in table III and are sketched in figure 9. The xy-planar location of the vortex which forms on the outboard panel for $\alpha \geqslant 0.87°$ is relatively independent of α. By contrast, the vortex which forms on the inboard portion of the wing for $\alpha \geqslant 2.96°$ apparently moves inboard and forward with increasing α. It is significant to note that the flow at station $y/(b/2) = 0.654$ is separated for all angles of attack greater than 2.96°. Although the detailed mechanism is not understood, the plain flow separation observed at $y/(b/2) = 0.654$ is thought to be related to the inboard wing crank where the sweep changes from 74° to 70°. This flow separation might be thought to be related to the outboard vertical fin; however, previous experiments have shown that the outboard vertical fin helps to contain the separated region and prevents it from spreading to the outboard wing panel.

Configuration With Deflected Leading Edge

Previous experimental investigations (see refs. 5 and 7) have shown that deflecting the entire leading edge results in a significant reduction in flow separation and delays the onset of vortex formation to higher angles of attack. These flow-field changes result in improved performance and a reduction in pitch-up. The investigation of reference 5, which was limited to consideration of uniformly deflected leading-edge conditions, indicated that $\delta_{le} = 30°$ was the preferred angle for the leading-edge deflections considered. However, the study also indicated that for this uniformly deflected condition, the inboard portion of leading edge may have been overdeflected and, hence, did not provide optimum performance. Based on this result, a continuously warped leading edge was devised to align the leading edge with the incoming flow along the entire span. (See ref. 7.) Although successful from an aerodynamic viewpoint, the mechanical complexity associated with implementing the

continuously warped leading edge may make the uniformly deflected leading edge a more viable concept.

Figure 10 presents the effect of leading-edge deflection on the longitudinal aerodynamic characteristics obtained for the present untwisted, uncambered model. As has been previously reported for the twisted and cambered configuration (see ref. 5), deflecting the leading edge through 30° extends the linear region of the pitching-moment coefficient to approximately $\alpha = 10°$ and results in substantial reductions in induced drag. However, this beneficial effect is accompanied by a reduction in the vortex-lift increment.

The leading-edge suction parameter S (see eq. (3)) is presented in figure 11 for $\delta_{le} = 0°$ and 30°. These results are compared with corresponding results for the twisted and cambered wing as published in reference 7. These data show that both twist and camber with leading-edge deflection result in marked improvements in leading-edge suction or correspondingly reduced drag. (For a representative climb lift coefficient, such as $C_L = 0.4$, a 1-percent increase in S is equivalent to a reduction in C_D of 0.00052.) Furthermore, these results indicate that the effects of twist and camber with leading-edge deflection, although not linearly additive, are favorable in combination.

Pressure data for the untwisted, uncambered configuration with $\delta_{le} = 30°$ are presented in figure 12. A summary of the interpretation of these data is provided in table IV. It should be noted that the pressure distributions presented in figure 12 show the existence of suction peaks on the flap shoulder. These suction peaks occur as a result of the increased curvature produced by simply deflecting the leading edges about the hinge line illustrated in figure 2.

For $\alpha = 2.51°$, the data of figure 12(a) show that the entire leading edge is overdeflected and that it experiences an upper-surface stagnation point. The data further show that for $y/(b/2) = 0.174$, the 30°-deflected leading edge remains overdeflected for $\alpha \leqslant 4.55°$, but it appears to align with the incoming flow for $\alpha = 6.64°$. The pressure data further indicate that with $\delta_{le} = 30°$, the separation problem previously discussed for the wing semispan stations of 0.654 and 0.862 (for $\delta_{le} = 0°$) is postponed to $\alpha \geqslant 8.59°$. These results are in good agreement with qualitative results from previous investigations for the twisted and cambered wing. In particular, in reference 7, it was reported that for the configuration with $\delta_{le} = 30°$, flow separation was first observed for $\alpha = 8°$ and occurred outboard at $y/(b/2) = 0.5$.

Effect of Trailing-Edge Flap Deflection

Previous investigations have shown a strong aerodynamic interaction between leading- and trailing-edge systems. For example, reference 5 indicated that the improvements in the wing flow field, which result from leading-edge deflection, are accompanied by increased trailing-edge flap effectiveness. The effect of trailing-edge flap deflection was examined in the present investigation to explore optimization of the high-lift system comprised of both leading- and trailing-edge flaps. For this experiment, the trailing-edge flap system was limited to segments t_1 and t_3 as sketched in figures 2 and 3. It should be noted that previous studies have included another flap segment located just inboard of the outboard vertical fins (see ref. 5) as part of the trailing-edge flap system; however, in recognition of lateral-control requirements (see ref. 16), this segment is now considered as a dedicated aileron.

Figure 13 presents the longitudinal aerodynamic characteristics of the present configuration with trailing-edge flap deflection as a parameter. For increasing values of C_L, improvements in untrimmed performance in terms of lift-drag polars are achieved with increased trailing-edge deflection for $0 \leqslant \delta_f \leqslant 20°$. In particular, at nominal take-off and climb lift coefficients of $C_L = 0.4$, a flap deflection of $\delta_f = 10°$ results in the lowest untrimmed drag. Furthermore, for values of δ_f greater than 20°, the performance is seen to be degraded (fig. 13(b)) for the entire range of lift coefficients considered.

The increment in lift produced by trailing-edge deflection (for the linear region of C_L plotted against α) is summarized in figure 14. Also presented for purposes of comparison is the theoretically predicted variation of ΔC_L with δ_f. As can be seen, the experimental flap effectiveness is linear for $\delta_f \leqslant 20°$ and is approximately 83 percent of the theoretical result. For flap deflections above $\delta_f = 20°$, the experimental increment in C_L becomes nonlinear. The overall trend for trailing-edge flap effectiveness as presented in figure 14 is similar to that determined for the twisted and cambered wing. (See ref. 16.) The variation of C_m with respect to α shown in figure 13 indicates that the onset of pitch-up occurs at lower angles of attack as flap deflection increases. This result was observed in reference 5 where it was hypothesized that the increased circulation accompanying trailing-edge deflection results in increased leading-edge separation and/or vortex formation.

Detailed pressure distributions are presented in figure 15 for the model with the various trailing-edge flap conditions investigated. The two inboard chordwise pressure rows (i.e., $y/(b/2) = 0.174$ and 0.425) are approximately centered on the trailing-edge segments t_1 and t_3. (See fig. 2.) Pressure data obtained for these inboard semispan stations clearly show the upper-surface suction peaks associated with simply deflecting the trailing edge about the hinge line. Most important, however, the data show that the leading-edge flow field at the two inboard stations is essentially unaffected by the deflection of segments t_1 and t_3, but that the leading-edge flow field at the two outboard stations (i.e., $y/(b/2) = 0.654$ and 0.862) is significantly influenced. For example, at $y/(b/2) = 0.862$ (fig.15(d)), the pressure data show that deflecting the trailing-edge segments t_1 and t_3 from $\delta_f = 0°$ to 30° results in a pressure distribution which is equivalent to that obtained by increasing α approximately 2°. The fact that deflecting trailing-edge flap segments t_1 and t_3 results in an increased upwash for the portion of the wing outboard of segments t_1 and t_3 is not surprising when the spanload distribution in the Trefftz plane is considered.

Optimization of the High-Lift System

The results of the preceding section indicate that for values of C_L on the order of 0.4 (i.e., typical climb C_L), the configuration with $\delta_{le} = 30°$ achieves the lowest untrimmed drag with $\delta_f = 10°$. However, it should be noted that this leading-edge deflection ($\delta_{le} = 30°$) was selected based on previous studies for which δ_{le} was varied while the trailing edge remained undeflected (i.e., $\delta_f = 0°$). Furthermore, as pointed out in a prior section, deflection of the trailing edge will alter the leading-edge flow field to some extent. Therefore, the high-lift condition, consisting of $\delta_{le} = 30°$ and $\delta_f = 10°$, would not necessarily be the optimum. To help define the best combination of δ_{le} and δ_f, a brief investigation was conducted in which the leading-edge deflection was varied while the trailing-edge deflection was held constant at $\delta_f = 10°$. Figure 16 presents the longitudinal aerodynamic characteristics of the configuration with $\delta_f = 10°$ and

δ_{le} = 20°, 30°, and 40°. As shown in figure 16 at the representative climb lift coefficient C_L of 0.4, δ_{le} = 30° results in slightly smaller values of untrimmed drag than either δ_{le} = 20° or 40°. Furthermore, the longitudinal stability characteristics (as indicated by the onset of pitch-up) of the configuration with δ_{le} = 30° are equal to or better than those achieved with either δ_{le} = 20° or 40°. Consequently, of the variables considered, it appears that δ_{le} = 30° and δ_f = 10° results in the best untrimmed aerodynamic performance.

Figure 17 presents corresponding pressure data for the various deflected leading-edge conditions discussed in the preceding paragraph. These data illustrate the effect of increasing leading-edge deflection. The data substantiate the statement of reference 5 which indicated that with δ_{le} = 30°, the inboard portion of the leading edge is overdeflected. For example, over the angle-of-attack range for which data are presented, it can be seen that δ_{le} = 20° is effective in inhibiting separation at the innermost semispan station (i.e., $y/(b/2) = 0.174$). It should be noted that a segmented leading-edge system would permit reduced deflections at inboard stations; however, such a system would also introduce surface discontinuities. Segmented leading-edge systems have been considered in previous investigations (see refs. 5 and 7), and the results showed that the drag penalty associated with the surface discontinuities overshadowed the beneficial effect of reducing the inboard leading-edge deflection.

Of particular interest is the pressure data for semispan station $y/(b/2) = 0.654$ which is located just forward of the wing leading-edge crank. (See fig. 2.) As can be seen from the data for $\alpha > 6.6°$, this semispan station experiences flow separation for all leading-edge deflections considered. As mentioned previously, the fluid mechanical phenomenon responsible for this separation is not understood; however, it is believed to be related to the inboard wing leading-edge crank. As noted in reference 16, elimination of this wing-planform discontinuity may alleviate this separation problem and thereby provide substantially improved aerodynamic performance.

SPOILER EFFECTIVENESS

Recent analytical studies (see ref. 17) have indicated potential benefits of steeper approach angles. The implementation of steeper approach angles, of course, depends on the ability to generate increased drag (e.g., with the use of spoilers) with minimum changes in lift and pitching moment. Most previous investigations of spoilers (e.g., ref. 8) have been limited to spoiler elements located just forward of the trailing-edge flap segments. Analysis of the data from these investigations reveals that spoiler deployment at this location would result in large changes in lift and pitching moment and thereby render such devices inappropriate for glide-path control.

The present investigation was conducted with individual spoiler elements s_1, s_2, s_3, and s_4, as depicted in figure 3. The wing leading edge was deflected 30° and tests were conducted for trailing-edge flap (segments t_1 and t_3) deflections of δ_f = 10° and 30°. Inasmuch as the results were similar for both trailing-edge flap deflections considered, the following discussion is limited to the δ_f = 30° condition. Information for the δ_f = 10° condition is contained in the tabulated data.

Figure 18 compares the longitudinal aerodynamic characteristics for the configuration with and without spoiler elements s_1, s_2, s_3, and s_4 individually

deployed. As expected, deflection of spoiler elements s_1 or s_3, located just ahead of the trailing-edge flap segments, results in a loss in lift and a change in pitching moment. Additionally, deflecting spoiler segment s_2 (located between the flap segments) results in an effect similar, but reduced, to that of deflecting either s_1 or s_3. Apparently, the aerodynamic interference produced by deflection of element s_2 is sufficient to spoil the flow partially over flap segments t_1 and t_3. (See fig. 3.) Most importantly, however, deployment of spoiler segment s_4, located just outboard of flap segment t_3, results in a substantial increment in drag with only a minimal change in the lift and pitching moment. (See figure 18(d).) Hence, spoiler segment s_4 appears to produce the desired aerodynamic qualities that would permit steeper approach angles to be achieved with minimum trim change.

SUMMARY OF RESULTS

An investigation was conducted to examine the wing flow field and the detailed effects of wing leading-edge deflection for a highly swept arrow-wing configuration. Limited tests were also conducted to determine the effects of spoiler deployment at various wing locations. The results may be summarized as follows:

1. Vortex separation is first observed on the outboard wing panel, and plain separation is first observed at a nondimensional semispan station of 0.654 for the configuration with undeflected leading edges and for angles of attack α as low as 3°. Vortex separation occurs at wing stations more inboard for angles of attack on the order of 7°, and these vortices move inboard and forward with increasing angle of attack.

2. Deflecting the entire wing leading edge to 30° is effective in delaying the onset of flow separation to $\alpha \geqslant 8°$. However, the data show that the inboard portion of the leading edge is overdeflected for this condition.

3. Deflecting the trailing-edge flaps results in an increase in the leading-edge upwash flow field on the portion of the wing outboard of the trailing-edge flap system.

4. Spoilers located ahead of the trailing-edge flap system produce substantial reductions in lift and positive increments in pitching moment which accompany the increase in drag. However, a spoiler located outboard of the trailing-edge flap system was effective in producing equivalent increases in drag with only a minimal effect on lift and pitching moment.

Langley Research Center
National Aeronautics and Space Administration
Hampton, VA 23665
July 12, 1983

APPENDIX

WIND-TUNNEL TEST SCHEDULE AND DATA TABULATION

As an aid to the reader, the appendix provides the wind-tunnel test schedule and tabulated longitudinal aerodynamic data.

TABLE AI.- TEST PROGRAM

Run	δ_{le}, deg	δ_f, deg	$\delta_{s,1}$, deg	$\delta_{s,2}$, deg	$\delta_{s,3}$, deg	$\delta_{s,4}$, deg
1	0	0	0	0	0	0
46	30	20				
57		0				
58		40				
61		10				
62		30				
67	40	10				
68	20					
69	30		60			
70			90			
71			0		60	
72					90	
73				60	0	
74				90		
75				0		60
76				0		90
77				60		60
78				90		90
94		30	60	0		0
95			90			
96			0		60	
97					90	
98				60	0	
99				90		
100				0		60
101				0		90

TABLE AII.- TABULATED DATA

RUN 1

ALPHA	CL	CD	CPM
-7.21	-.2980	.0431	-.0239
-5.16	-.2035	.0242	-.0117
-3.12	-.1108	.0133	-.0072
-1.11	-.0346	.0095	-.0040
.87	.0368	.0096	-.0005
2.96	.1156	.0133	.0027
4.95	.2032	.0229	.0066
6.99	.2988	.0401	.0144
9.05	.3964	.0646	.0264
11.04	.4947	.0956	.0394
13.10	.5981	.1358	.0569
15.09	.6981	.1825	.0775
17.08	.8002	.2378	.0995

RUN 46

ALPHA	CL	CD	CPM
-3.57	-.0275	.0300	-.0566
-2.60	-.0011	.0270	-.0531
-1.58	.0483	.0241	-.0492
-.58	.0885	.0217	-.0443
.46	.1196	.0223	-.0422
1.62	.1691	.0231	-.0376
2.62	.2168	.0248	-.0341
3.60	.2406	.0278	-.0338
4.57	.2794	.0311	-.0304
5.58	.3229	.0360	-.0273
6.70	.3627	.0423	-.0277
7.59	.3944	.0479	-.0258
8.70	.4372	.0576	-.0255
9.70	.4769	.0679	-.0238
10.75	.5237	.0812	-.0196
11.67	.5612	.0948	-.0170
12.64	.6057	.1114	-.0119
13.72	.6734	.1361	-.0054
14.74	.7180	.1568	.0017

RUN 57

ALPHA	CL	CD	CPM
-7.57	-.3589	.0725	-.0551
-6.52	-.2884	.0559	-.0427
-5.59	-.2643	.0481	-.0398
-4.62	-.2137	.0380	-.0327
-3.59	-.1776	.0302	-.0260
-2.60	-.1399	.0244	-.0204
-1.60	-.0956	.0190	-.0149
-.46	-.0385	.0148	-.0094
.49	-.0002	.0129	-.0082
1.51	.0458	.0119	-.0061
2.44	.0783	.0118	-.0042
3.54	.1191	.0127	-.0018
.48	-.0019	.0129	-.0081
2.51	.0807	.0118	-.0040
4.55	.1546	.0146	-.0004
5.70	.1955	.0176	.0026
6.64	.2296	.0209	.0041
7.54	.2595	.0247	.0059
8.59	.3032	.0310	.0085
9.72	.3435	.0391	.0109
10.63	.3868	.0489	.0129
11.68	.4347	.0628	.0148
12.71	.4866	.0783	.0198
13.62	.5423	.0966	.0261
14.72	.5889	.1160	.0320

RUN 58

ALPHA	CL	CD	CPM
-7.60	-.0637	.0771	-.1185
-6.61	-.0426	.0723	-.1119
-5.53	-.0006	.0657	-.0953
-4.41	.0305	.0619	-.0870
-3.38	.0744	.0573	-.0793
-2.48	.1196	.0547	-.0744
-1.54	.1558	.0535	-.0695
-.50	.1901	.0541	-.0658
.55	.2270	.0557	-.0629
1.53	.2689	.0578	-.0594
2.56	.2969	.0610	-.0569
3.61	.3309	.0653	-.0546
4.61	.3711	.0706	-.0531
5.67	.4045	.0760	-.0516
6.61	.4513	.0834	-.0515
6.62	.4459	.0832	-.0506
7.59	.4856	.0913	-.0507
8.62	.5334	.1020	-.0506
9.70	.5704	.1143	-.0475
10.67	.6088	.1279	-.0418
11.69	.6543	.1436	-.0360
12.70	.7025	.1629	-.0297
13.68	.7537	.1856	-.0222

RUN 61

ALPHA	CL	CD	CPM
-7.54	-.2682	.0612	-.0794
-6.65	-.2235	.0509	-.0685
-5.58	-.1912	.0424	-.0638
-4.54	-.1313	.0330	-.0489
-3.48	-.1019	.0270	-.0421
-2.50	-.0586	.0217	-.0364
-1.51	-.0129	.0177	-.0321
-.47	.0345	.0154	-.0285
.55	.0696	.0147	-.0259
1.51	.1014	.0148	-.0239
2.58	.1473	.0159	-.0202
3.49	.1782	.0175	-.0182
4.60	.2190	.0207	-.0161
6.63	.2950	.0287	-.0116
6.55	.2886	.0284	-.0120
7.56	.3286	.0340	-.0099
8.60	.3689	.0412	-.0083
9.68	.4178	.0513	-.0057
10.68	.4545	.0626	-.0035
11.71	.5087	.0779	.0003
12.75	.5530	.0941	.0043
13.69	.6007	.1127	.0086
14.78	.6589	.1359	.0178

RUN 62

ALPHA	CL	CD	CPM
-7.57	-.1048	.0617	-.1081
-6.53	-.0754	.0557	-.1027
-5.58	-.0380	.0496	-.0827
-4.55	-.0134	.0455	-.0782
-3.46	.0332	.0397	-.0698
-2.43	.0642	.0377	-.0666
-1.40	.1004	.0364	-.0629
-.43	.1484	.0350	-.0597
.63	.1917	.0357	-.0550
1.59	.2279	.0368	-.0514
2.55	.2597	.0396	-.0493
3.58	.2913	.0430	-.0468
4.69	.3372	.0485	-.0448
5.59	.3685	.0531	-.0434
6.57	.4091	.0598	-.0423
7.58	.4469	.0678	-.0416
8.59	.4405	.0697	-.0375
9.65	.5372	.0896	-.0386
10.65	.5741	.1031	-.0346
11.70	.6270	.1210	-.0294
12.68	.6740	.1390	-.0252
13.60	.7185	.1583	-.0207
14.64	.7793	.1846	-.0105

RUN 67

ALPHA	CL	CD	CPM
-7.64	-.2714	.0682	-.0845
-6.69	-.2315	.0582	-.0777
-5.71	-.1898	.0486	-.0691
-4.54	-.1428	.0388	-.0594
-3.57	-.1123	.0328	-.0533
-2.61	-.0687	.0271	-.0442
-1.53	-.0118	.0217	-.0360
-.60	.0074	.0201	-.0351
.58	.0642	.0181	-.0297
1.51	.1125	.0173	-.0271
2.52	.1438	.0183	-.0250
3.51	.1715	.0195	-.0224
4.52	.2162	.0223	-.0197
5.62	.2564	.0263	-.0175
6.63	.2921	.0307	-.0151
7.60	.3378	.0361	-.0125
8.60	.3672	.0426	-.0107
9.59	.4054	.0505	-.0083
10.63	.4459	.0601	-.0053
11.61	.4800	.0703	-.0033
12.72	.5271	.0851	.0014
13.70	.5698	.1005	.0049
14.50	.6179	.1181	.0088

RUN 68

ALPHA	CL	CD	CPM
-7.45	-.2565	.0532	-.0681
-6.64	-.2284	.0452	-.0625
-5.58	-.1796	.0359	-.0527
-4.43	-.1153	.0261	-.0419
-3.45	-.0887	.0217	-.0363
-2.51	-.0343	.0167	-.0302
-1.55	.0020	.0143	-.0260
-.55	.0321	.0130	-.0262
.47	.0751	.0128	-.0223
1.49	.1104	.0135	-.0204
2.48	.1482	.0152	-.0185
3.51	.1881	.0173	-.0163
4.51	.2189	.0206	-.0143
5.57	.2543	.0250	-.0121
6.56	.2988	.0307	-.0108
7.56	.3471	.0391	-.0097
8.60	.3861	.0484	-.0065
9.55	.4269	.0593	-.0046
10.69	.4866	.0764	.0002
11.68	.5425	.0940	.0054
12.71	.5916	.1121	.0115
13.74	.6451	.1332	.0183
14.53	.6841	.1506	.0237

TABLE AII.- Continued

RUN 69

ALPHA	CL	CD	CPM
-7.68	-.3182	.0776	-.0758
-6.51	-.2688	.0636	-.0668
-5.34	-.1961	.0498	-.0495
-4.54	-.1928	.0461	-.0497
-3.57	-.1381	.0377	-.0392
-2.52	-.1024	.0321	-.0328
-1.55	-.0725	.0276	-.0292
-.54	-.0244	.0239	-.0241
.52	.0183	.0221	-.0205
1.50	.0654	.0214	-.0181
2.45	.1011	.0216	-.0164
3.32	.1307	.0228	-.0137
4.53	.1697	.0248	-.0111
5.64	.2146	.0282	-.0069
6.53	.2278	.0312	-.0066
7.54	.2693	.0359	-.0040
8.53	.3107	.0423	-.0007
9.67	.3631	.0513	.0001
10.72	.3980	.0613	.0033
11.76	.4420	.0750	.0060
12.77	.4941	.0918	.0098
13.79	.5601	.1129	.0182
14.77	.6129	.1330	.0264

RUN 70

ALPHA	CL	CD	CPM
-7.58	-.3069	.0777	-.0785
-6.62	-.2703	.0677	-.0710
-5.59	-.2240	.0563	-.0625
-4.56	-.1867	.0481	-.0550
-3.54	-.1387	.0402	-.0435
-2.59	-.1203	.0360	-.0401
-1.55	-.0603	.0298	-.0313
-.56	-.0156	.0262	-.0269
.52	.0281	.0240	-.0237
1.50	.0634	.0238	-.0215
2.50	.1006	.0239	-.0187
3.52	.1461	.0256	-.0162
4.48	.1692	.0275	-.0146
5.56	.2012	.0306	-.0115
6.49	.2366	.0334	-.0092
7.61	.2719	.0384	-.0060
8.60	.3168	.0448	-.0029
9.58	.3471	.0525	-.0007
10.53	.3781	.0605	-.0000
11.67	.4426	.0762	.0039
12.69	.4762	.0898	.0071
13.57	.5391	.1090	.0144
14.75	.5898	.1294	.0210

RUN 71

ALPHA	CL	CD	CPM
-7.58	-.2512	.0660	-.0885
-6.66	-.2193	.0570	-.0777
-5.54	-.1856	.0480	-.0710
-4.48	-.1324	.0385	-.0562
-3.51	-.1008	.0331	-.0463
-2.53	-.0681	.0284	-.0415
-1.50	-.0172	.0242	-.0363
-.51	.0092	.0227	-.0333
.47	.0725	.0209	-.0270
1.46	.0974	.0216	-.0258
2.47	.1365	.0221	-.0229
3.53	.1734	.0237	-.0214
4.54	.2055	.0271	-.0189
5.52	.2477	.0299	-.0156
6.53	.2849	.0345	-.0140
7.57	.3227	.0403	-.0108
8.57	.3575	.0457	-.0096
9.61	.3960	.0542	-.0080
10.70	.4540	.0683	-.0044
11.67	.4896	.0808	-.0031
12.76	.5574	.1025	.0020
13.63	.5829	.1169	.0044
14.67	.6382	.1397	.0094

RUN 72

ALPHA	CL	CD	CPM
-7.46	-.2311	.0643	-.0877
-6.64	-.2115	.0577	-.0831
-5.65	-.1693	.0482	-.0709
-4.59	-.1452	.0423	-.0628
-3.55	-.1014	.0354	-.0501
-2.56	-.0663	.0306	-.0431
-1.50	-.0075	.0256	-.0360
-.53	.0146	.0242	-.0342
.46	.0625	.0231	-.0306
1.44	.0947	.0234	-.0283
2.51	.1324	.0239	-.0243
3.47	.1672	.0260	-.0231
4.54	.2161	.0287	-.0197
5.48	.2372	.0321	-.0187
6.64	.2798	.0367	-.0153
7.61	.3181	.0410	-.0121
8.61	.3511	.0476	-.0096
9.59	.3851	.0563	-.0086
10.63	.4368	.0675	-.0060
11.70	.5022	.0849	-.0046
12.73	.5454	.1019	-.0009
13.72	.6027	.1252	.0014
14.77	.6559	.1494	.0110

RUN 73

ALPHA	CL	CD	CPM
-7.64	-.2671	.0708	-.0850
-6.59	-.2243	.0595	-.0743
-5.64	-.1871	.0511	-.0639
-4.67	-.1548	.0440	-.0560
-3.51	-.1137	.0367	-.0477
-2.60	-.0750	.0312	-.0401
-1.54	-.0244	.0271	-.0341
-.47	.0061	.0245	-.0321
.42	.0512	.0230	-.0293
1.56	.0876	.0232	-.0245
2.65	.1307	.0236	-.0231
3.52	.1615	.0249	-.0207
4.49	.1922	.0271	-.0179
5.45	.2264	.0304	-.0159
6.47	.2590	.0348	-.0145
7.42	.2925	.0387	-.0119
8.59	.3451	.0464	-.0094
9.52	.3795	.0538	-.0053
10.70	.4295	.0669	-.0029
11.72	.4707	.0800	-.0004
12.68	.5158	.0946	.0026
13.66	.5650	.1122	.0077
14.70	.6346	.1361	.0169

RUN 74

ALPHA	CL	CD	CPM
-3.51	-.1062	.0381	-.0487
-1.52	-.0315	.0292	-.0379
.40	.0533	.0248	-.0295
2.47	.1326	.0254	-.0248
4.51	.1968	.0297	-.0203
6.63	.2709	.0371	-.0146
8.59	.3423	.0485	-.0090
10.55	.4020	.0646	-.0027
12.56	.5090	.0952	.0017
14.55	.6214	.1351	.0141

RUN 75

ALPHA	CL	CD	CPM
-3.56	-.0955	.0360	-.0474
-1.59	-.0107	.0257	-.0335
.47	.0692	.0227	-.0258
2.52	.1350	.0236	-.0208
4.48	.2014	.0283	-.0171
6.58	.2798	.0367	-.0128
8.54	.3552	.0482	-.0074
10.53	.4438	.0679	-.0036
12.51	.5583	.0985	.0031
14.69	.6614	.1342	.0186

RUN 76

ALPHA	CL	CD	CPM
-3.59	-.0838	.0383	-.0433
-1.52	-.0240	.0304	-.0347
.51	.0659	.0242	-.0272
2.49	.1401	.0256	-.0226
4.64	.2199	.0315	-.0179
6.64	.2930	.0401	-.0136
8.68	.3629	.0524	-.0081
10.61	.4462	.0715	-.0047
12.64	.5499	.0977	.0034
14.80	.6723	.1357	.0200

TABLE AII.- Concluded

RUN 77

ALPHA	CL	CD	CPM
-3.58	-.1207	.0463	-.0489
-1.55	-.0248	.0339	-.0329
.45	.0461	.0297	-.0284
2.94	.1290	.0308	-.0222
4.59	.1898	.0347	-.0180
6.67	.2578	.0428	-.0120
8.59	.3266	.0528	-.0066
10.59	.4089	.0709	-.0003
12.57	.5025	.0965	.0017
14.61	.6113	.1296	.0149

RUN 78

ALPHA	CL	CD	CPM
-3.56	-.1120	.0500	-.0484
-1.22	-.0157	.0383	-.0333
.50	.0416	.0345	-.0306
2.50	.1226	.0352	-.0254
4.53	.1848	.0395	-.0210
6.58	.2608	.0474	-.0139
8.50	.3233	.0575	-.0069
10.63	.4147	.0773	.0001
12.65	.5173	.1004	.0021
14.63	.6354	.1361	.0175

RUN 94

ALPHA	CL	CD	CPM
-3.67	-.0666	.0518	-.0621
-1.43	.0381	.0411	-.0446
.49	.1026	.0395	-.0406
2.64	.1776	.0413	-.0337
4.62	.2460	.0469	-.0295
6.67	.3156	.0557	-.0257
8.53	.3995	.0700	-.0229
10.66	.4782	.0915	-.0174
12.59	.5628	.1211	-.0110
14.50	.6668	.1615	.0044

RUN 95

ALPHA	CL	CD	CPM
-3.63	-.0610	.0540	-.0625
-1.54	.0292	.0440	-.0490
.43	.0983	.0417	-.0427
2.58	.1780	.0430	-.0357
3.53	.2088	.0454	-.0339
4.60	.2494	.0487	-.0306
6.57	.3072	.0567	-.0271
8.63	.3900	.0712	-.0248
10.55	.4672	.0912	-.0191
12.65	.5673	.1247	-.0121
14.45	.6606	.1610	.0040

RUN 96

ALPHA	CL	CD	CPM
-3.53	.0167	.0462	-.0722
-1.50	.0898	.0411	-.0625
.49	.1670	.0406	-.0534
2.59	.2374	.0444	-.0460
4.48	.2958	.0514	-.0420
6.54	.3774	.0620	-.0362
8.55	.4690	.0795	-.0337
10.61	.5476	.1042	-.0301
12.71	.6406	.1398	-.0210
14.65	.7401	.1860	-.0060

RUN 97

ALPHA	CL	CD	CPM
-3.63	.0101	.0484	-.0754
-1.48	.1018	.0416	-.0619
.60	.1732	.0420	-.0543
2.57	.2342	.0455	-.0479
4.56	.2940	.0526	-.0425
6.54	.3675	.0636	-.0378
8.59	.4558	.0808	-.0345
10.58	.5256	.1029	-.0312
12.67	.6338	.1405	-.0238
14.68	.7279	.1871	-.0104

RUN 98

ALPHA	CL	CD	CPM
-3.65	-.0165	.0507	-.0720
-1.49	.0791	.0428	-.0586
.40	.1401	.0420	-.0532
2.56	.2228	.0448	-.0444
4.50	.2860	.0514	-.0395
6.45	.3606	.0604	-.0346
8.55	.4387	.0766	-.0327
10.63	.5087	.0993	-.0265
12.90	.6496	.1442	-.0153
14.70	.7174	.1775	-.0039

RUN 99

ALPHA	CL	CD	CPM
-3.63	.0012	.0500	-.0718
-1.52	.0691	.0444	-.0624
.54	.1553	.0433	-.0530
2.82	.2147	.0477	-.0467
4.68	.2894	.0529	-.0404
6.66	.3607	.0621	-.0354
8.57	.4374	.0774	-.0339
10.92	.5290	.1065	-.0243
12.53	.6031	.1334	-.0195
13.85	.6747	.1605	-.0107
14.60	.7093	.1758	-.0037

RUN 100

ALPHA	CL	CD	CPM
-3.61	.0208	.0479	-.0777
-1.58	.0999	.0431	-.0636
.50	.1709	.0443	-.0582
2.59	.2539	.0481	-.0497
4.59	.3294	.0572	-.0437
6.64	.3940	.0681	-.0401
8.65	.4659	.0863	-.0366
10.67	.5620	.1101	-.0350
12.68	.6738	.1455	-.0270
14.61	.7763	.1829	-.0115

RUN 101

ALPHA	CL	CD	CPM
-3.57	.0276	.0499	-.0772
-1.56	.1045	.0453	-.0643
.50	.1830	.0467	-.0585
2.44	.2513	.0511	-.0516
4.62	.3218	.0601	-.0465
6.65	.3919	.0709	-.0415
8.69	.4624	.0885	-.0380
10.54	.5498	.1108	-.0349
12.68	.6630	.1439	-.0258

REFERENCES

1. Robins, A. Warner; Morris, Odell A.; and Harris, Roy V., Jr.: Recent Research Results in the Aerodynamics of Supersonic Vehicles. J. Aircr., vol. 3, no. 6, Nov.-Dec. 1966, pp. 573-577.

2. Robins, A. Warner; Lamb, Milton; and Miller, David S.: Aerodynamic Characteristics at Mach Numbers of 1.5, 1.8, and 2.0 of a Blended Wing-Body Configuration With and Without Integral Canards. NASA TP-1427, 1979.

3. Coe, Paul L., Jr.; McLemore, H. Clyde; and Shivers, James P.: Effects of Upper-Surface Blowing and Thrust Vectoring on Low-Speed Aerodynamic Characteristics of a Large-Scale Supersonic Transport Model. NASA TN D-8296, 1976.

4. Coe, Paul L., Jr.; Smith, Paul M.; and Parlett, Lysle P.: Low-Speed Wind Tunnel Investigation of an Advanced Supersonic Cruise Arrow-Wing Configuration. NASA TM-74043, 1977.

5. Coe, Paul L., Jr.; and Weston, Robert P.: Effects of Wing Leading-Edge Deflection on Low-Speed Aerodynamic Characteristics of a Low-Aspect-Ratio Highly Swept Arrow-Wing Configuration. NASA TP-1434, 1979.

6. Coe, Paul L., Jr.; and Thomas, James L.: Theoretical and Experimental Investigation of Ground-Induced Effects for a Low-Aspect-Ratio Highly Swept Arrow-Wing Configuration. NASA TP-1508, 1979.

7. Coe, Paul L., Jr.; Huffman, Jarrett K.; and Fenbert, James W.: Leading-Edge Deflection Optimization for a Highly Swept Arrow-Wing Configuration. NASA TP-1777, 1980.

8. Gentry, Garl L., Jr.; and Coe, Paul L., Jr.: Low-Speed Aerodynamic Characteristics of a Highly Swept Arrow-Wing Configuration With Several Deflected Leading-Edge Concepts. NASA TM-80180, 1980.

9. Craidon, Charlotte B.: Description of a Digital Computer Program for Airplane Configuration Plots. NASA TM X-2074, 1970.

10. Gillis, Clarence L.; Polhamus, Edward C.; and Gray, Joseph L., Jr.: Charts for Determining Jet-Boundary Corrections for Complete Models in 7- by 10-Foot Closed Rectangular Wind Tunnels. NACA WR L-123, 1945. (Formerly NACA ARR L5G31.)

11. Pope, Alan; and Harper, John J.: Low-Speed Wind Tunnel Testing. John Wiley & Sons, Inc., c.1966.

12. Braslow, Albert L.; and Knox, Eugene C.: Simplified Method for Determination of Critical Height of Distributed Roughness Particles for Boundary-Layer Transition at Mach Numbers From 0 to 5. NACA TN 4363, 1958.

13. Tulinius, J.: Unified Subsonic, Transonic, and Supersonic NAR Vortex Lattice. TFD-72-523, Los Angeles Div., North American Rockwell, Apr. 27, 1972.

14. Henderson, William P.: Studies of Various Factors Affecting Drag Due to Lift at Subsonic Speeds. NASA TN D-3584, 1966.

15. Hess, John L.: Calculation of Potential Flow About Arbitrary Three-Dimensional Lifting Bodies. Rep. No. MDC J5679-01 (Contract N00019-71-C-0524), McDonnell Douglas Corp., Oct. 1972. (Available from DTIC as AD 755 480.)

16. Coe, Paul L., Jr.; Thomas, James L.; Huffman, Jarrett K.; Weston, Robert P.; Schoonover, Ward E., Jr.; and Gentry, Garl L., Jr.: Overview of the Langley Subsonic Research Effort on SCR Configurations. Supersonic Cruise Research '79 - Part 1, NASA CP-2108, 1980, pp. 13-33.

17. Grantham, William D.; Smith, Paul M.; and Deal, Perry L.: A Simulator Study for the Development and Evaluation of Operating Procedures on a Supersonic Cruise Research Transport To Minimize Airport-Community Noise. NASA TP-1742, 1980.

TABLE I.- GEOMETRIC CHARACTERISTICS OF MODEL

Wing:	
Aspect ratio	1.904
Reference area, m^2 (ft^2)	0.834 (8.972)
Gross area, m^2 (ft^2)	0.919 (9.889)
Span, m (ft)	1.260 (4.133)
Root chord, m (ft)	1.674 (5.492)
Tip chord, m (ft)	0.161 (0.529)
Reference mean aerodynamic chord, m (ft)	0.880 (2.887)
Gross mean aerodynamic chord, m (ft)	1.038 (3.406)
Leading-edge sweep, deg:	
At body station 0.530 m (1.738 ft)	74.0
At body station 1.569 m (5.149 ft)	70.5
At body station 2.027 m (6.651 ft)	60.0
Vertical fin (each):	
Span, m (ft)	0.107 (0.350)
Root chord, m (ft)	0.326 (1.069)
Tip chord, m (ft)	0.048 (0.158)
Leading-edge sweep, deg	73.4
Taper ratio	0.148

TABLE II.- COMPUTER CARDS FOR NUMERICAL MODEL OF CONFIGURATION

(a) SI Units; all dimensions are given in centimeters

```
 AST-200 LOW-SPEED MODEL    .03259 SCALE  UNCAMBERED (COF) (8/2/79)
   -1 -1  1  1  1 -1 20 28  1 19 30                          2 20  2 10  1 10
0.       .125    .25     .5      .75     1.0     1.5     2.5     5.0     10.       XAF 10
 15.     20.     25.     30.     35.     40.     45.     50.     55.     60.       XAF 20
65.     70.     75.     80.     85.     90.     95.     100.                       XAF 28
 52.979  0.000  0.000167.406                                                       WORG 1
 58.471  1.575  0.000161.884                                                       WORG 2
 63.965  3.150  0.000156.357                                                       WORG 3
 71.742  5.380  0.000148.547                                                       WORG 3A
 74.948  6.299  0.000145.306                                                       WORG 4
 85.931  9.449  0.000134.259                                                       WORG 5
 96.914 12.598  0.000123.208                                                       WORG 6
107.899 15.748  0.000112.161                                                       WORG 7
126.324 21.031  0.000 93.624                                                       WORG 8
140.851 25.197  0.000 80.239                                                       WORG 9
156.939 29.809  0.000 65.410                                                       WORG 10
170.619 34.564  0.000 53.030                                                       WORG 11
179.913 37.795  0.000 46.586                                                       WORG 12
188.976 40.945  0.000 40.307                                                       WORG 13
202.717 45.720  0.000 30.785                                                       WORG 14
202.717 45.723  0.000 30.785                                                       WORG 15
203.817 46.355  0.000 30.249                                                       WORG 15A
210.810 50.394  0.000 26.820                                                       WORG 16
221.722 56.693  0.000 21.476                                                       WORG 17
232.634 62.992  0.000 16.129                                                       WORG 18
0.      .137    .180    .242    .298    .339    .413    .521    .726    .996       WORD1.1
1.181   1.318   1.419   1.490   1.532   1.543   1.543   1.543   1.543   1.543      WORD1.2
1.388   1.213   1.021   .819    .615    .413    .212    0.                         WORD1.3
0.      .137    .180    .242    .298    .339    .413    .521    .726    .996       WORD2.1
1.181   1.318   1.419   1.490   1.532   1.543   1.543   1.543   1.543   1.543      WORD2.2
1.388   1.213   1.021   .819    .615    .413    .212    0.                         WORD2.3
0.      .137    .180    .242    .298    .339    .413    .521    .726    .996       WORD3.1
1.181   1.318   1.419   1.490   1.532   1.543   1.543   1.543   1.543   1.543      WORD3.2
1.388   1.213   1.021   .819    .615    .413    .212    0.                         WORD3.3
0.      .137    .179    .241    .297    .339    .412    .523    .724    .994       WORD3A.1
1.177   1.315   1.416   1.487   1.528   1.539   1.539   1.539   1.539   1.539      WORD3A.2
1.384   1.210   1.018   .817    .614    .412    .211    0.                         WORD3A.3
0.      .136    .178    .237    .291    .333    .405    .514    .712    .978       WORD4.1
1.157   1.292   1.391   1.461   1.501   1.512   1.512   1.512   1.512   1.512      WORD4.2
1.363   1.192   1.003   .806    .606    .406    .208    0.                         WORD4.3
0.      .128    .168    .225    .277    .316    .386    .490    .679    .931       WORD5.1
1.103   1.232   1.326   1.392   1.430   1.441   1.441   1.441   1.441   1.437      WORD5.2
1.294   1.132   .953    .765    .576    .385    .197    0.                         WORD5.3
0.      .118    .160    .216    .266    .304    .370    .470    .651    .894       WORD6.1
1.059   1.182   1.273   1.336   1.373   1.383   1.383   1.383   1.383   1.341      WORD6.2
1.208   1.056   .889    .714    .537    .360    .184    0.                         WORD6.3
0.      .110    .153    .208    .257    .294    .358    .455    .631    .866       WORD7.1
1.025   1.144   1.231   1.293   1.328   1.338   1.338   1.338   1.338   1.277      WORD7.2
1.151   1.006   .848    .681    .512    .343    .175    0.                         WORD7.3


0.      .101    .145    .200    .247    .283    .344    .438    .607    .833       WORD8.1
.987    1.101   1.184   1.244   1.278   1.287   1.287   1.287   1.287   1.186      WORD8.2
1.069   .935    .788    .633    .476    .319    .163    0.                         WORD8.3
0.      .100    .144    .198    .245    .280    .341    .435    .602    .827       WORD9.1
.979    1.092   1.175   1.234   1.268   1.277   1.277   1.277   1.260   1.161      WORD9.2
1.046   .915    .771    .619    .466    .312    .159    0.                         WORD9.3
0.      .102    .146    .201    .248    .284    .345    .440    .609    .836       WORD10.1
.990    1.105   1.189   1.248   1.283   1.292   1.292   1.292   1.247   1.149      WORD10.2
1.035   .906    .763    .613    .461    .309    .156    0.                         WORD10.3
0.      .111    .154    .209    .258    .295    .359    .457    .632    .868       WORD11.1
1.028   1.148   1.235   1.297   1.330   1.342   1.342   1.342   1.263   1.164      WORD11.2
1.049   .917    .773    .621    .467    .313    .160    0.                         WORD11.3
0.      .118    .160    .216    .266    .304    .370    .470    .651    .894       WORD12.1
1.059   1.181   1.272   1.335   1.372   1.382   1.382   1.382   1.300   1.198      WORD12.2
1.080   .945    .796    .639    .481    .322    .164    0.                         WORD12.3
0.      .125    .166    .222    .274    .313    .381    .484    .670    .920       WORD13.1
1.090   1.216   1.309   1.375   1.413   1.423   1.423   1.423   1.339   1.234      WORD13.2
1.112   .972    .819    .658    .495    .331    .169    0.                         WORD13.3
0.      .138    .177    .235    .289    .330    .402    .510    .706    .969       WORD14.1
1.148   1.282   1.380   1.449   1.489   1.500   1.500   1.500   1.411   1.300      WORD14.2
1.171   1.024   .862    .692    .521    .349    .178    0.                         WORD14.3
0.      .0069   .0144   .0294   .0440   .0590   .0884   .1462   .2853   .541       WORD15.1
.766    .961    1.126   1.261   1.365   1.440   1.485   1.500   1.485   1.440      WORD15.2
1.365   1.261   1.126   .961    .766    .541    .285    0.                         WORD15.3
0.      .0069   .0144   .0294   .0440   .0590   .0884   .1462   .2853   .541       WORD15A.
.766    .961    1.126   1.261   1.365   1.440   1.485   1.500   1.485   1.440      WORD15A.
1.365   1.261   1.126   .961    .766    .541    .285    0.                         WORD15A.
0.      .0069   .0144   .0294   .0440   .0590   .0884   .1462   .2853   .541       WORD16.1
.766    .961    1.126   1.261   1.365   1.440   1.485   1.500   1.485   1.440      WORD16.2
1.365   1.261   1.126   .961    .766    .541    .285    0.                         WORD16.3
0.      .0069   .0144   .0294   .0440   .0590   .0884   .1462   .2853   .541       WORD17.1
.766    .961    1.126   1.261   1.365   1.440   1.485   1.500   1.485   1.440      WORD17.2
1.365   1.261   1.126   .961    .766    .541    .285    0.                         WORD17.3
0.      .0069   .0144   .0294   .0440   .0590   .0884   .1462   .2853   .541       WORD18.1
.766    .961    1.126   1.261   1.365   1.440   1.485   1.500   1.485   1.440      WORD18.2
1.365   1.261   1.126   .961    .766    .541    .285    0.                         WORD18.3
  0.000   9.934  19.868  29.802  39.736  49.670  59.604  69.535  79.469  89.403   XFUS 10
 99.337109.271119.205129.139139.073149.007158.941168.874178.808188.740   XFUS 20
198.674208.608218.542228.476                                             XFUS
  0.000   7.006  19.535  35.032  53.581  74.993  95.819106.671109.335104.503   AFUS 10
 97.890  97.593  99.271101.639104.800108.845113.677116.735117.626118.413   AFUS 20
118.219116.638112.497105.884                                             AFUS
```

TABLE II.- Concluded

(b) U.S. Customary Units; all dimensions are given in inches

AST-200 LOW-SPEED MODEL .03259 SCALE UNCAMBERED (COE) (8/2/79)

-1 -1 1 1 1 -1 20 28 1 19 30 2 20 2 10 1 10

0.	.125	.25	.5	.75	1.0	1.5	2.5	5.0	10.	XAF 10
15.	20.	25.	30.	35.	40.	45.	50.	55.	60.	XAF 20
65.	70.	75.	80.	85.	90.	95.	100.			XAF 28
20.858	0.000	0.	65.908							WORG 1
23.020	.620	0.	63.734							WORG 2
25.183	1.240	0.	61.558							WORG 3
28.245	2.118	0.	58.483							WORG 3A
29.507	2.480	0.	57.207							WORG 4
33.831	3.720	0.	52.858							WORG 5
38.155	4.960	0.	48.507							WORG 6
42.480	6.200	0.	44.158							WORG 7
49.734	8.280	0.	36.860							WORG 8
55.453	9.920	0.	31.590							WORG 9
61.787	11.736	0.	25.752							WORG 10
67.173	13.608	0.	20.878							WORG 11
70.832	14.880	0.	18.341							WORG 12
74.400	16.120	0.	15.869							WORG 13
79.810	18.000	0.	12.120							WORG 14
79.810	18.001	0.	12.120							WORG 15
80.243	18.250	0.	11.909							WORG 15A
82.996	19.840	0.	10.559							WORG 16
87.292	22.320	0.	8.455							WORG 17
91.588	24.800	0.	6.350							WORG 18
0.	.137	.180	.242	.298	.339	.413	.521	.726	.996	WORD1.1
1.181	1.318	1.419	1.490	1.532	1.543	1.543	1.543	1.543	1.543	WORD1.2
1.388	1.213	1.021	.819	.615	.413	.212	0.			WORD1.3
0.	.137	.180	.242	.298	.339	.413	.521	.726	.996	WORD2.1
1.181	1.318	1.419	1.490	1.532	1.543	1.543	1.543	1.543	1.543	WORD2.2
1.388	1.213	1.021	.819	.615	.413	.212	0.			WORD2.3
0.	.137	.180	.242	.298	.339	.413	.521	.726	.996	WORD3.1
1.181	1.318	1.419	1.490	1.532	1.543	1.543	1.543	1.543	1.543	WORD3.2
1.388	1.213	1.021	.819	.615	.413	.212	0.			WORD3.3
0.	.137	.179	.241	.297	.339	.412	.523	.724	.994	WORD3A.1
1.177	1.315	1.416	1.487	1.528	1.539	1.539	1.539	1.539	1.539	WORD3A.2
1.384	1.210	1.018	.817	.614	.412	.211	0.			WORD3A.3
0.	.136	.178	.237	.291	.333	.405	.514	.712	.978	WORD4.1
1.157	1.292	1.391	1.461	1.501	1.512	1.512	1.512	1.512	1.512	WORD4.2
1.363	1.192	1.003	.806	.606	.406	.208	0.			WORD4.3
0.	.128	.168	.225	.277	.316	.386	.490	.679	.931	WORD5.1
1.103	1.232	1.326	1.392	1.430	1.441	1.441	1.441	1.441	1.437	WORD5.2
1.294	1.132	.953	.765	.576	.385	.197	0.			WORD5.3
0.	.118	.160	.216	.266	.304	.370	.470	.651	.894	WORD6.1
1.059	1.182	1.273	1.336	1.373	1.383	1.383	1.383	1.383	1.341	WORD6.2
1.208	1.056	.889	.714	.537	.360	.184	0.			WORD6.3
0.	.110	.153	.208	.257	.294	.358	.455	.631	.866	WORD7.1
1.025	1.144	1.231	1.293	1.328	1.338	1.338	1.338	1.338	1.277	WORD7.2
1.151	1.006	.848	.681	.512	.343	.175	0.			WORD7.3
0.	.101	.145	.200	.247	.283	.344	.438	.607	.833	WORD8.1
.987	1.101	1.184	1.244	1.278	1.287	1.287	1.287	1.287	1.186	WORD8.2
1.069	.935	.788	.633	.476	.319	.163	0.			WORD8.3
0.	.100	.144	.198	.245	.280	.341	.435	.602	.827	WORD9.1
.979	1.092	1.175	1.234	1.268	1.277	1.277	1.277	1.260	1.161	WORD9.2
1.046	.915	.771	.619	.466	.312	.159	0.			WORD9.3
0.	.102	.146	.201	.248	.284	.345	.440	.609	.836	WORD10.1
.990	1.105	1.189	1.248	1.283	1.292	1.292	1.292	1.247	1.149	WORD10.2
1.035	.906	.763	.613	.461	.309	.156	0.			WORD10.3
0.	.111	.154	.209	.258	.295	.359	.457	.632	.868	WORD11.1
1.028	1.148	1.235	1.297	1.330	1.342	1.342	1.342	1.263	1.164	WORD11.2
1.049	.917	.773	.621	.467	.313	.160	0.			WORD11.3
0.	.118	.160	.216	.266	.304	.370	.470	.651	.894	WORD12.1
1.059	1.181	1.272	1.335	1.372	1.382	1.382	1.382	1.300	1.198	WORD12.2
1.080	.945	.796	.639	.481	.322	.164	0.			WORD12.3
0.	.125	.166	.222	.274	.313	.381	.484	.670	.920	WORD13.1
1.090	1.216	1.309	1.375	1.413	1.423	1.423	1.423	1.339	1.234	WORD13.2
1.112	.972	.819	.658	.495	.331	.169	0.			WORD13.3
0.	.138	.177	.235	.289	.330	.402	.510	.706	.969	WORD14.1
1.148	1.282	1.380	1.449	1.489	1.500	1.500	1.500	1.411	1.300	WORD14.2
1.171	1.024	.862	.692	.521	.349	.178	0.			WORD14.3
0.	.0069	.0144	.0294	.0440	.0590	.0884	.1462	.2853	.541	WORD15.1
.766	.961	1.126	1.261	1.365	1.440	1.485	1.500	1.485	1.440	WORD15.2
1.365	1.261	1.126	.961	.766	.541	.285	0.			WORD15.3
0.	.0069	.0144	.0294	.0440	.0590	.0884	.1462	.2853	.541	WORD15A.
.766	.961	1.126	1.261	1.365	1.440	1.485	1.500	1.485	1.440	WORD15A.
1.365	1.261	1.126	.961	.766	.541	.285	0.			WORD15A.
0.	.0069	.0144	.0294	.0440	.0590	.0884	.1462	.2853	.541	WORD16.1
.766	.961	1.126	1.261	1.365	1.440	1.485	1.500	1.485	1.440	WORD16.2
1.365	1.261	1.126	.961	.766	.541	.285	0.			WORD16.3
0.	.0069	.0144	.0294	.0440	.0590	.0884	.1462	.2853	.541	WORD17.1
.766	.961	1.126	1.261	1.365	1.440	1.485	1.500	1.485	1.440	WORD17.2
1.365	1.261	1.126	.961	.766	.541	.285	0.			WORD17.3
0.	.0069	.0144	.0294	.0440	.0590	.0884	.1462	.2853	.541	WORD18.1
.766	.961	1.126	1.261	1.365	1.440	1.485	1.500	1.485	1.440	WORD18.2
1.365	1.261	1.126	.961	.766	.541	.285	0.			WORD18.3
0.000	3.911	7.822	11.733	15.644	19.555	23.466	27.376	31.287	35.198	XFUS 10
39.109	43.020	46.931	50.842	54.753	58.664	62.575	66.486	70.397	74.307	XFUS 20
78.218	82.129	86.040	89.951							XFUS
0.000	1.086	3.028	5.430	8.305	11.624	14.852	16.534	16.947	16.198	AFUS 10
15.173	15.127	15.387	15.754	16.244	16.871	17.620	18.094	18.232	18.354	AFUS 20
18.324	18.079	17.437	16.412							AFUS

TABLE III.- SUMMARY OF EXPERIMENTAL VORTEX CORE LOCATIONS

α, deg	Values of η at location of vortex intersection with chordwise row located along semispan station -				Values of γ at location of vortex intersection with spanwise row located along -		
	$y/\frac{b}{2}$ = 0.170	$y/\frac{b}{2}$ = 0.425	$y/\frac{b}{2}$ = 0.654	$y/\frac{b}{2}$ = 0.862	ξ = 0.472	ξ = 0.731	ξ = 0.98
0.87	None	None	None	None	None	None	None
2.96	↓	None	Plain separation	0.225	None	None	0.95
4.95	↓	0.025	↓	↓	0.94	0.96	↓
6.99	↓	.28	↓	↓	.86	.78	↓
9.05	0.04	.30	↓	↓	.86	.78	↓
11.04	.04	.36	↓	↓	.76	.78	↓
13.10	.06	.40	↓	↓	.76	.78	↓
15.09	.07	.43	↓	↓	.76	.62	↓

TABLE IV.- SPANWISE LEADING-EDGE CHARACTERISTICS BASED ON INTERPRETATION OF PRESSURE DATA WITH δ_{le} = 30°

α, deg	Leading-edge characteristics at semispan station -			
	$y/\frac{b}{2}$ = 0.170	$y/\frac{b}{2}$ = 0.425	$y/\frac{b}{2}$ = 0.654	$y/\frac{b}{2}$ = 0.862
2.51	Over deflected	Over deflected	Over deflected	Over deflected
4.55	Over deflected	Attached	Attached	Attached
6.64	Aligned	↓	Attached	Attached
8.59	Attached	↓	Separated	Separation bubble at leading edge
10.63	↓	↓	↓	↓
12.71	↓	↓	↓	↓

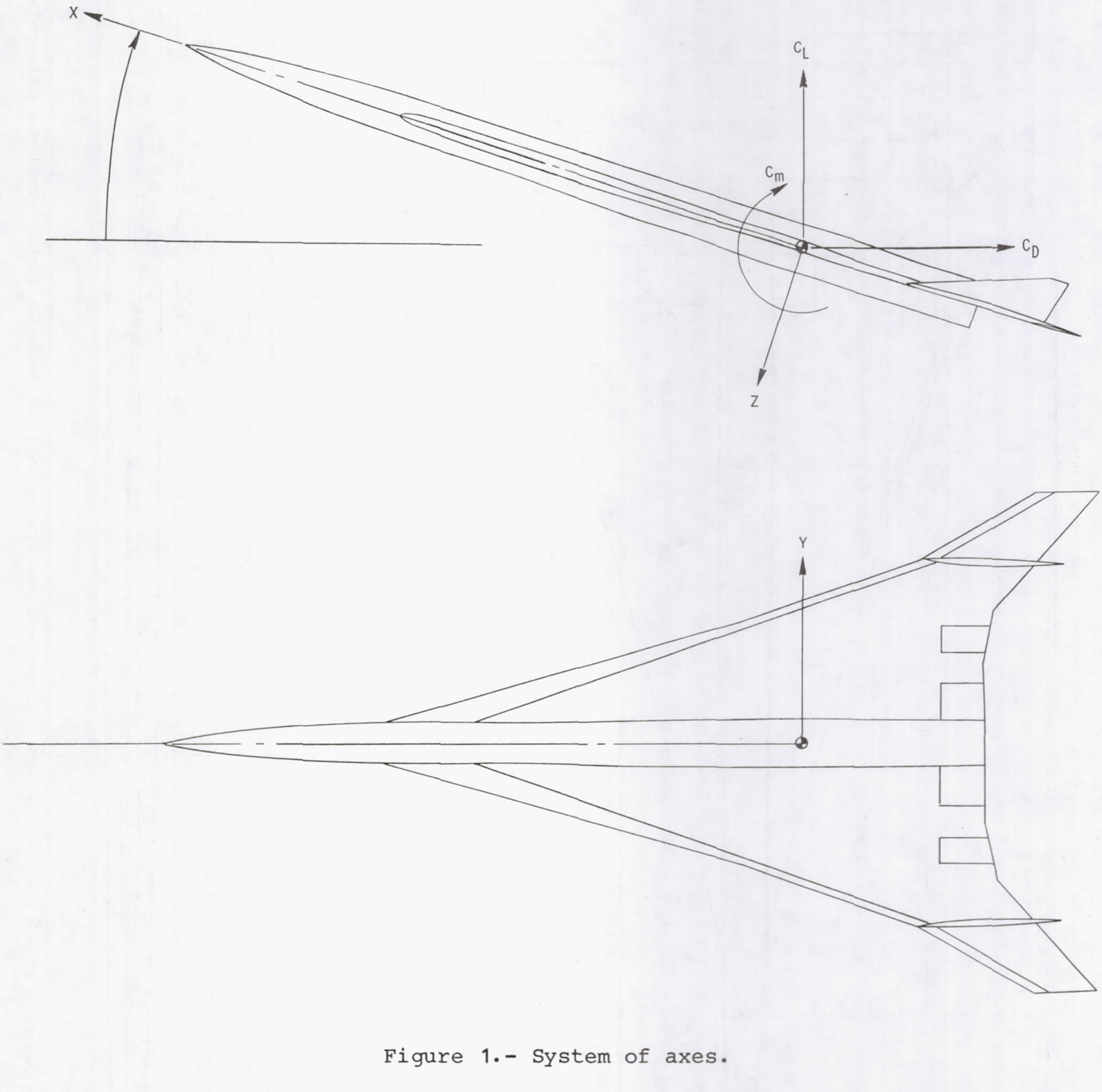

Figure 1.- System of axes.

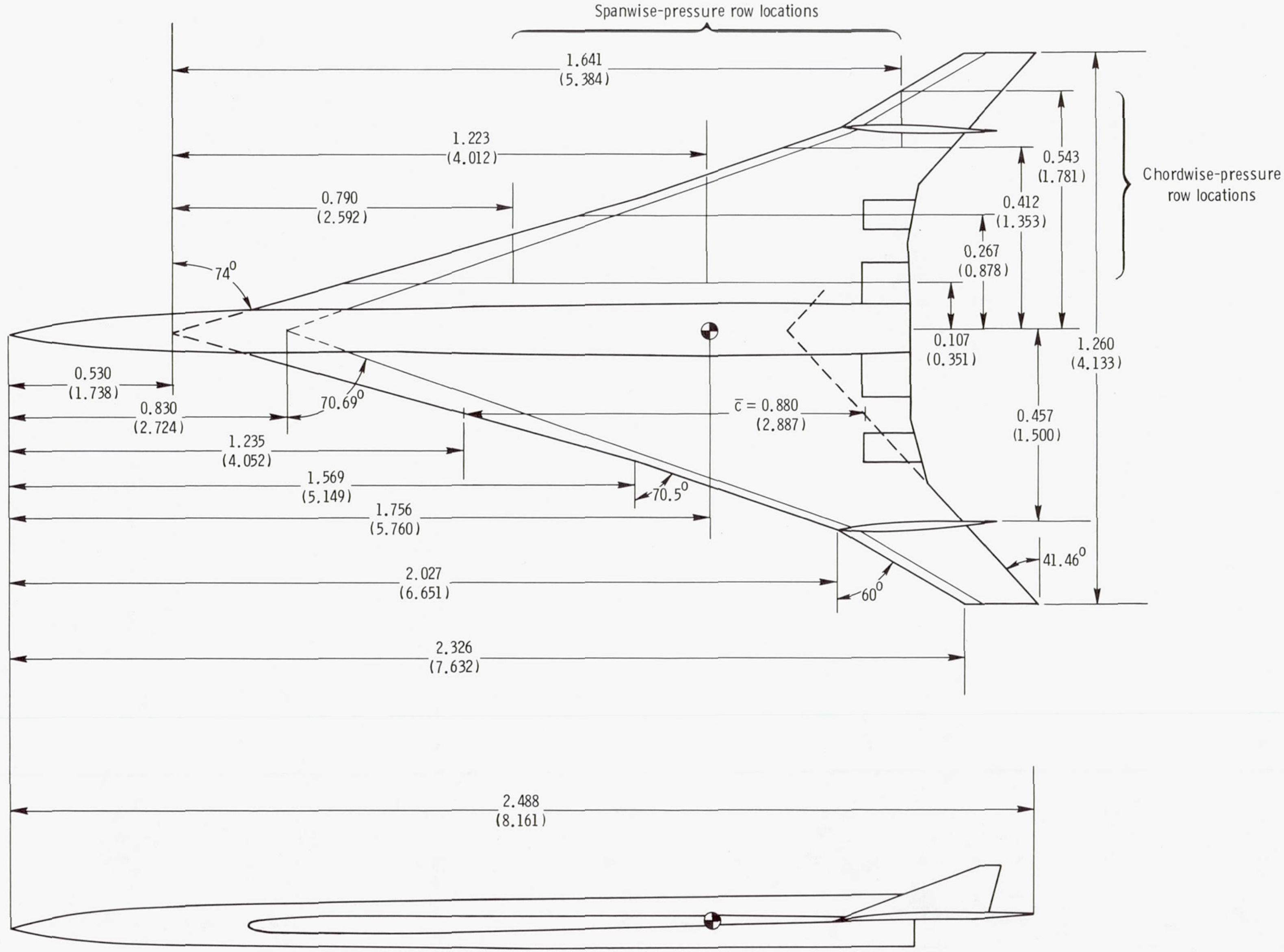

Figure 2.- Geometric characteristics. Dimensions are given in meters (feet) unless otherwise specified.

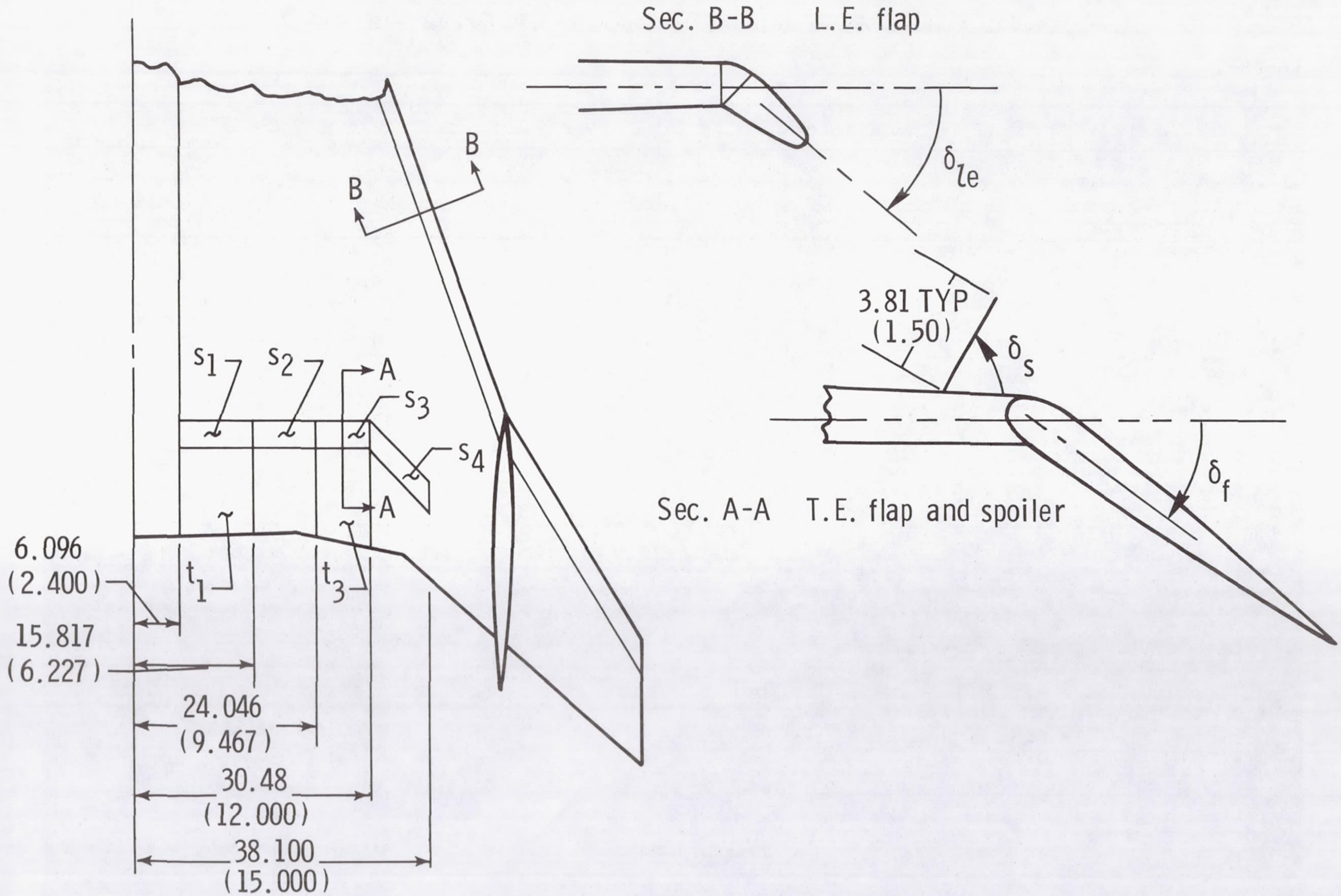

Figure 3.- Sketch of flaps and spoilers. Dimensions are given in centimeters (inches).

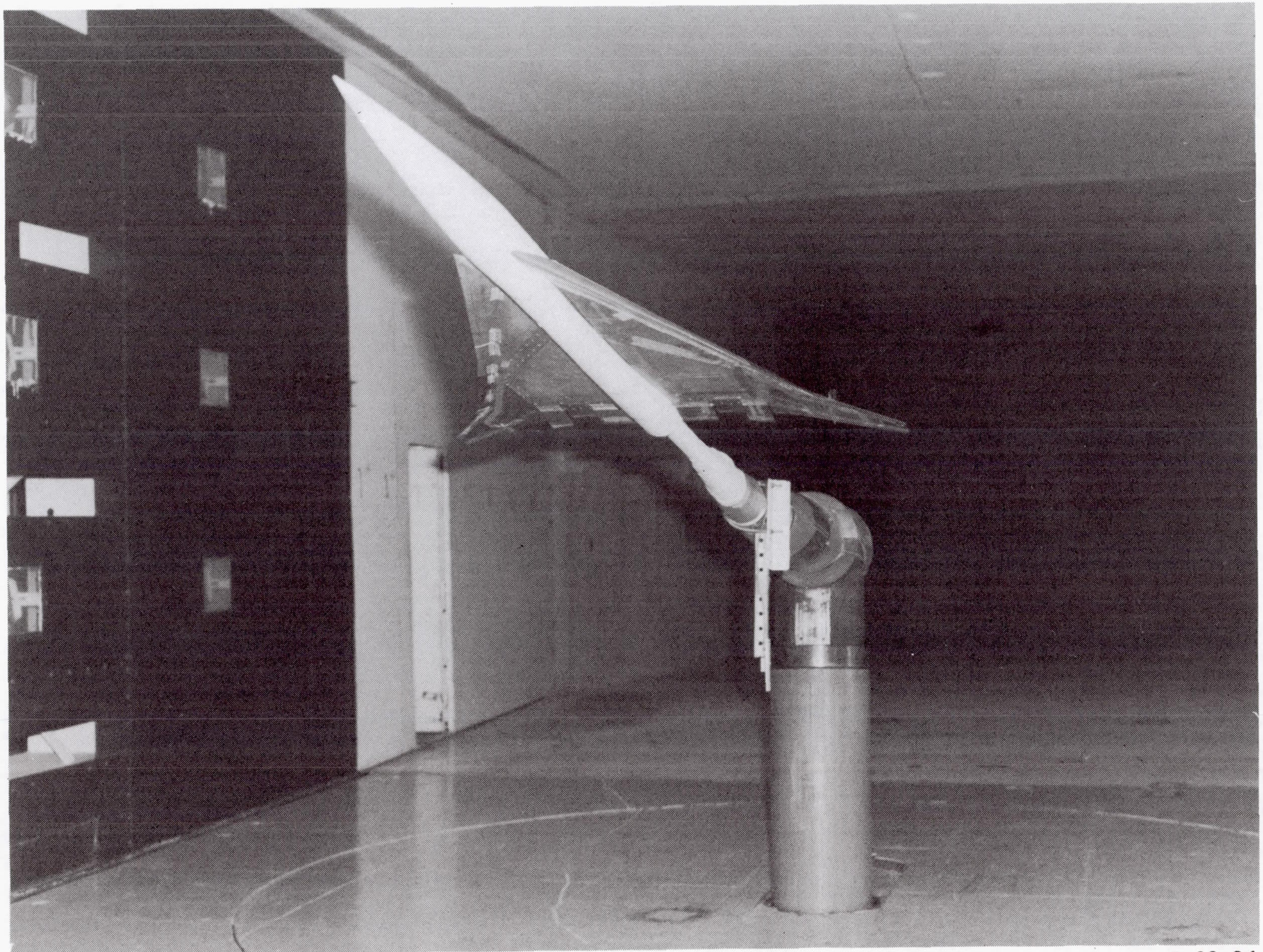

L-83-91

Figure 4.- Photograph of model in Langley 4- by 7-Meter Tunnel.

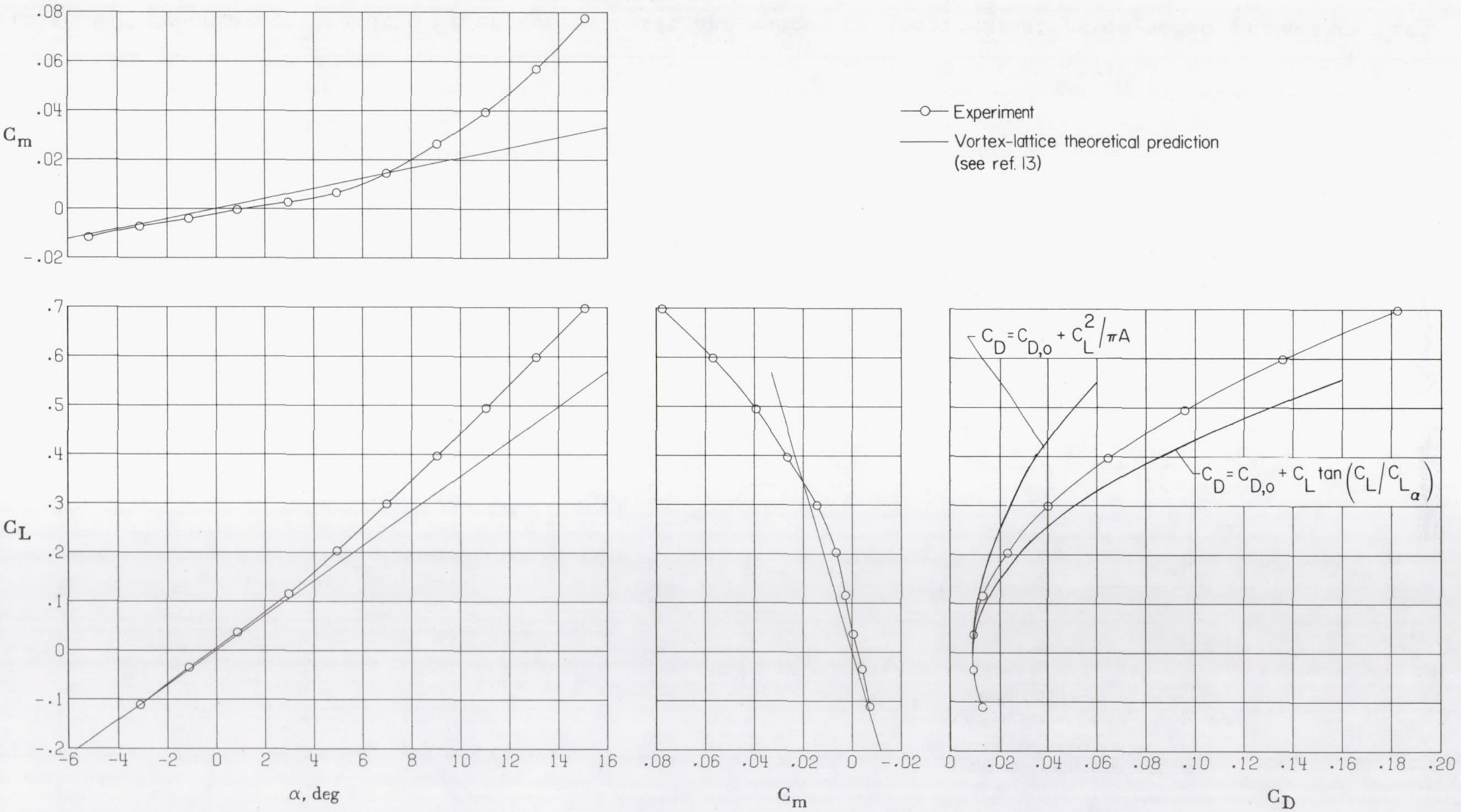

Figure 5.- Longitudinal aerodynamic characteristics of configuration. $\delta_{le} = 0°$; $\delta_f = 0°$.

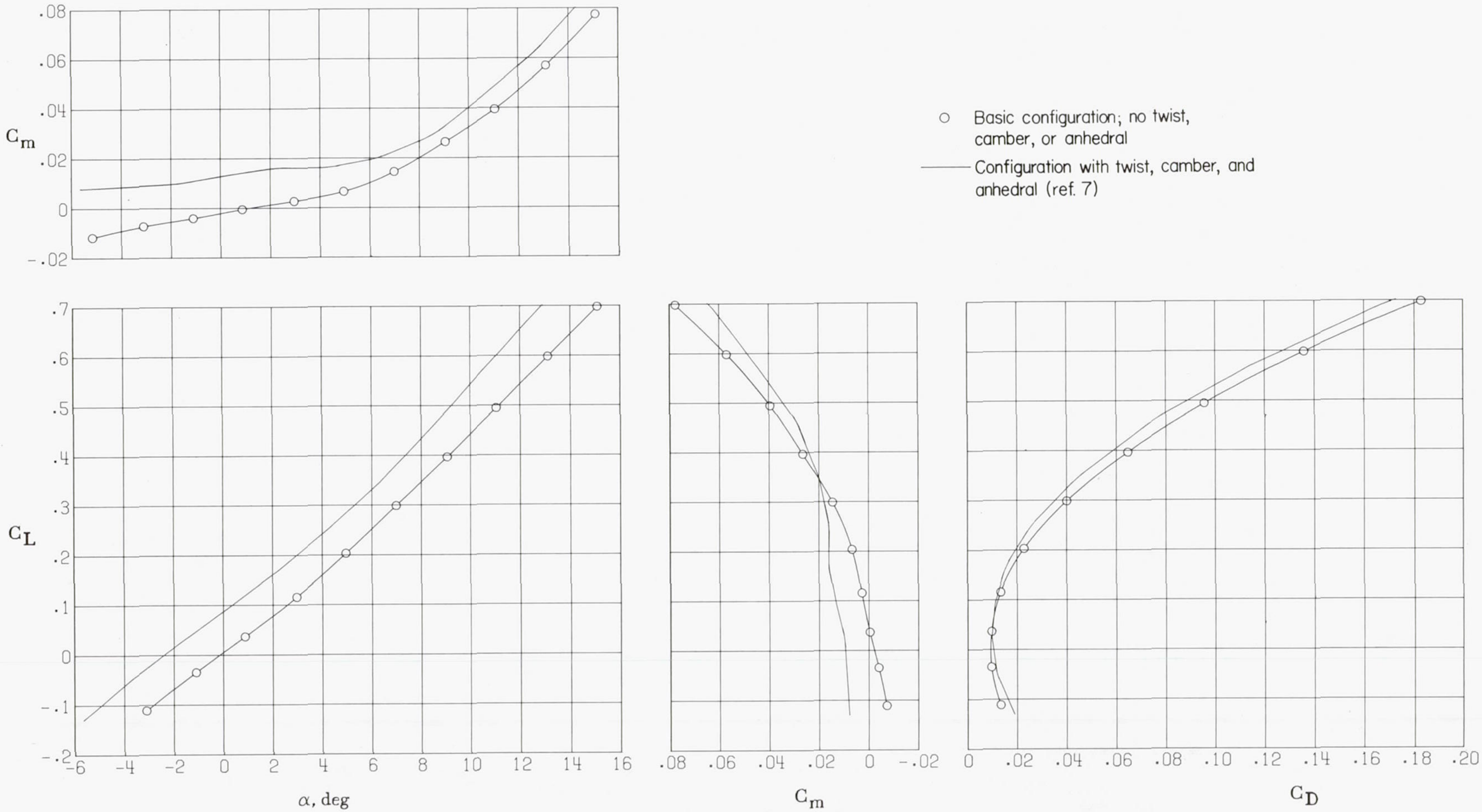

Figure 6.- Experimental results of effect of twist and camber on longitudinal aerodynamic characteristics of basic configuration. $\delta_{le} = 0°$; $\delta_f = 0°$.

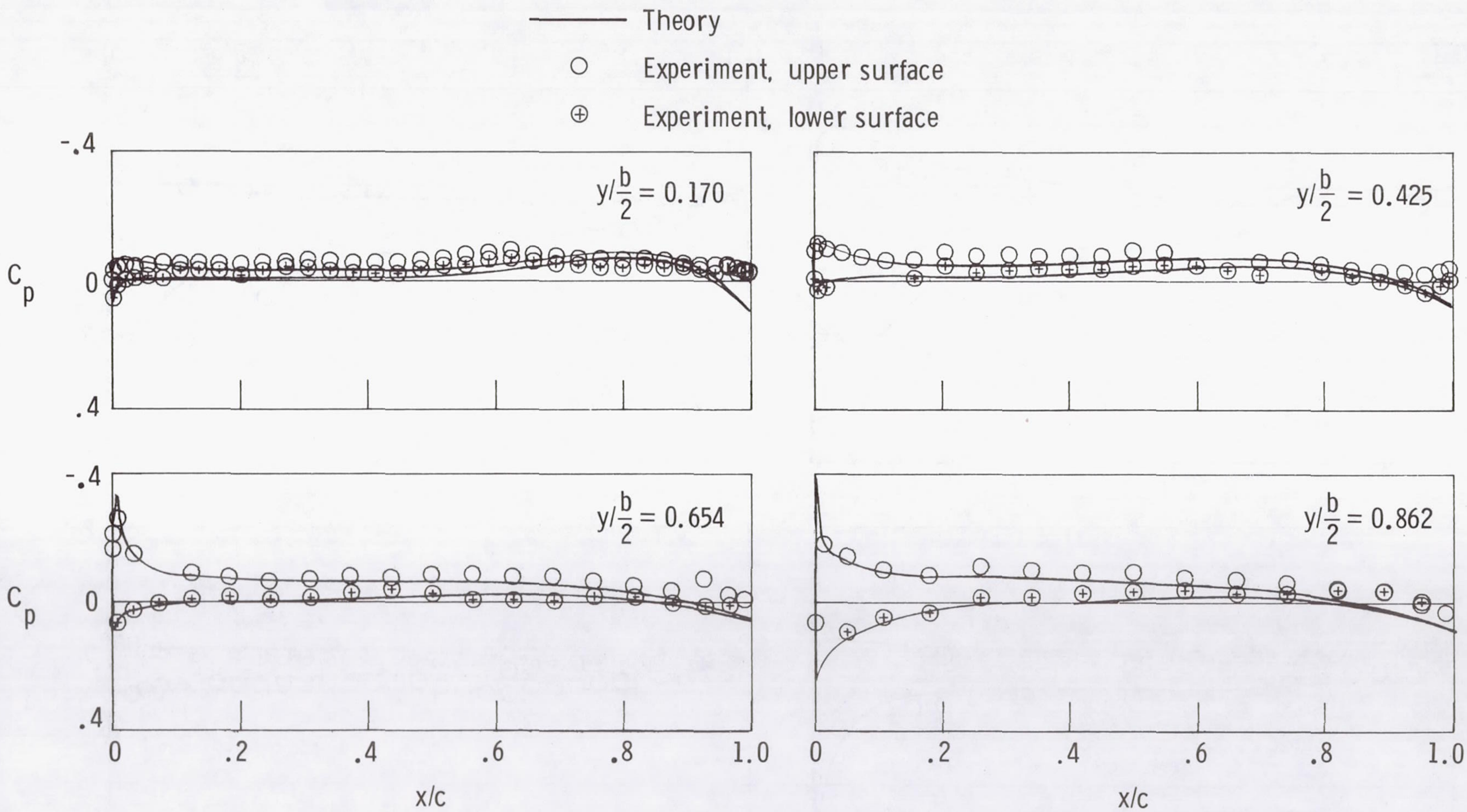

(a) $\alpha = 0.87°$.

Figure 7.- Comparison of theoretical and experimental chordwise wing pressure distributions. $\delta_{le} = 0°$; $\delta_f = 0°$.

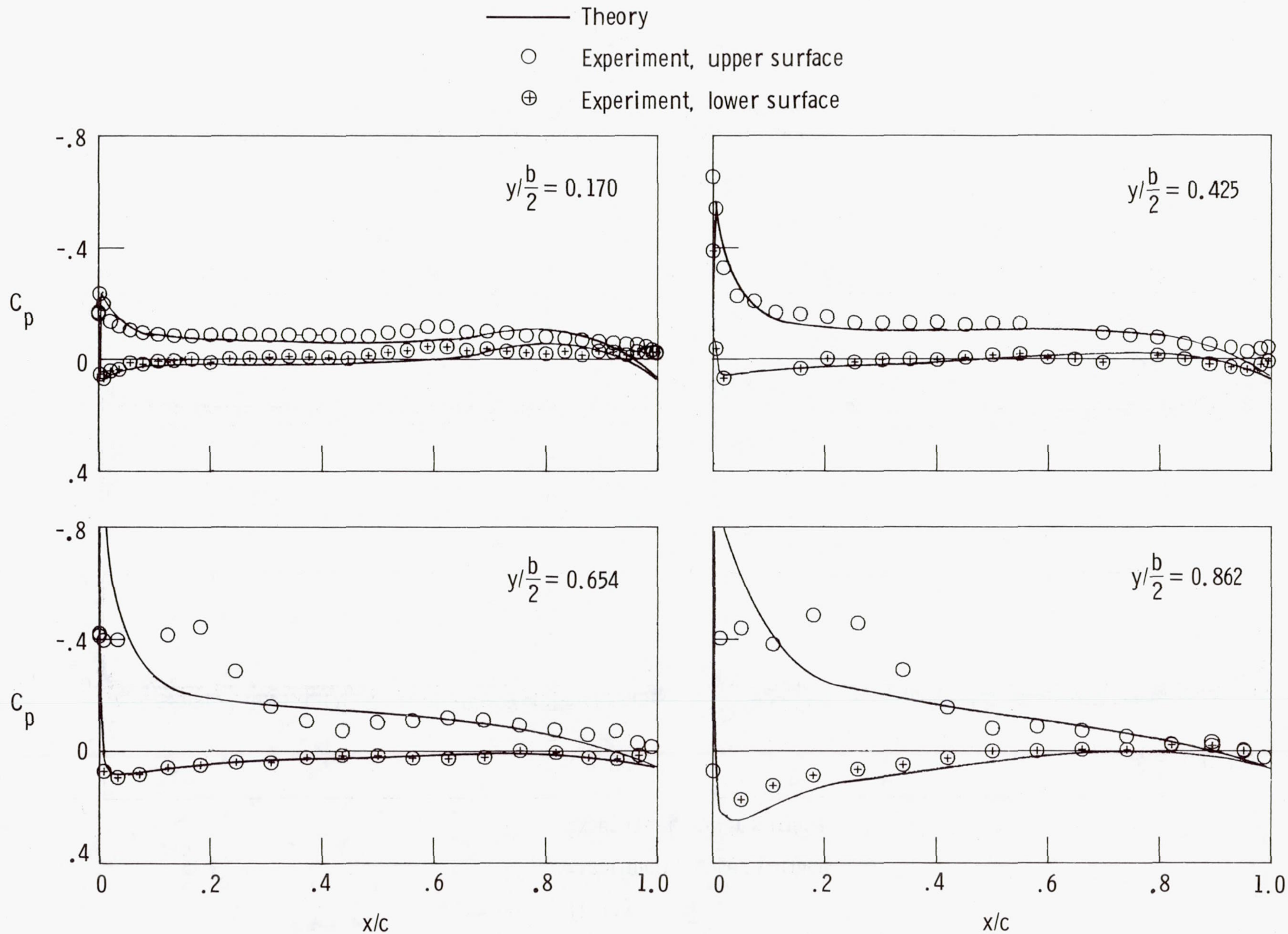

(b) $\alpha = 2.96°$.

Figure 7.- Continued.

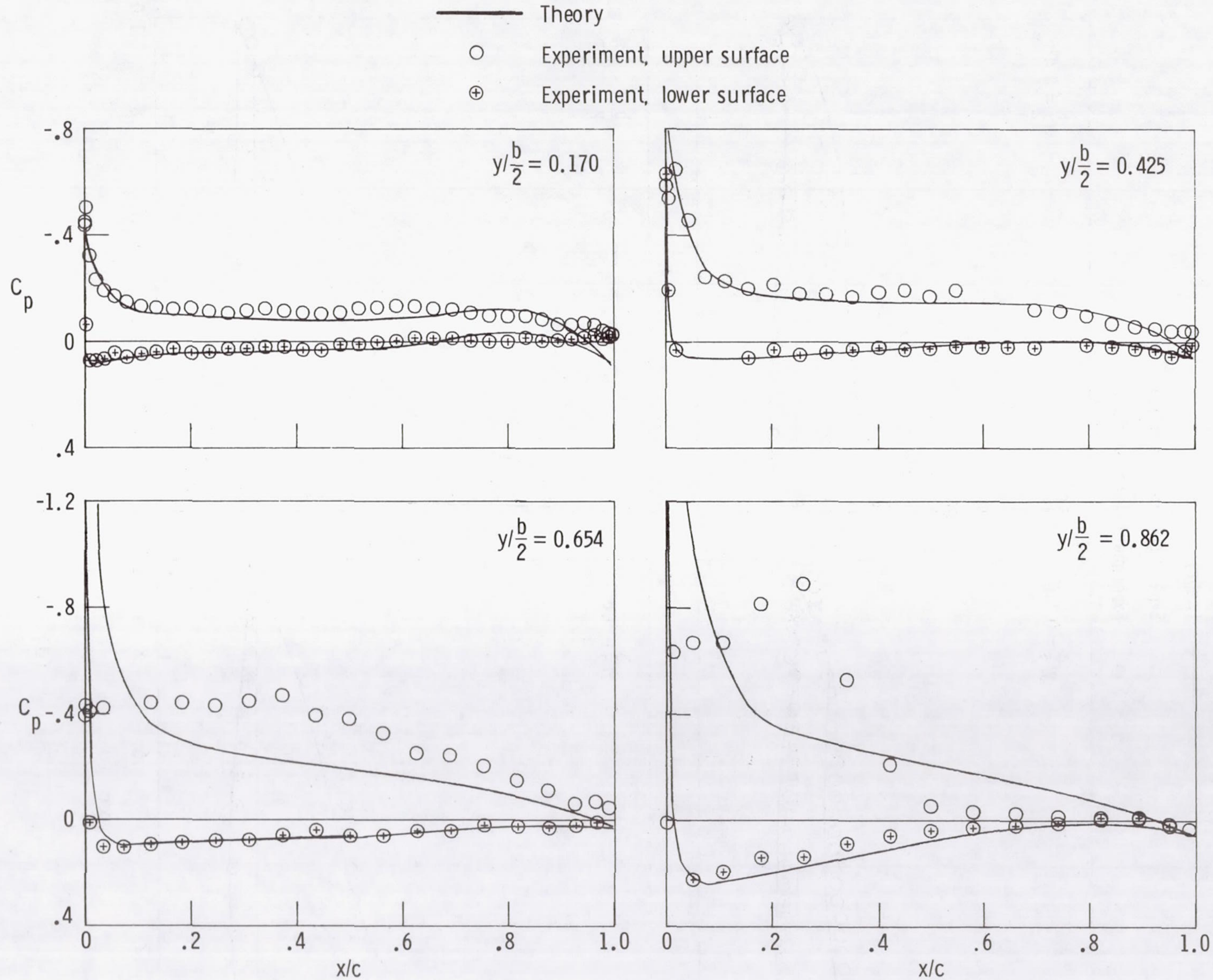

(c) α = 4.95°.

Figure 7.- Continued.

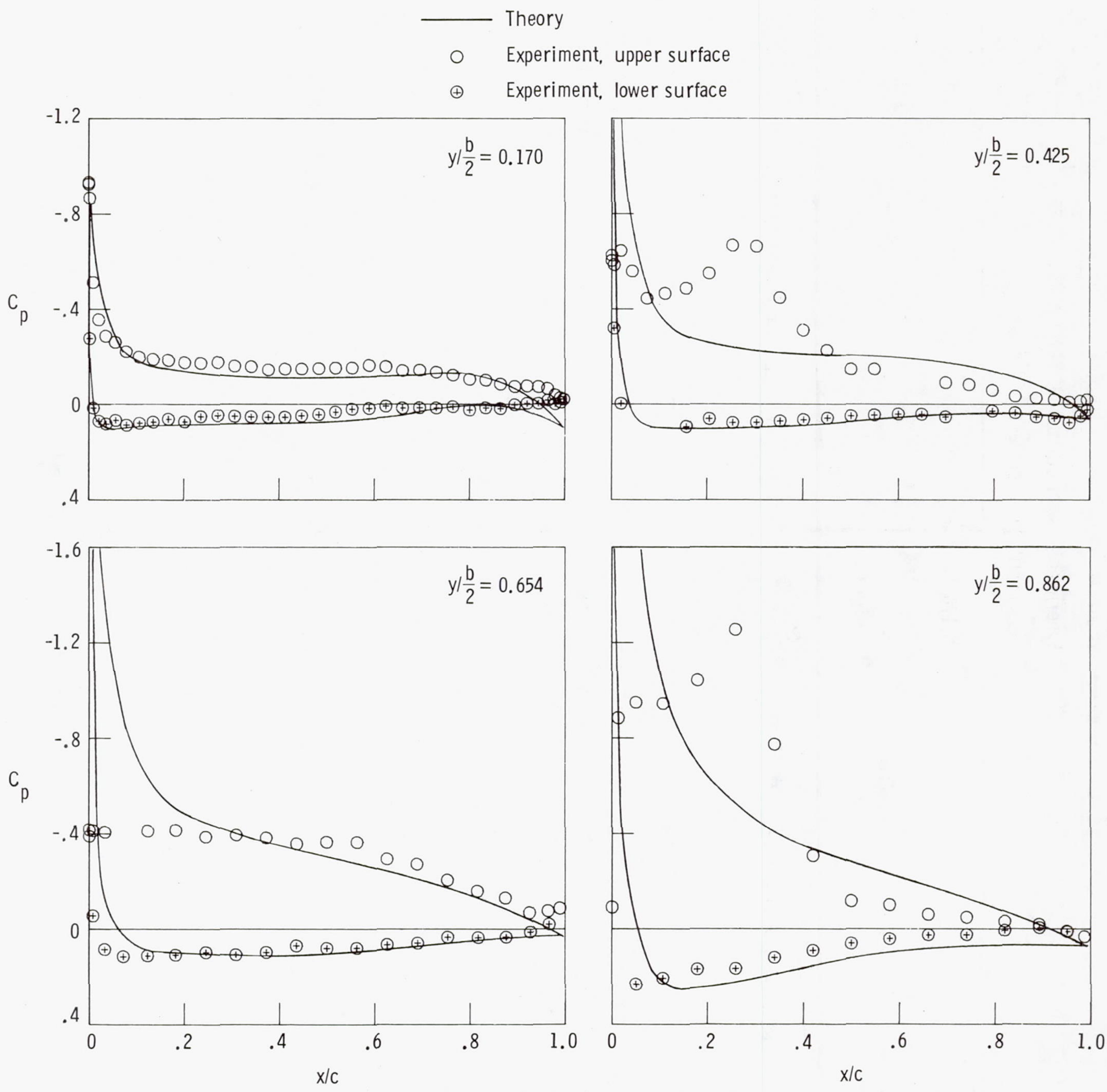

(d) α = 6.99°.

Figure 7.- Continued.

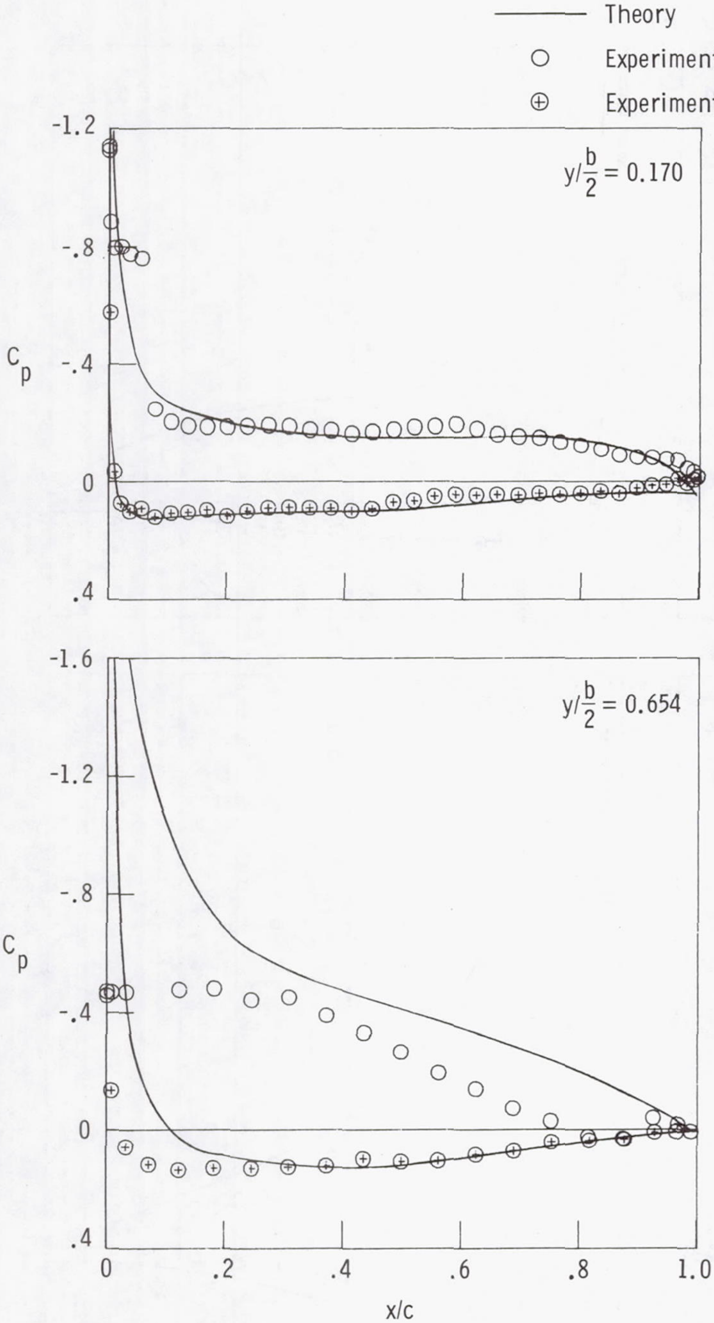

(e) α = 9.05°.

Figure 7.- Continued.

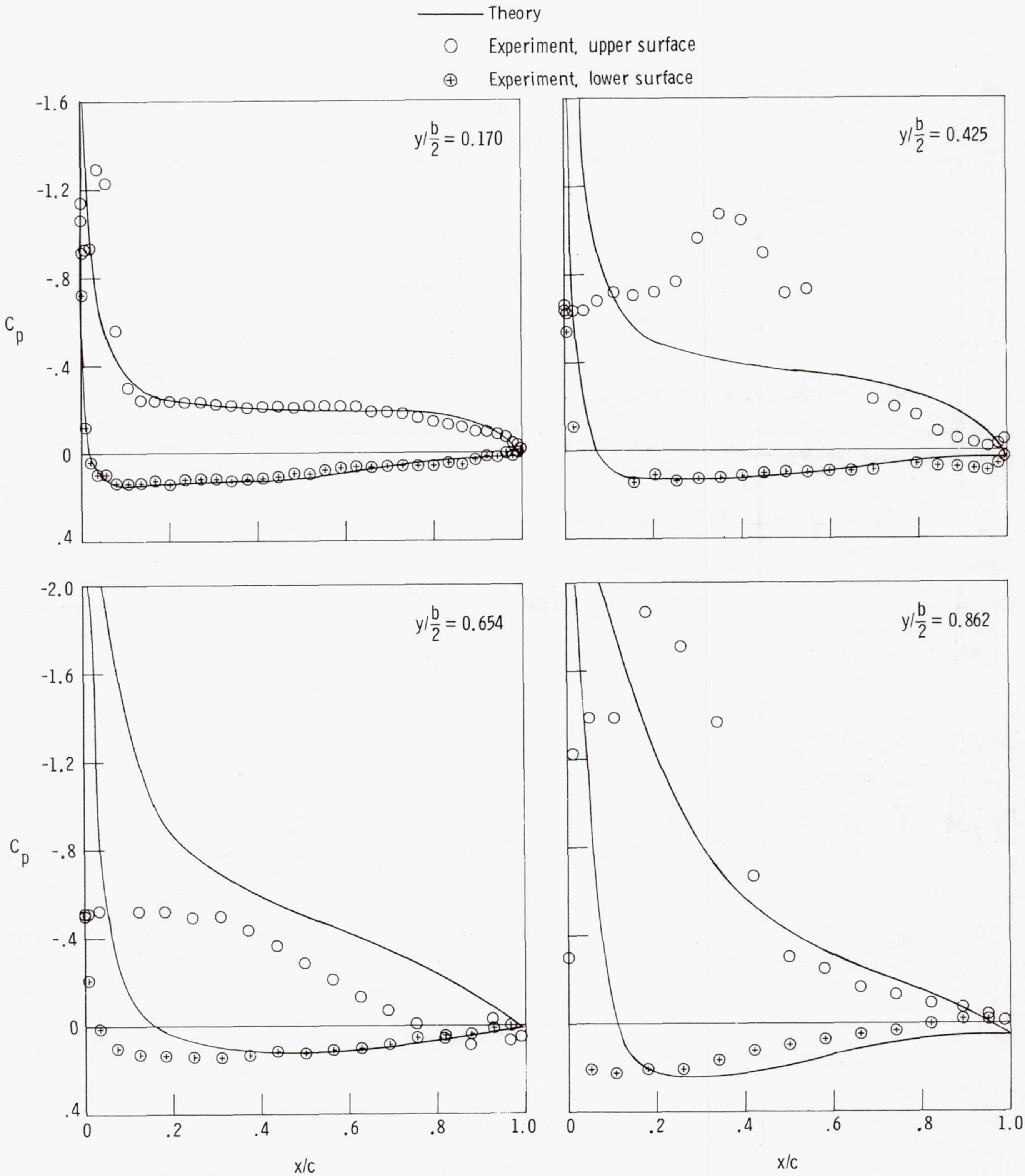

(f) $\alpha = 11.04°$.

Figure 7.- Continued.

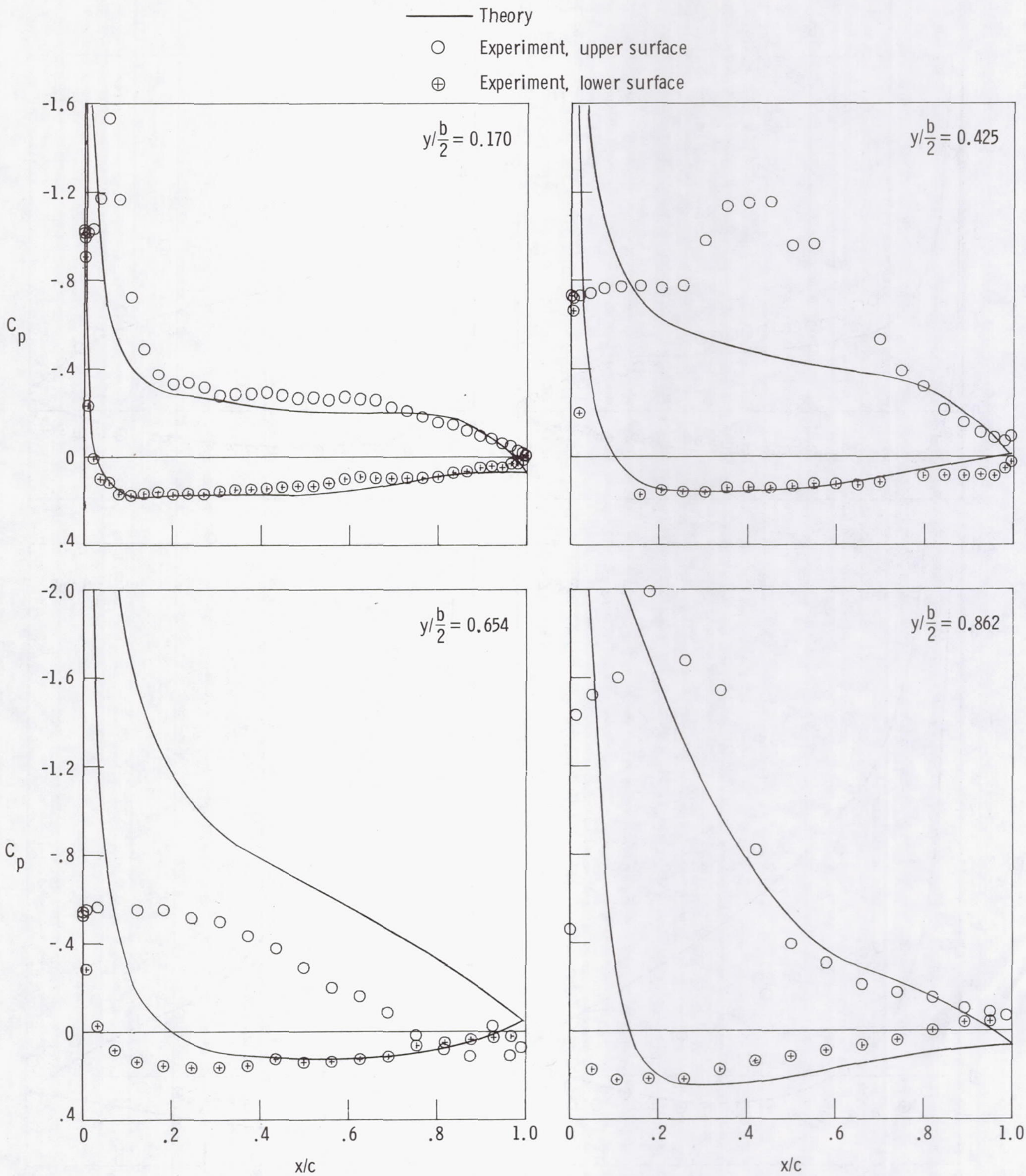

(g) $\alpha = 13.10°$.

Figure 7.- Continued.

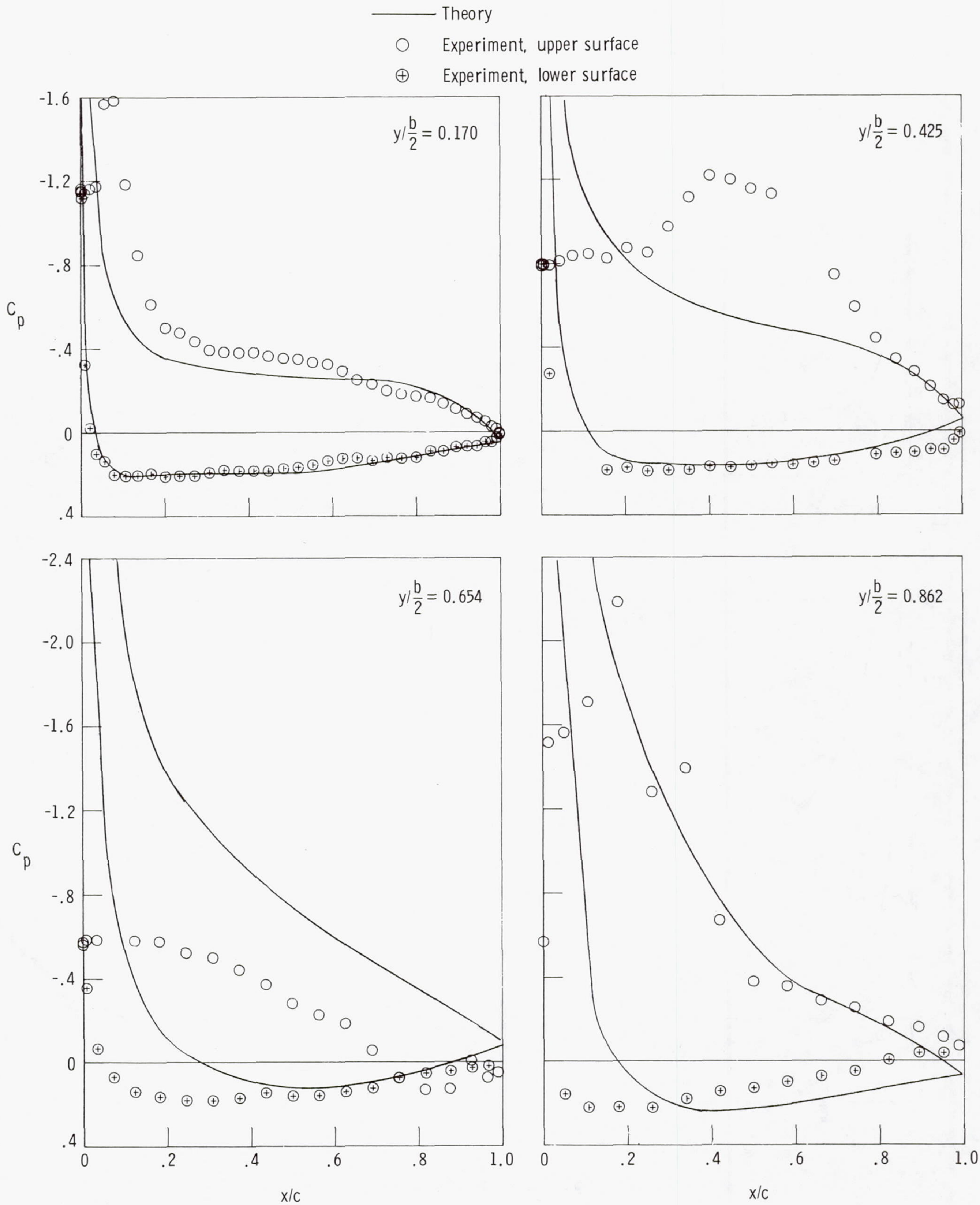

(h) α = 15.09°.

Figure 7.- Concluded.

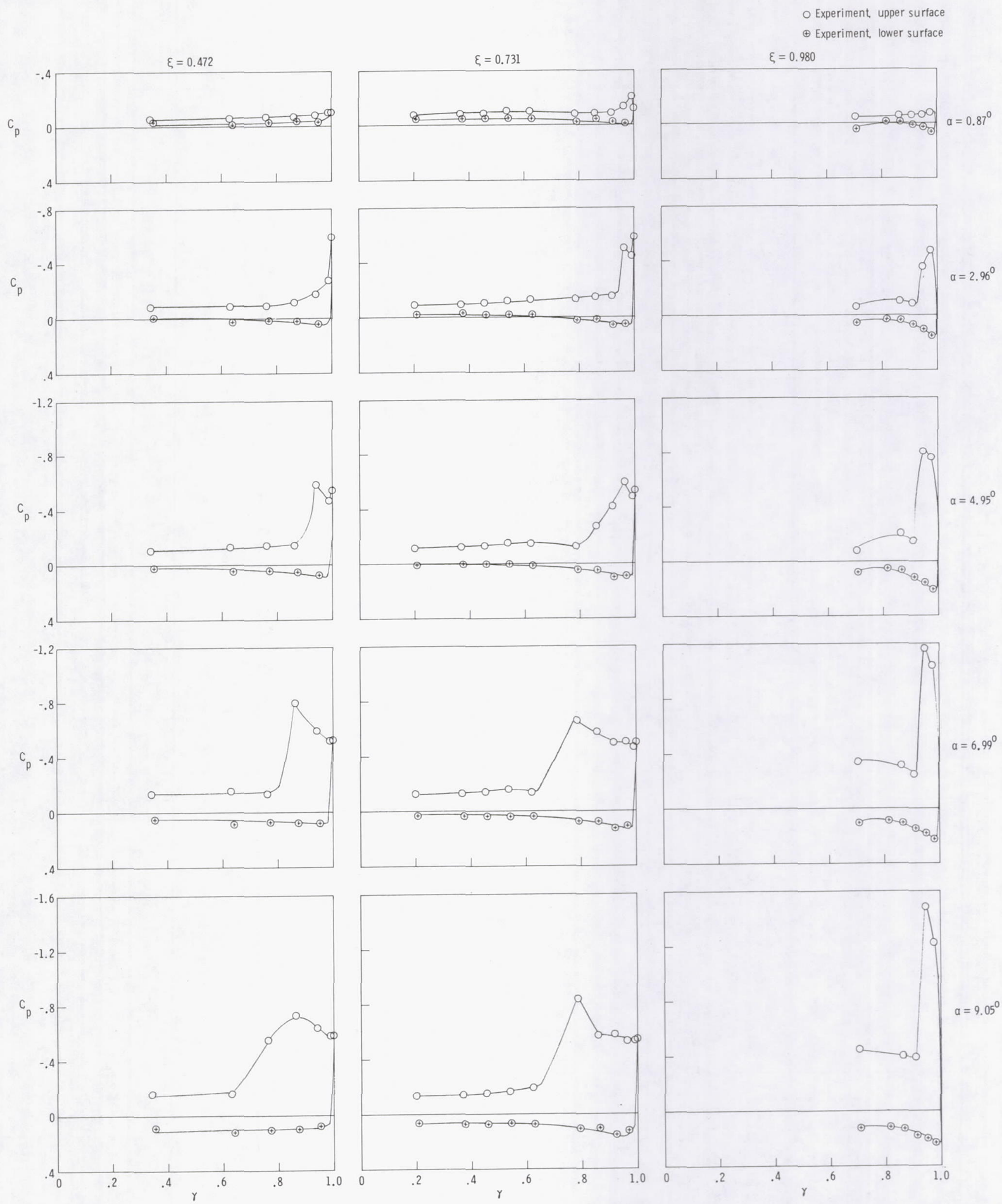

(a) α = 0.87°, 2.96°, 4.95°, 6.99°, and 9.05°.

Figure 8.- Spanwise wing pressure distributions. δ_{le} = 0°; δ_f = 0°.

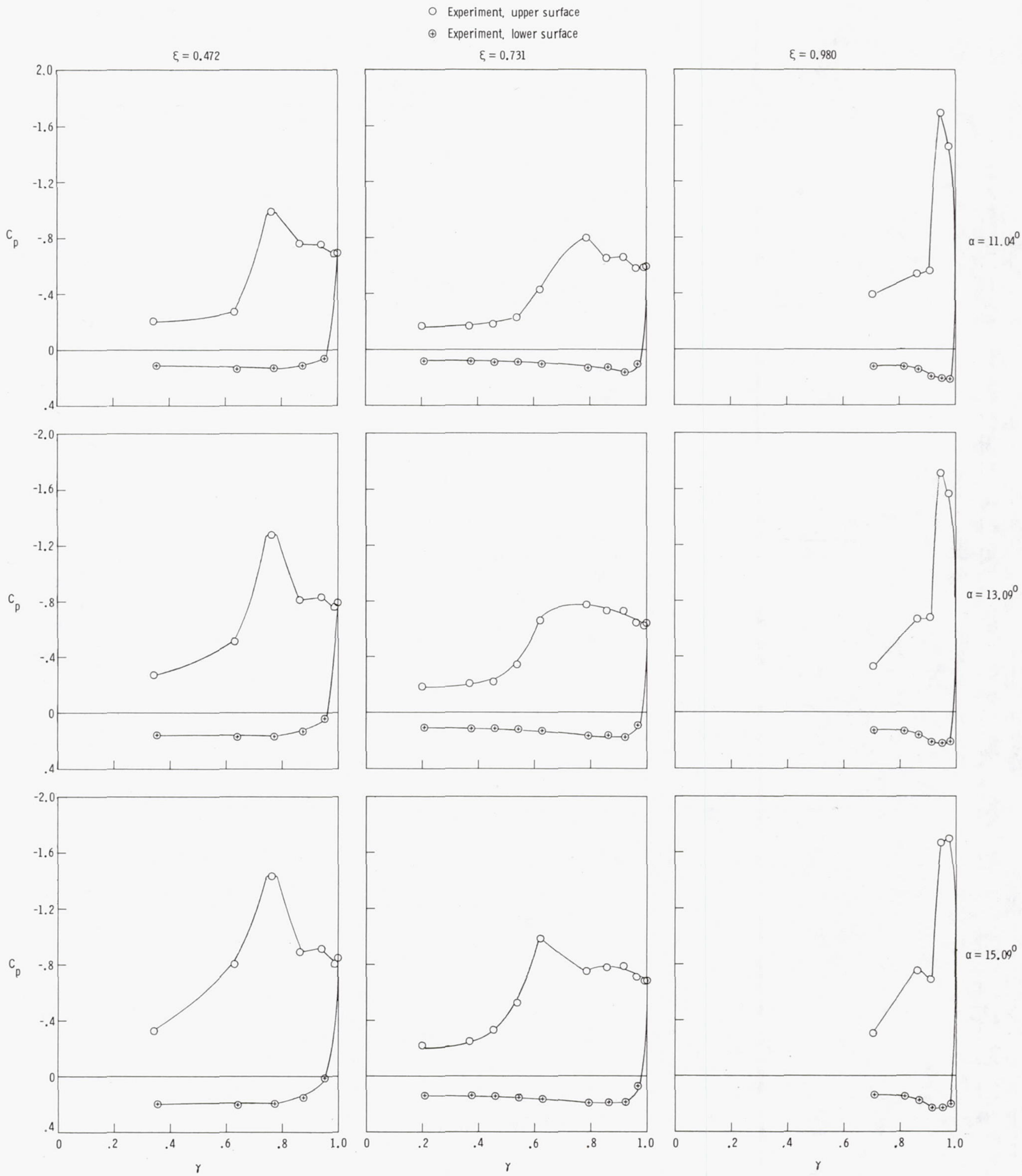

(b) α = 11.04°, 13.09°, and 15.09°.

Figure 8.- Concluded.

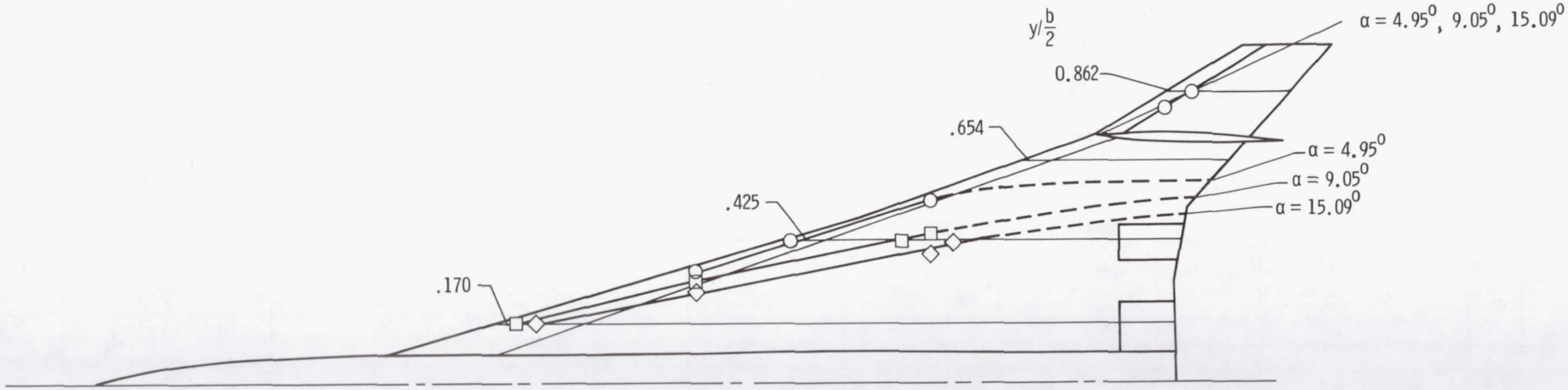

Figure 9.- Sketch of experimentally determined vortex locations. Dashed portion of curve indicates extrapolated result. $\delta_{le} = 0°$; $\delta_f = 0°$.

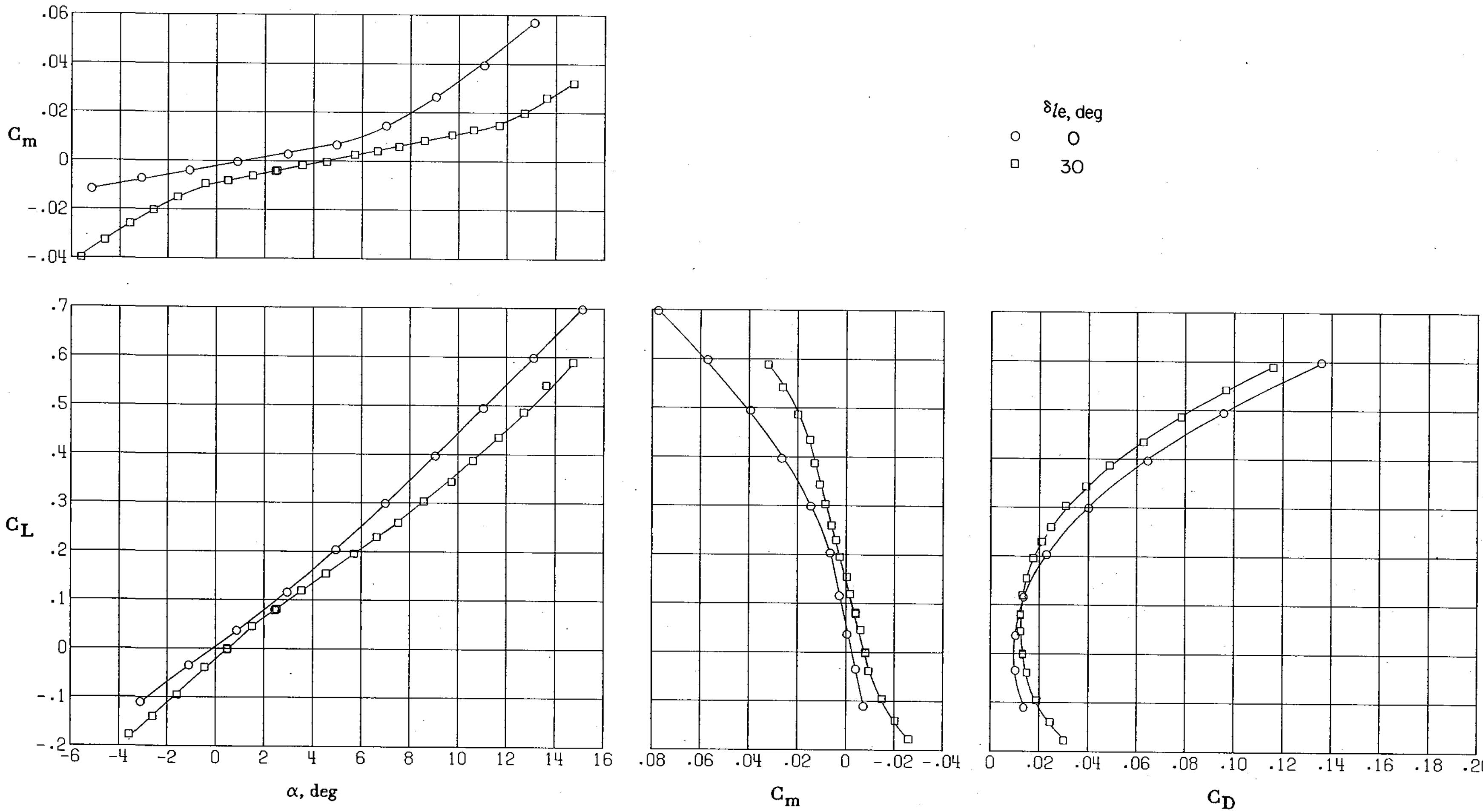

Figure 10.- Effect of leading-edge deflection on longitudinal aerodynamic characteristics of configuration. $\delta_f = 0°$.

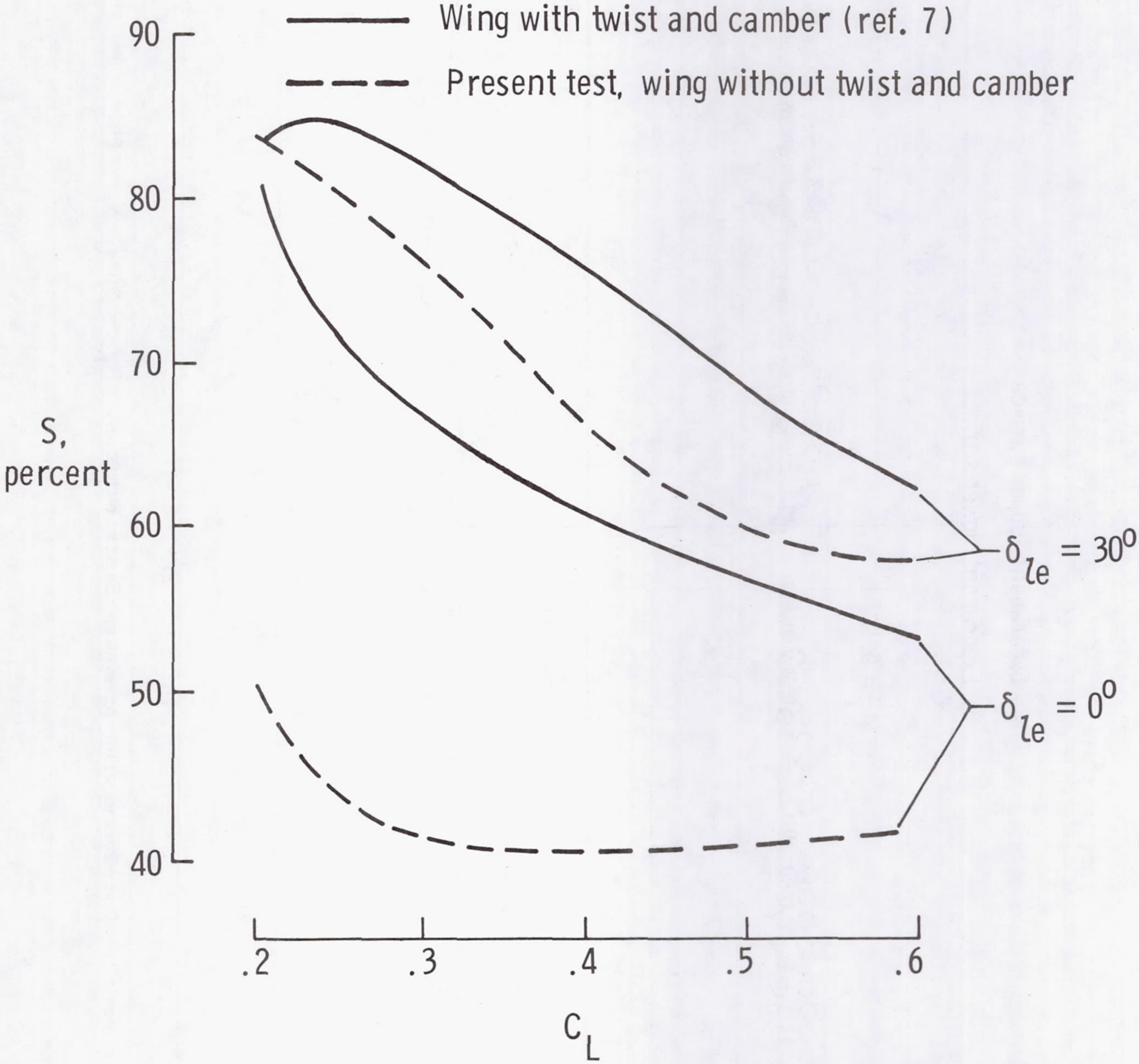

Figure 11.- Effect of twist and camber with leading-edge deflection on leading-edge suction parameter.

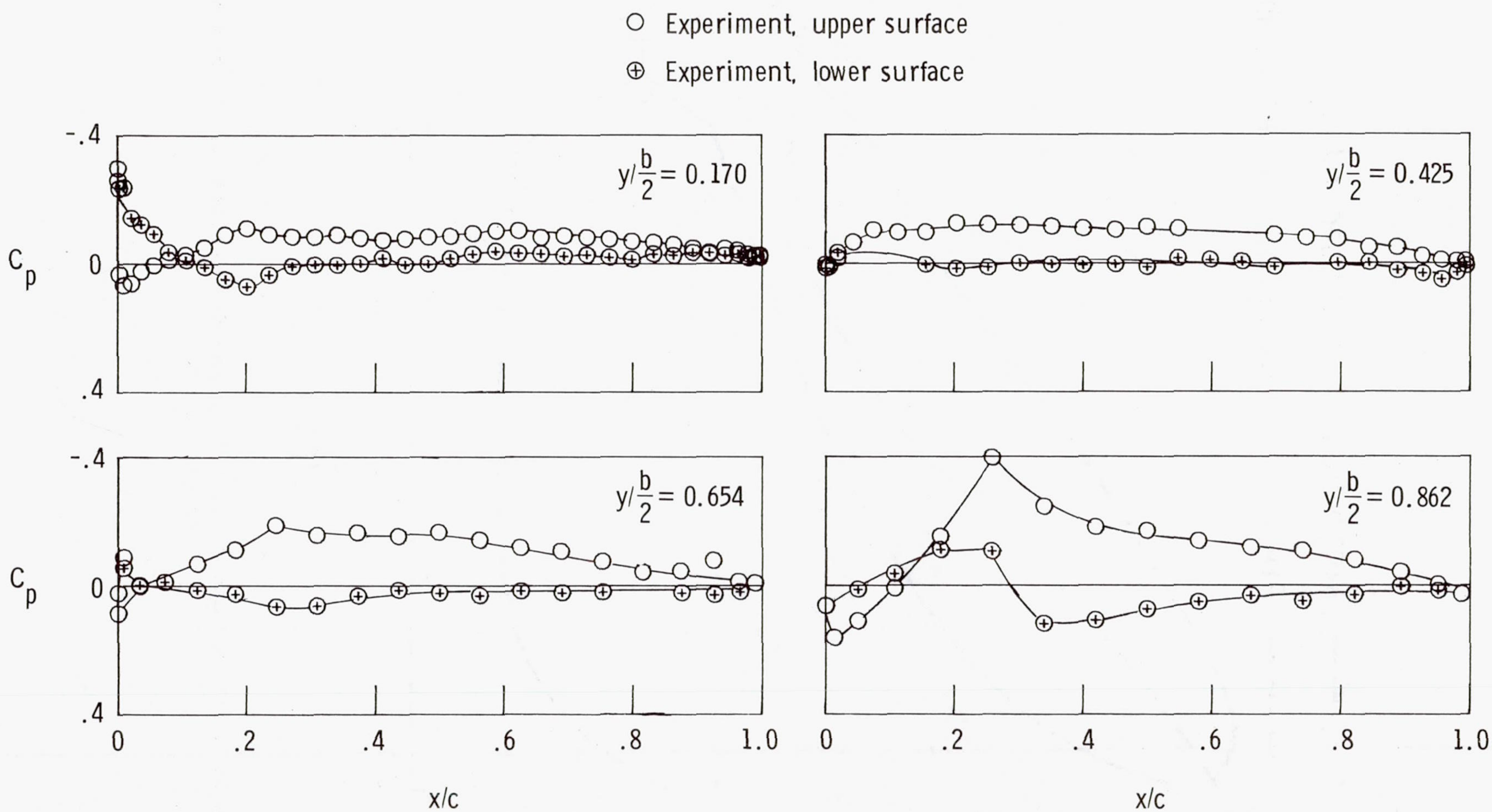

(a) $\alpha = 2.51°$.

Figure 12.- Chordwise wing pressure distributions. $\delta_{le} = 30°$; $\delta_f = 0°$.

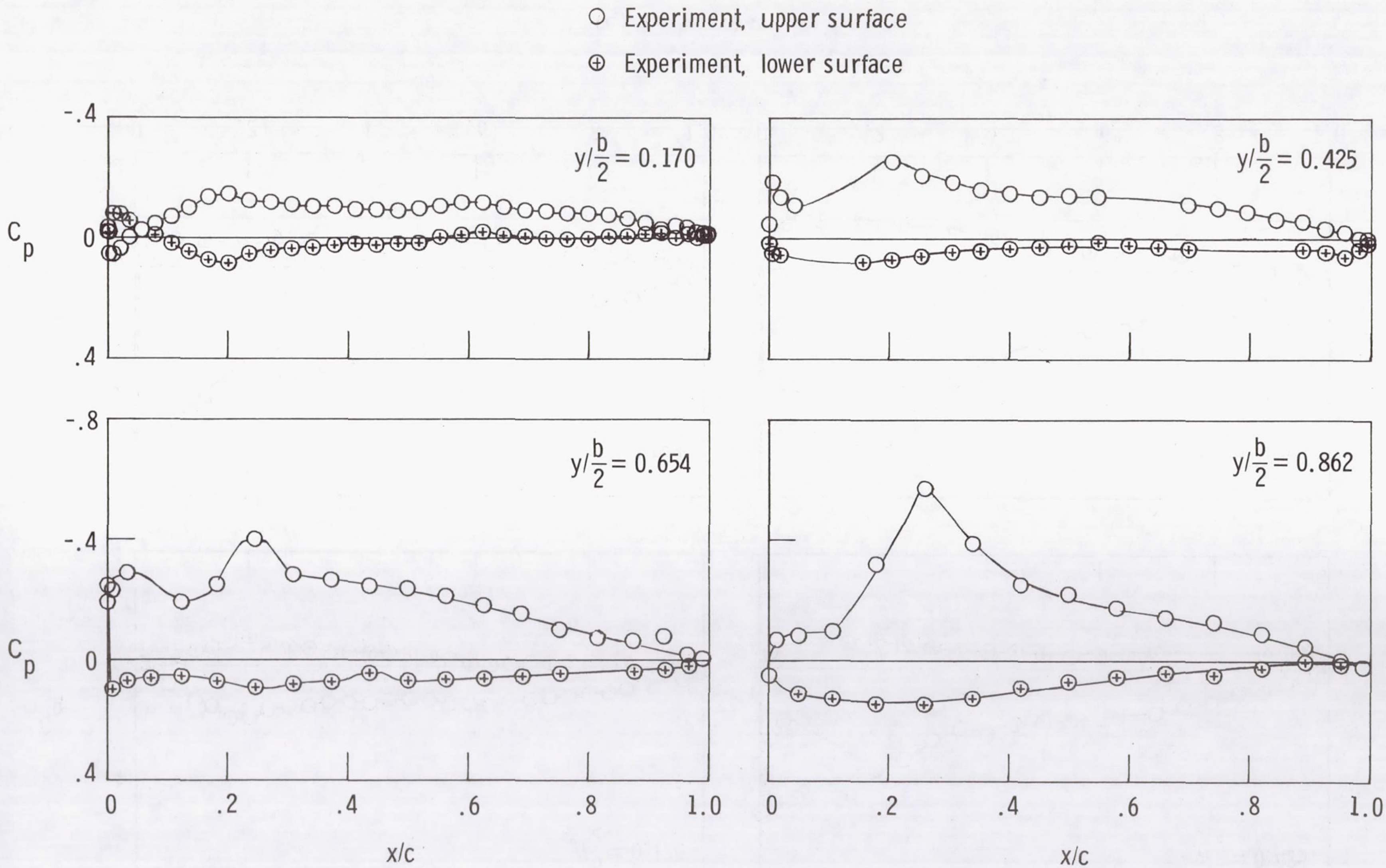

(b) α = 4.55°.

Figure 12.- Continued.

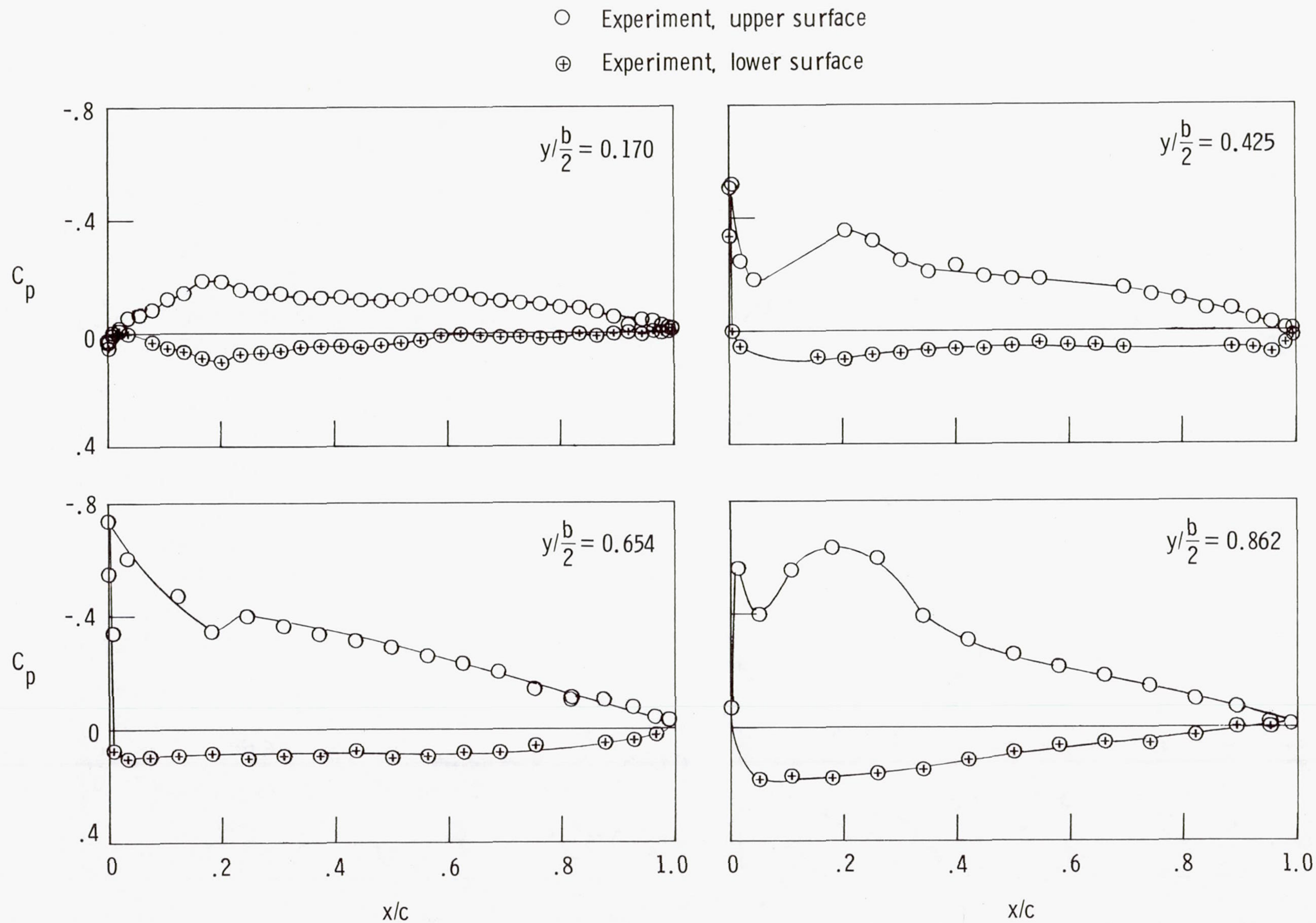

(c) $\alpha = 6.64°$.

Figure 12.- Continued.

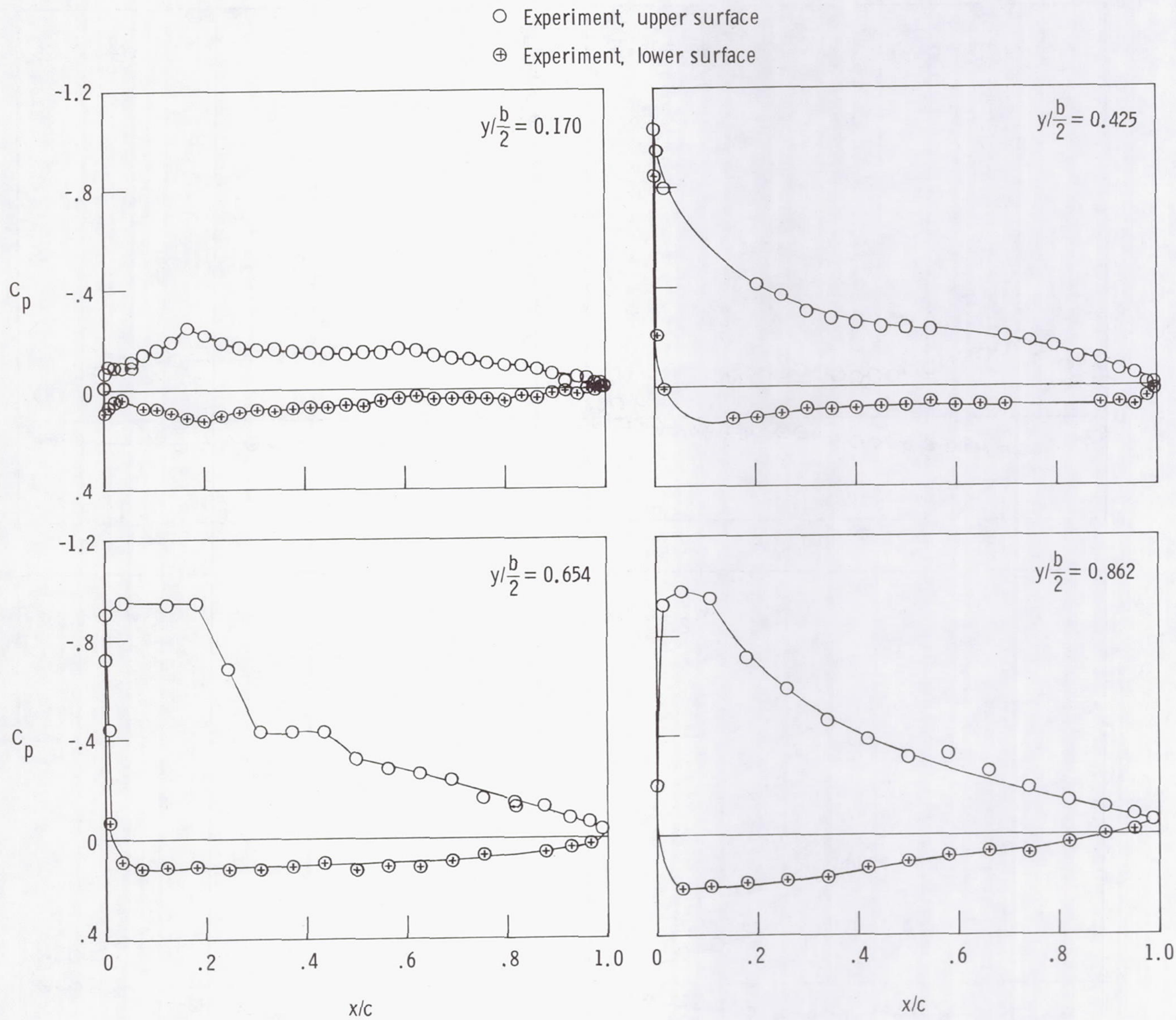

(d) $\alpha = 8.59°$.

Figure 12.- Continued.

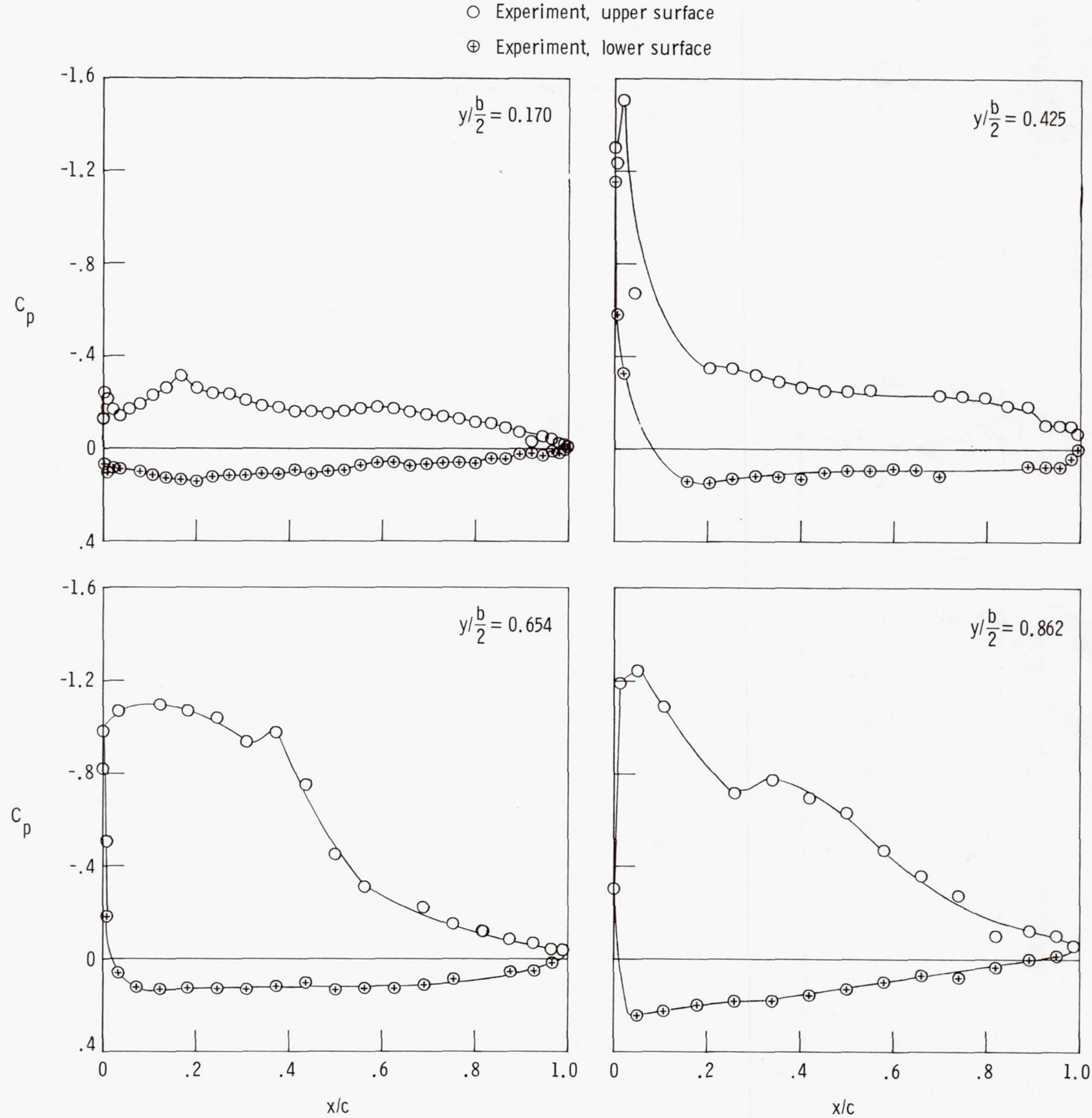

(e) $\alpha = 10.63°$.

Figure 12.- Continued.

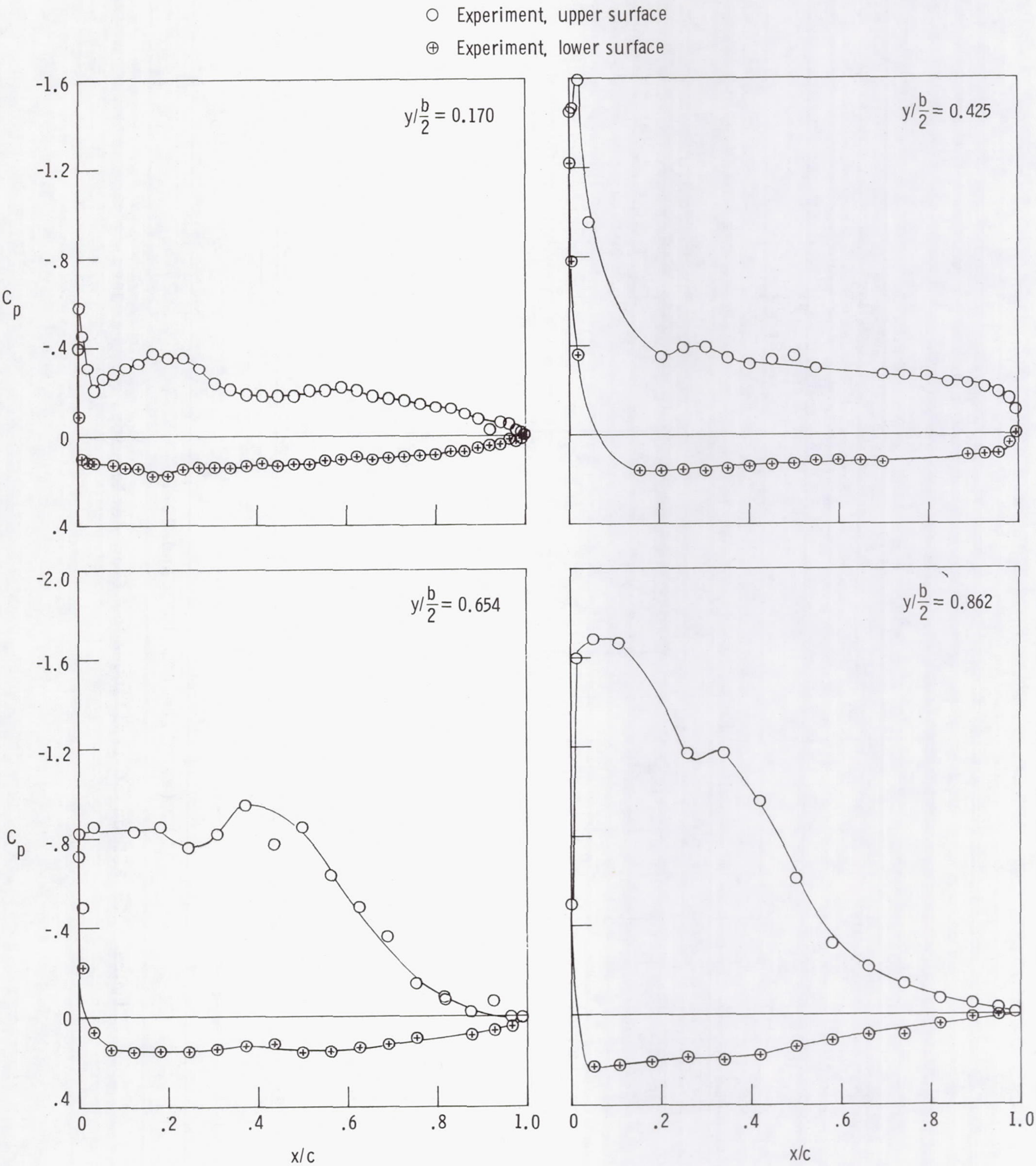

(f) $\alpha = 12.71°$.

Figure 12.- Concluded.

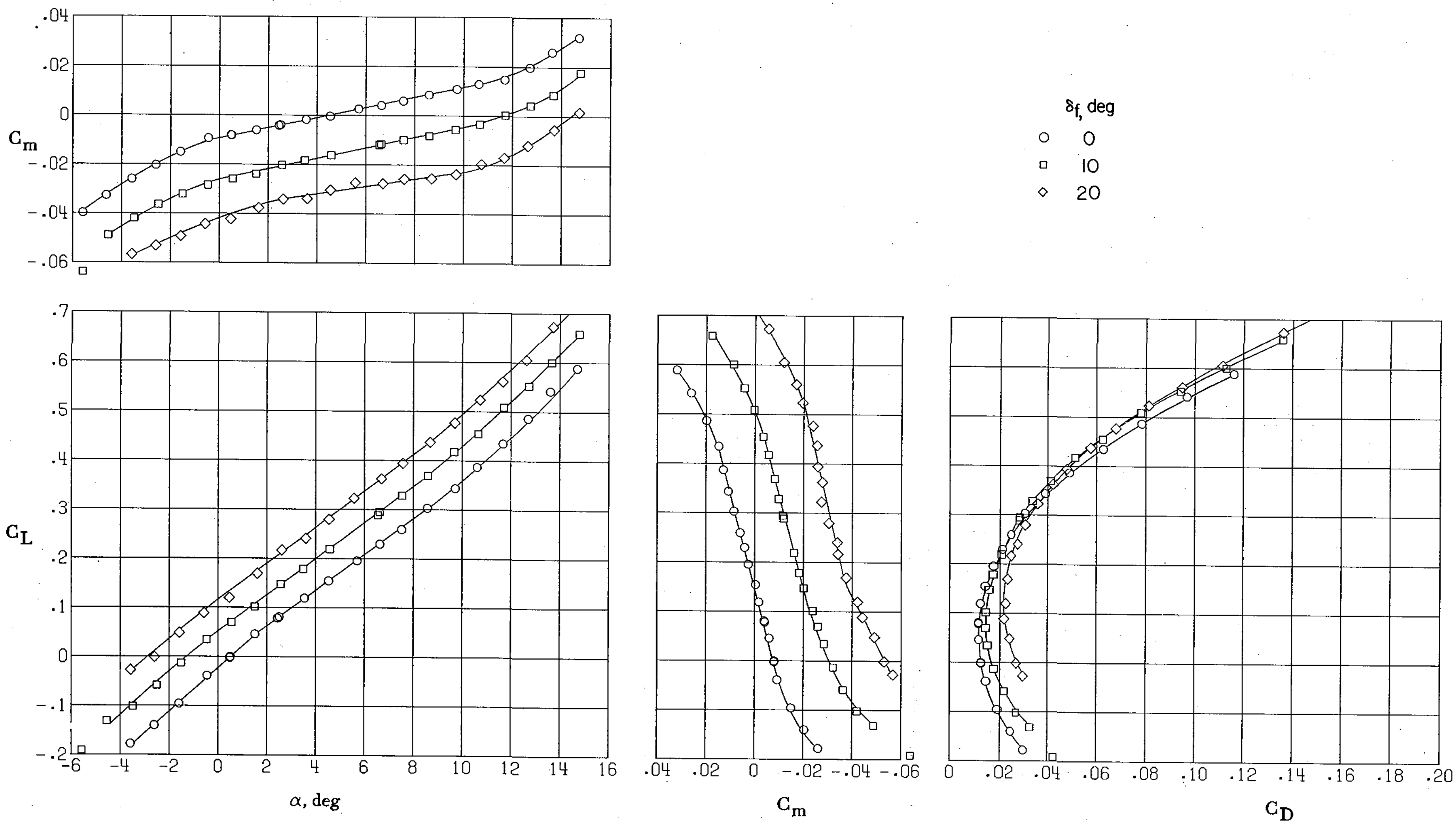

(a) δ_f = 0°, 10°, and 20°.

Figure 13.- Effect of trailing-edge flap deflection. δ_{le} = 30°.

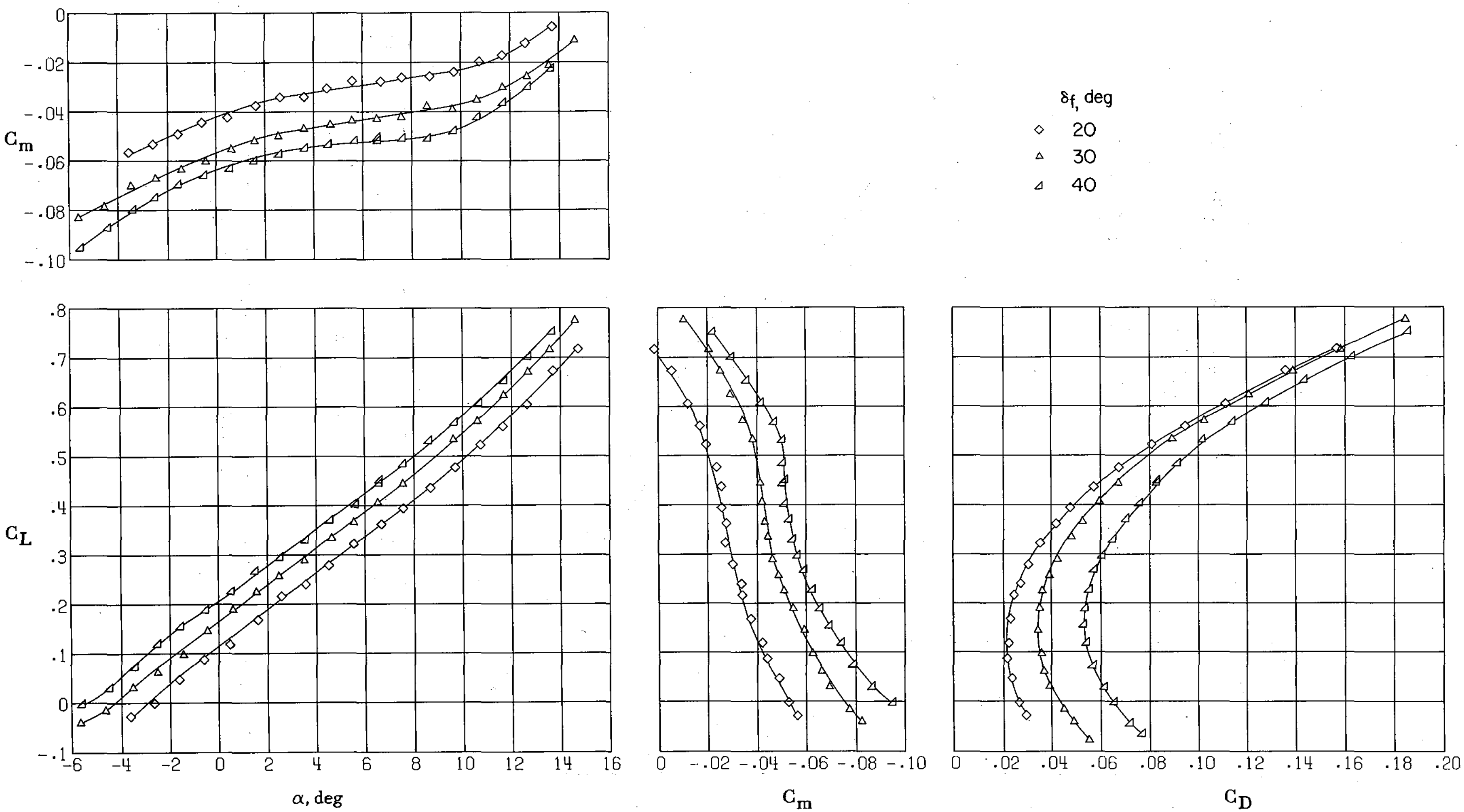

(b) $\delta_f = 20°, 30°, \text{and } 40°$.

Figure 13.- Concluded.

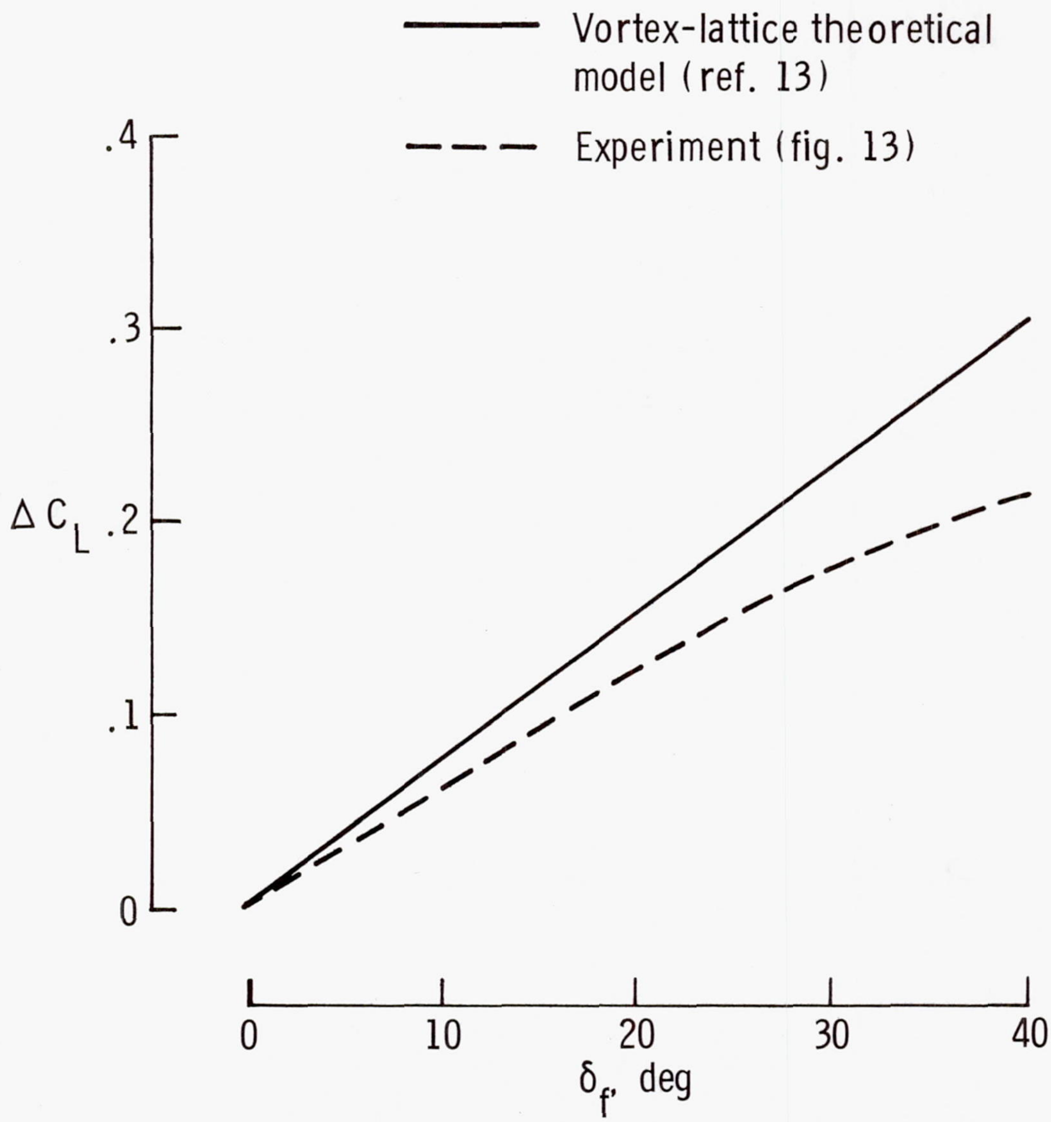

Figure 14.- Comparison of theoretical and experimental trailing-edge flap effectiveness. Segments t_1 and t_3.

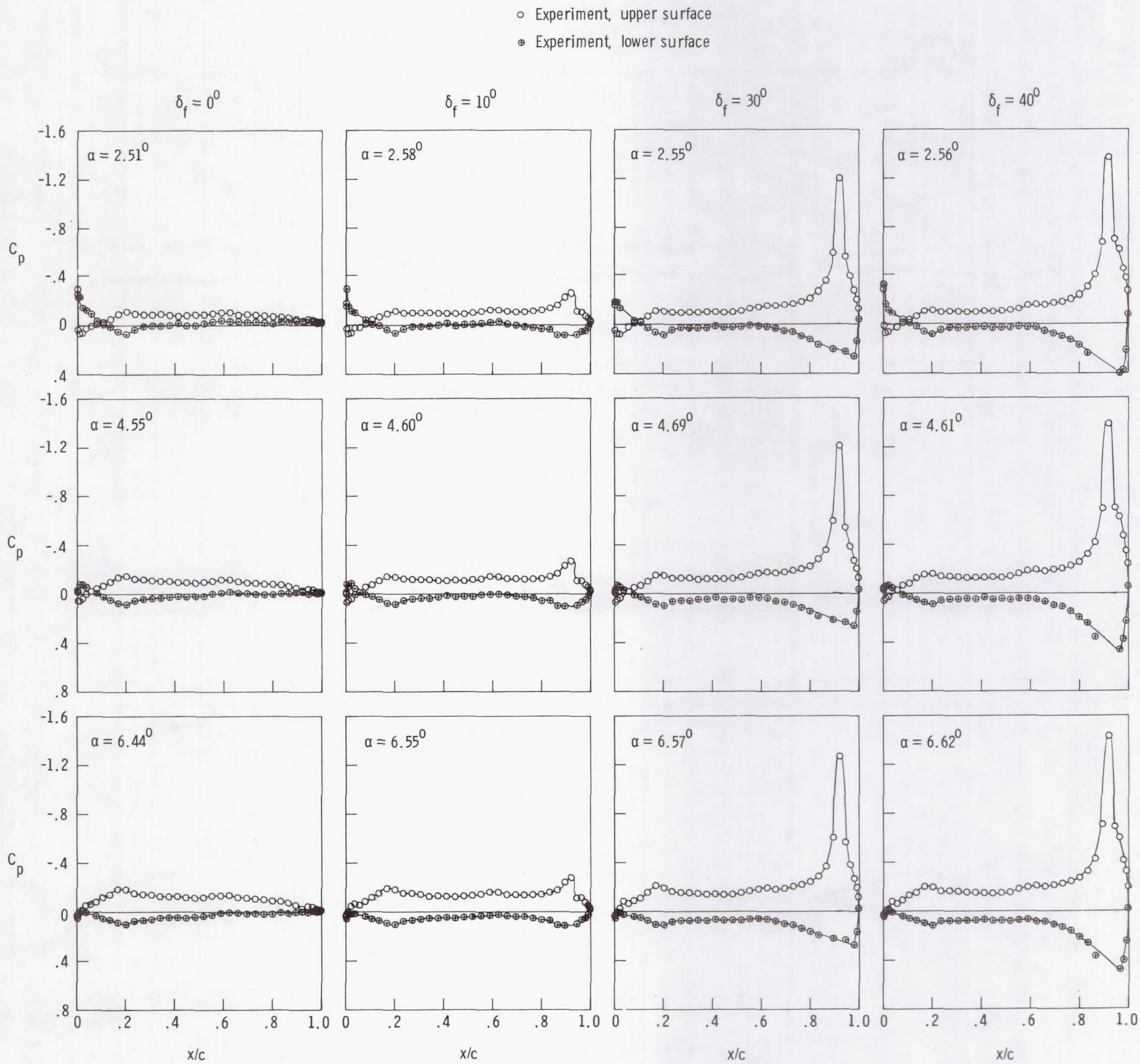

(a) $y/\frac{b}{2} = 0.170.$

Figure 15.- Effect of trailing-edge flap deflection on wing chordwise pressure distributions. $\delta_{le} = 30°$.

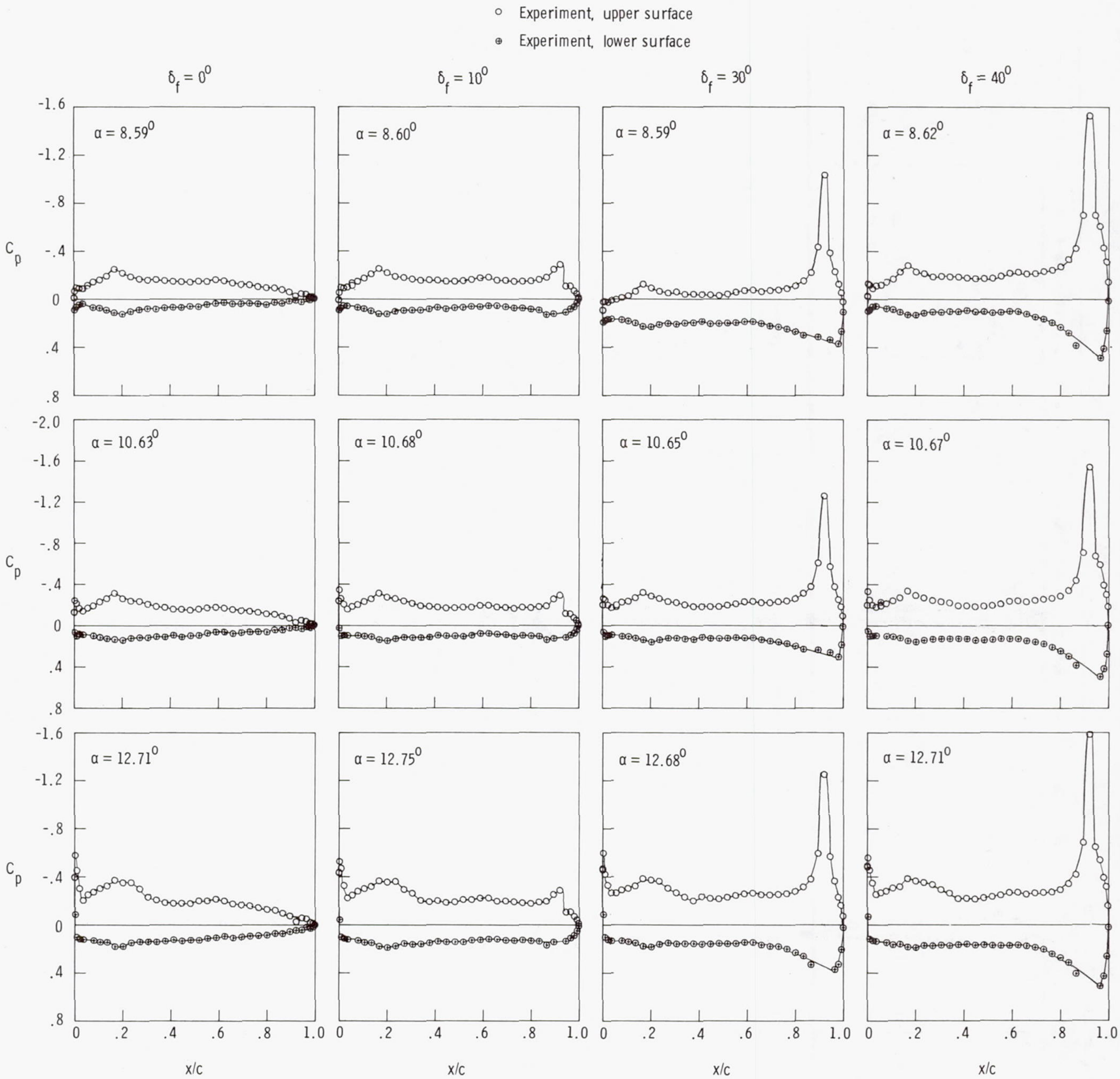

(a) Concluded.

Figure 15.- Continued.

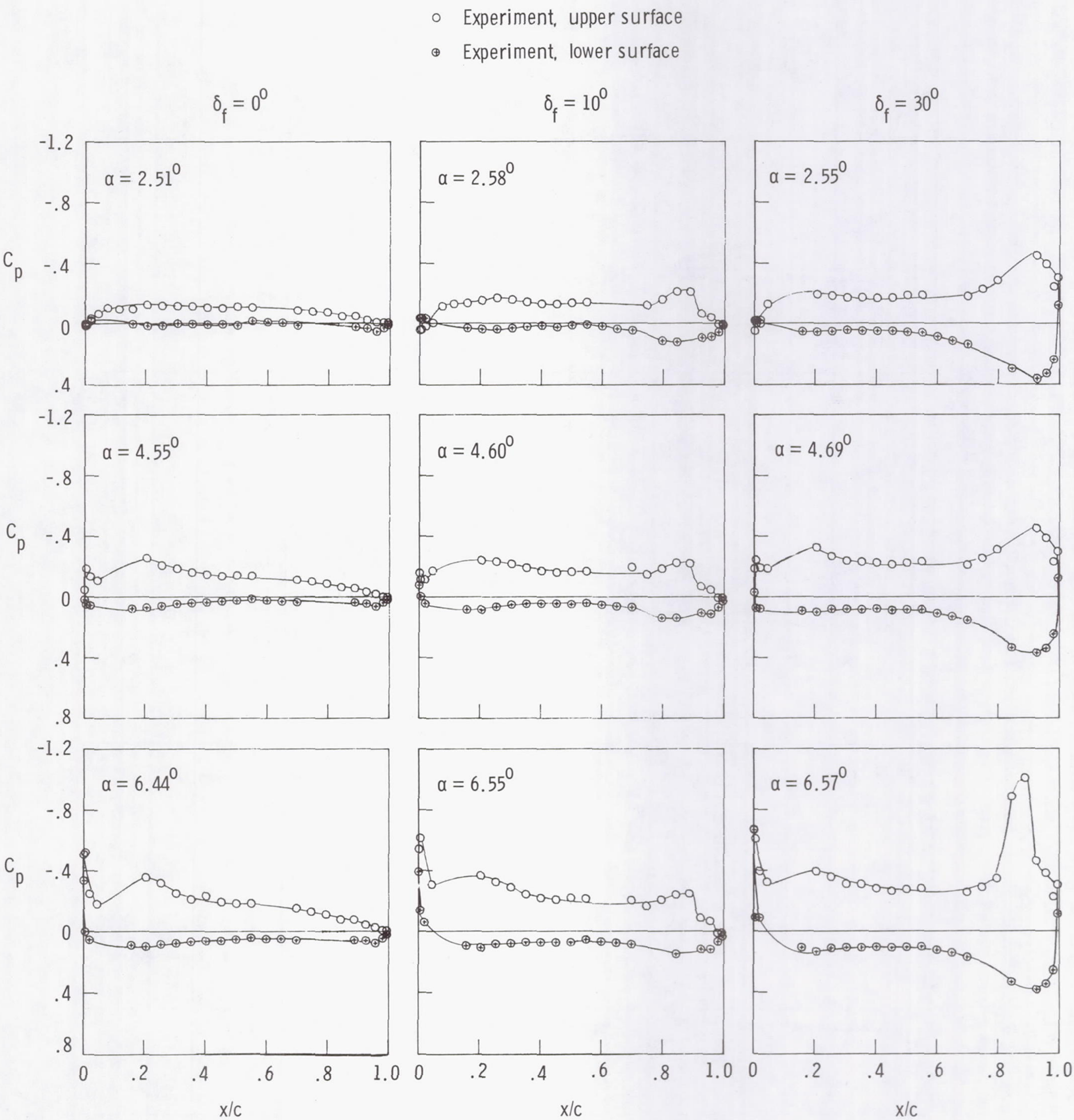

(b) $y/\frac{b}{2} = 0.425.$

Figure 15.- Continued.

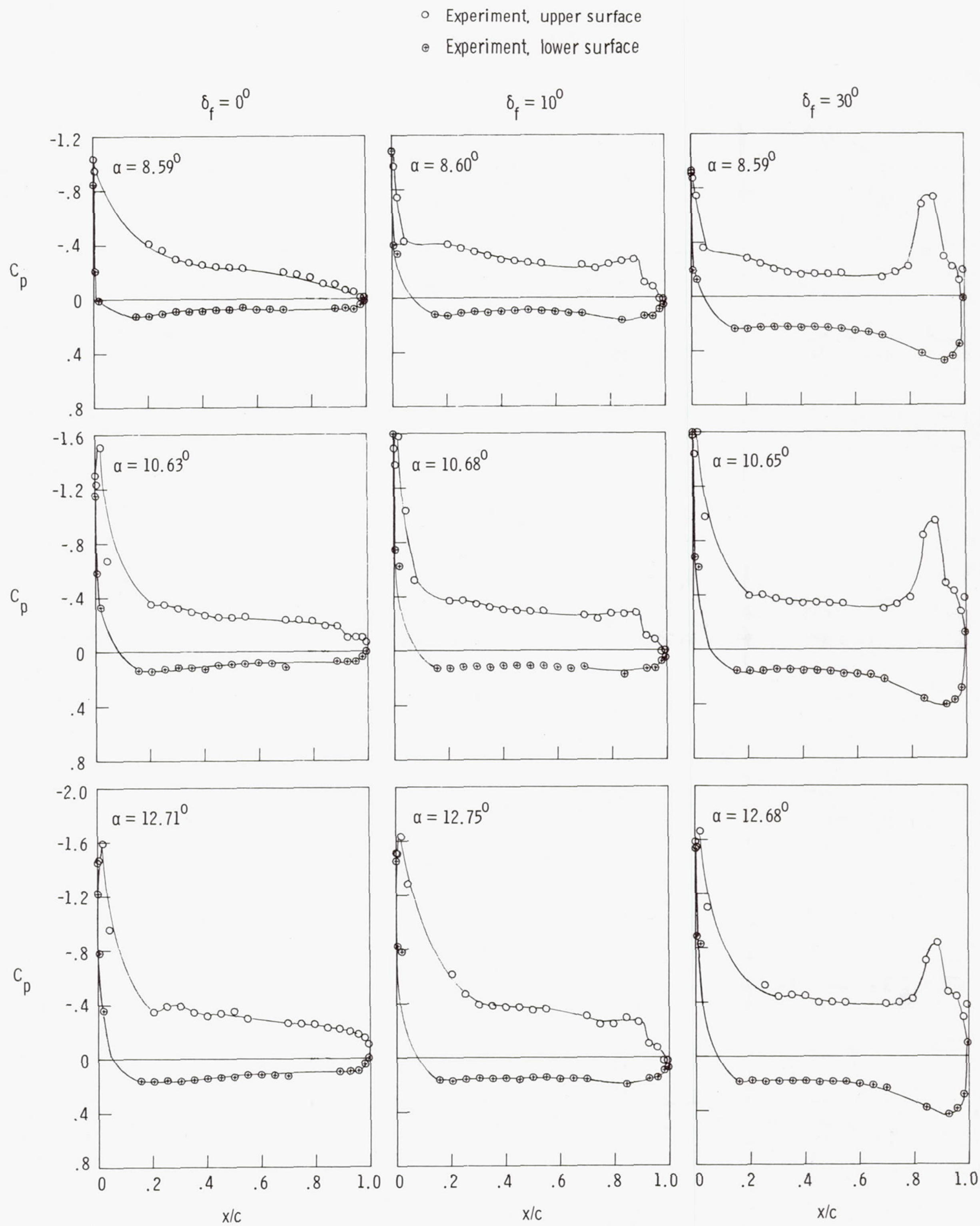

(b) Concluded.

Figure 15.- Continued.

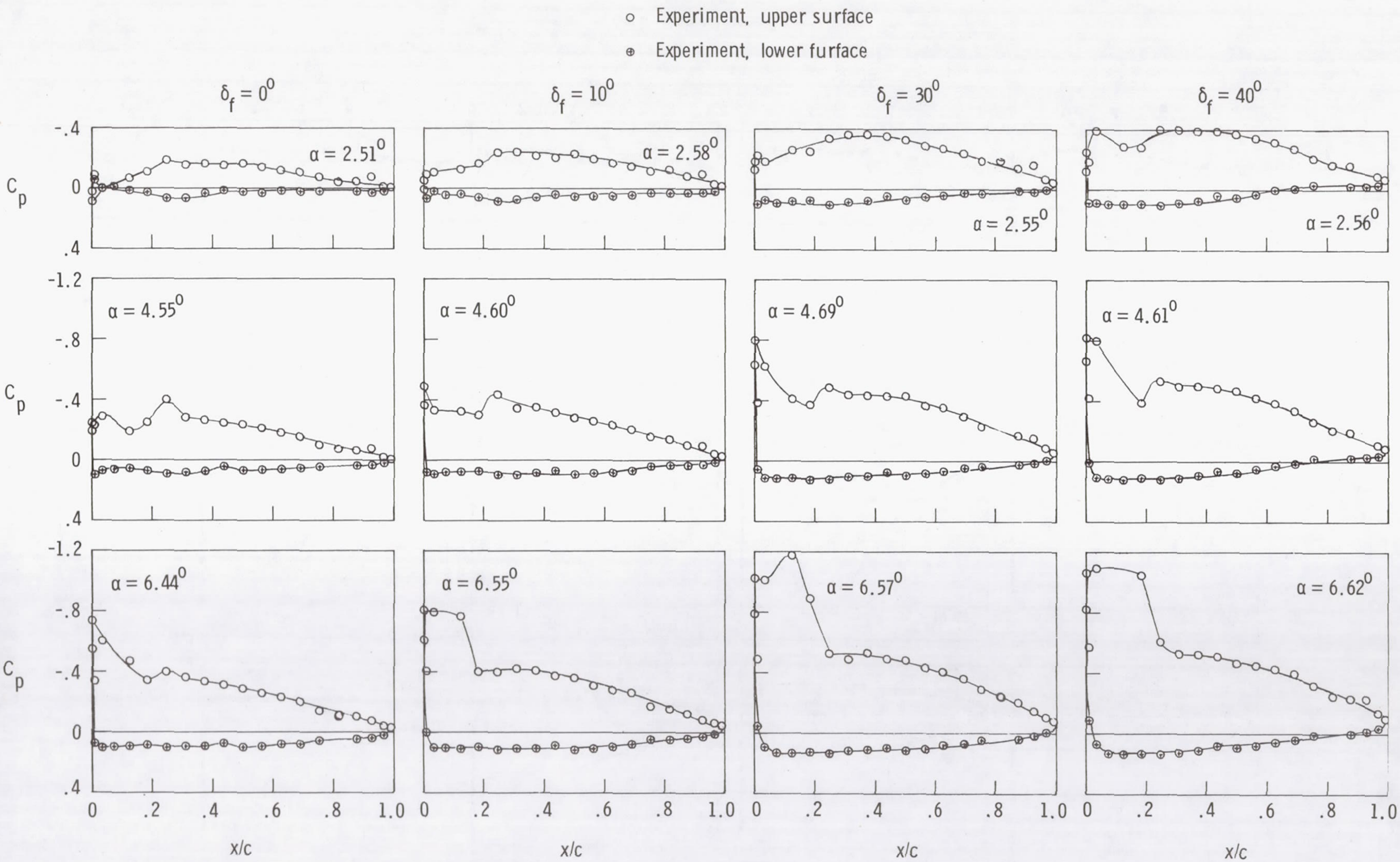

(c) $y/\frac{b}{2} = 0.654$.

Figure 15.- Continued.

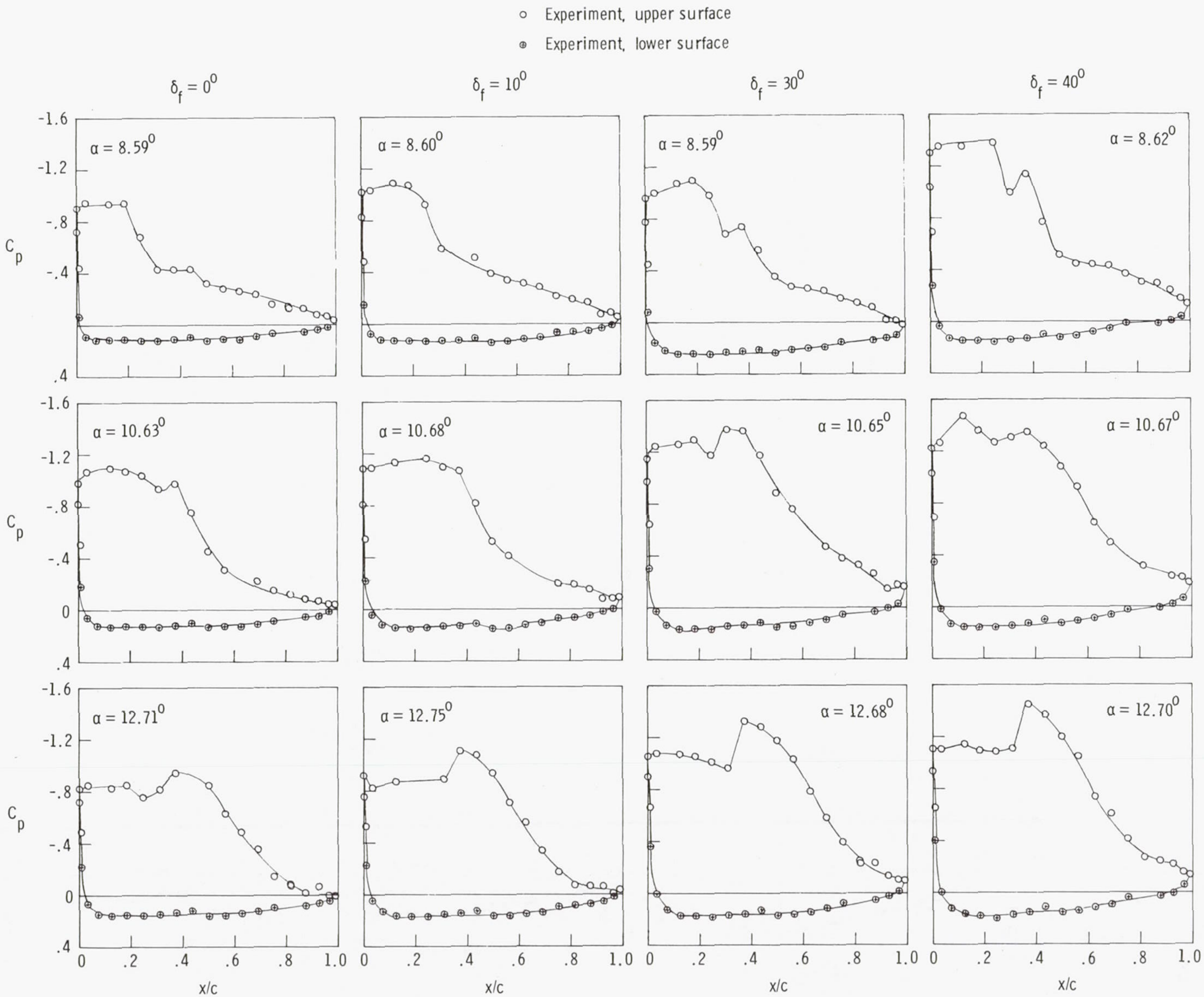

(c) Concluded.

Figure 15.- Continued.

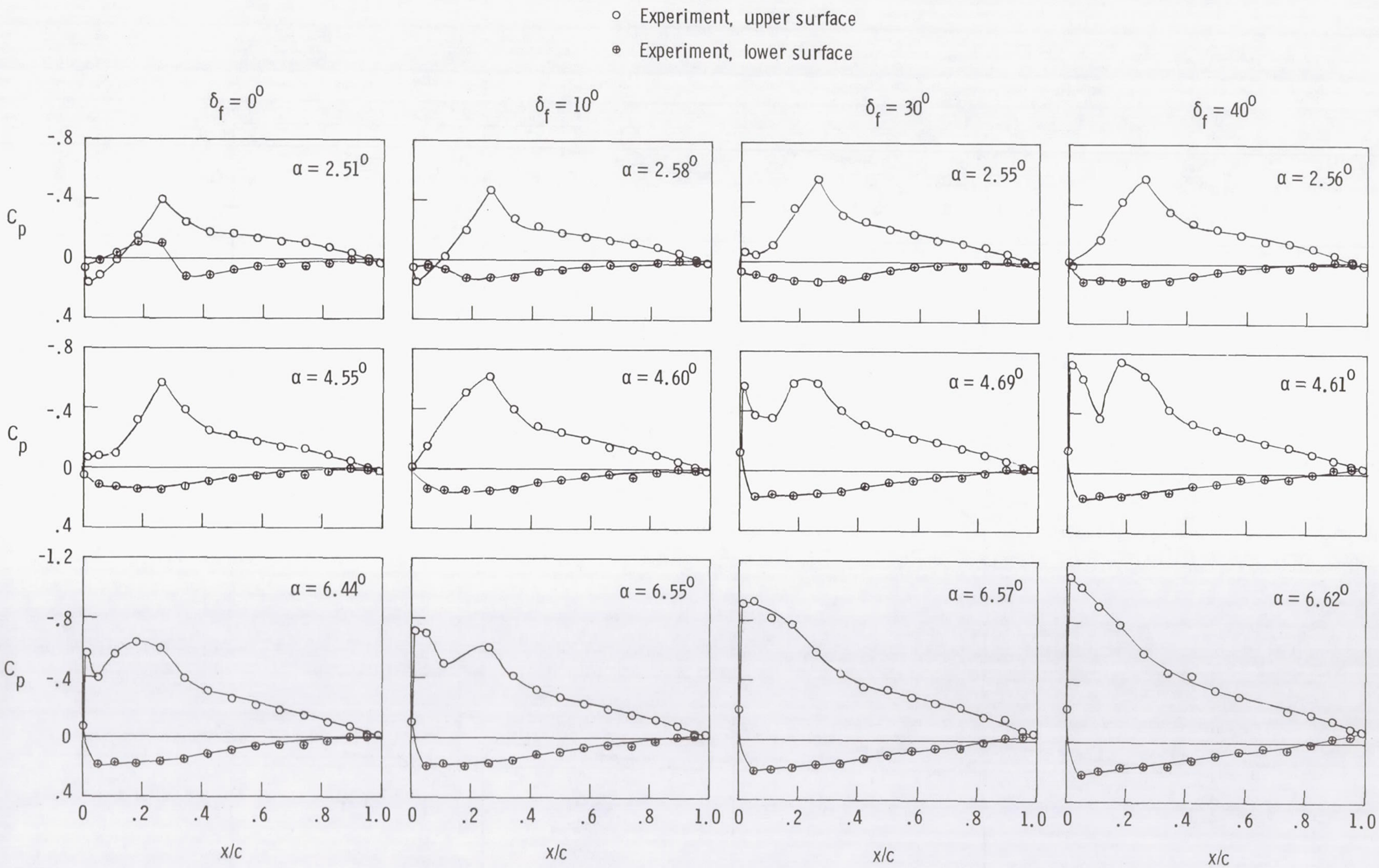

(d) $y/\frac{b}{2} = 0.862.$

Figure 15.- Continued.

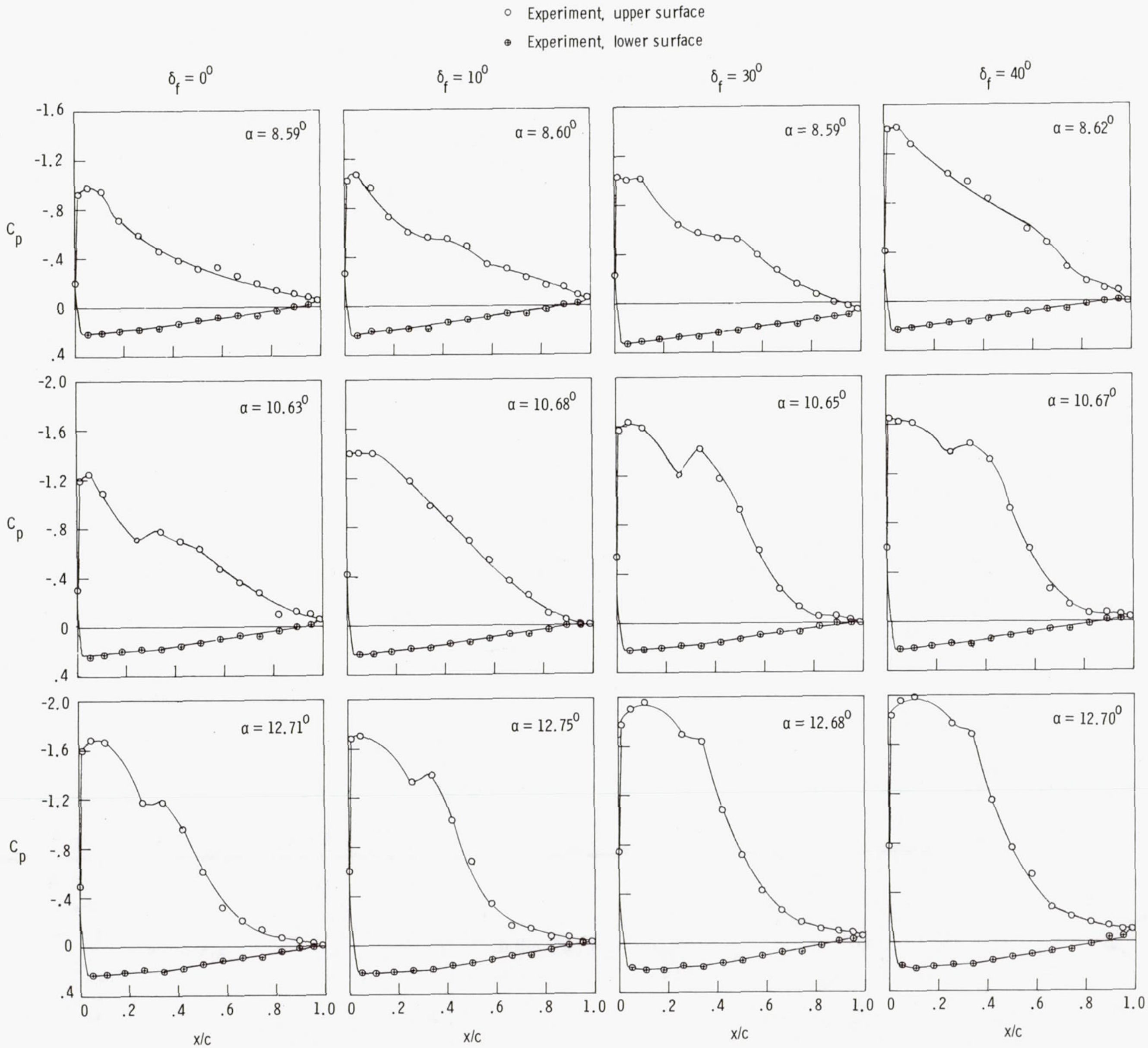

(d) Concluded.

Figure 15.- Concluded.

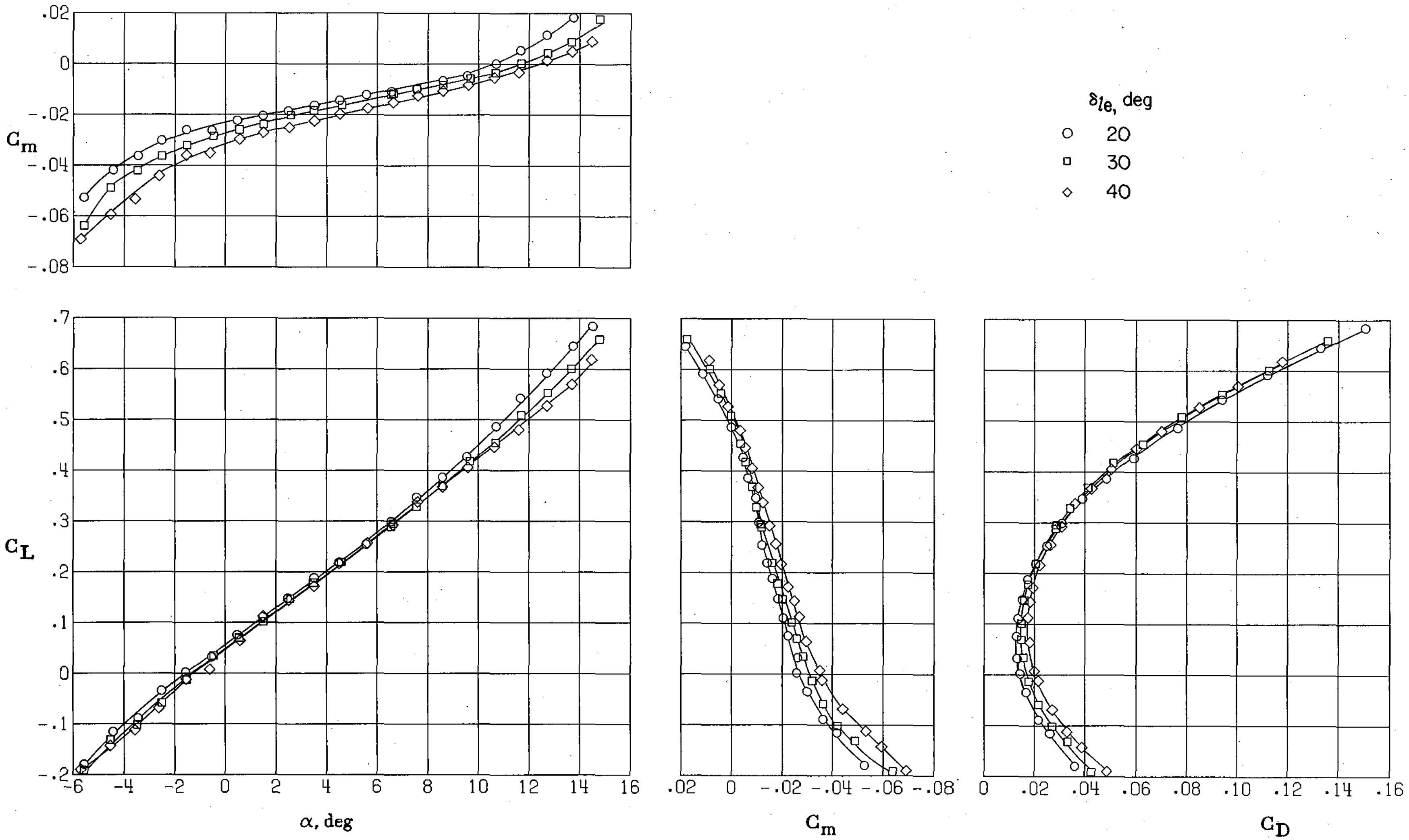

Figure 16.- Effect of leading-edge deflection on longitudinal aerodynamic characteristics. $\delta_f = 10°$.

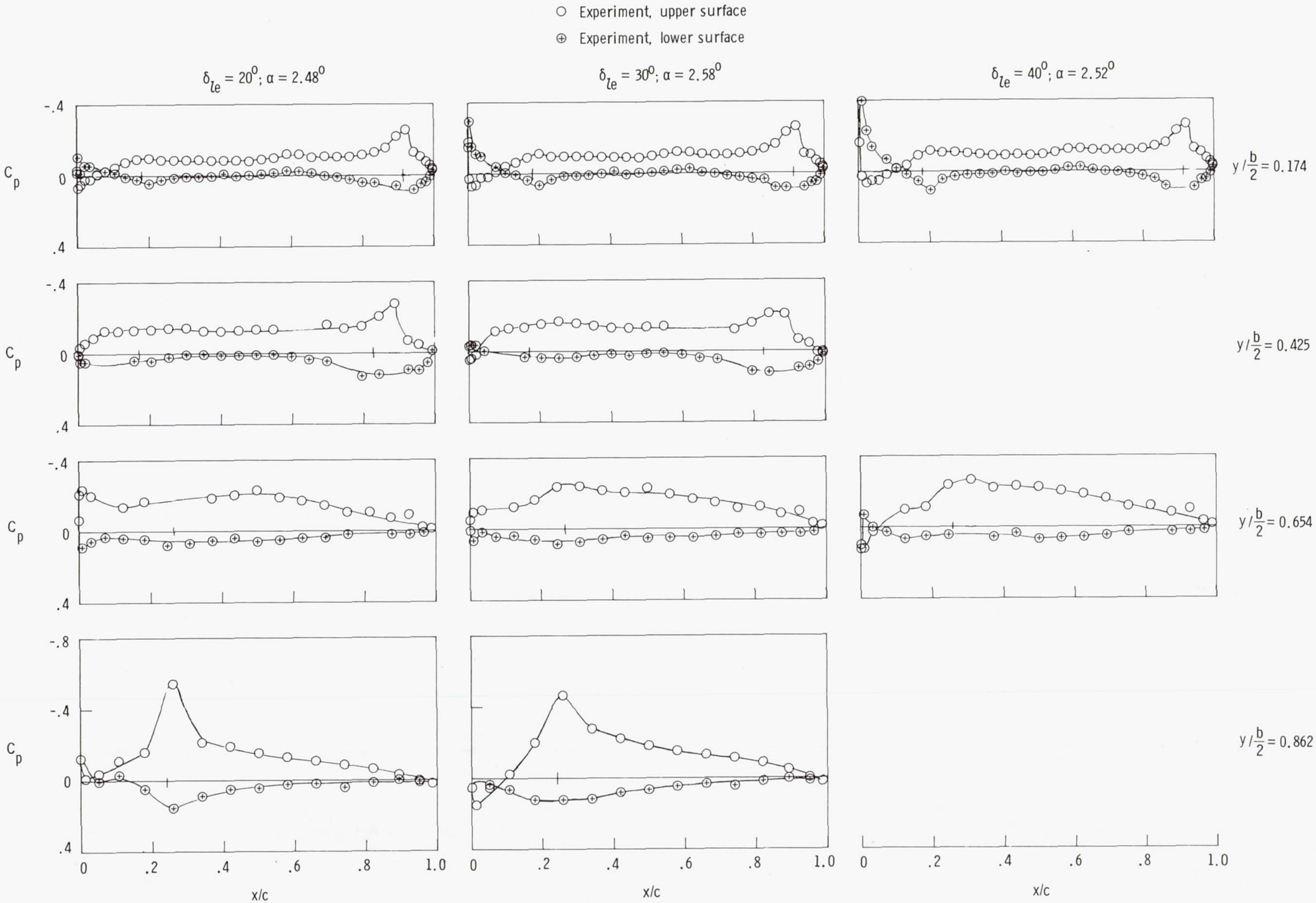

(a) $\alpha = 2.5°$.

Figure 17.- Effect of wing leading-edge deflection on wing chordwise pressure distributions. $\delta_f = 10°$.

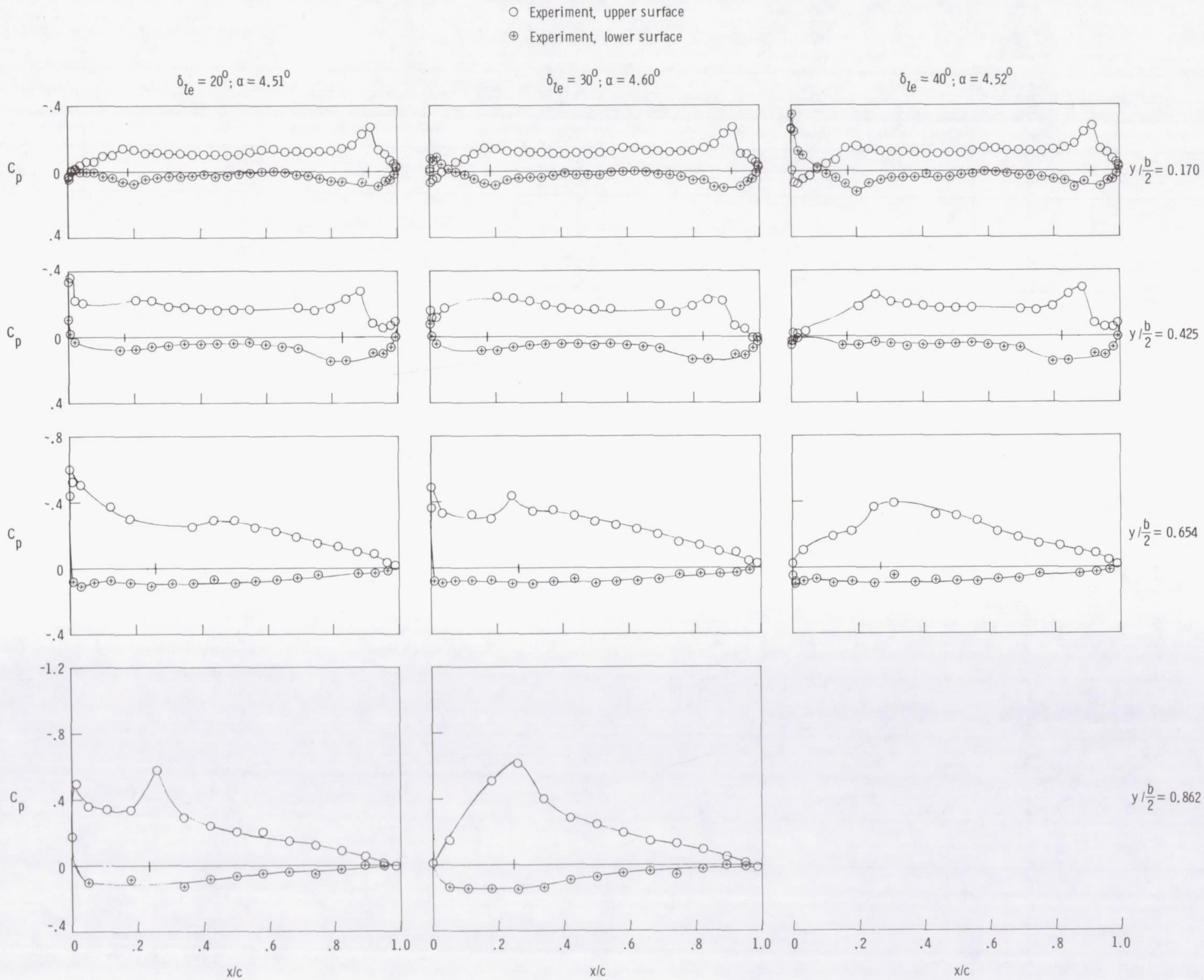

(b) $\alpha = 4.5°$.

Figure 17.- Continued.

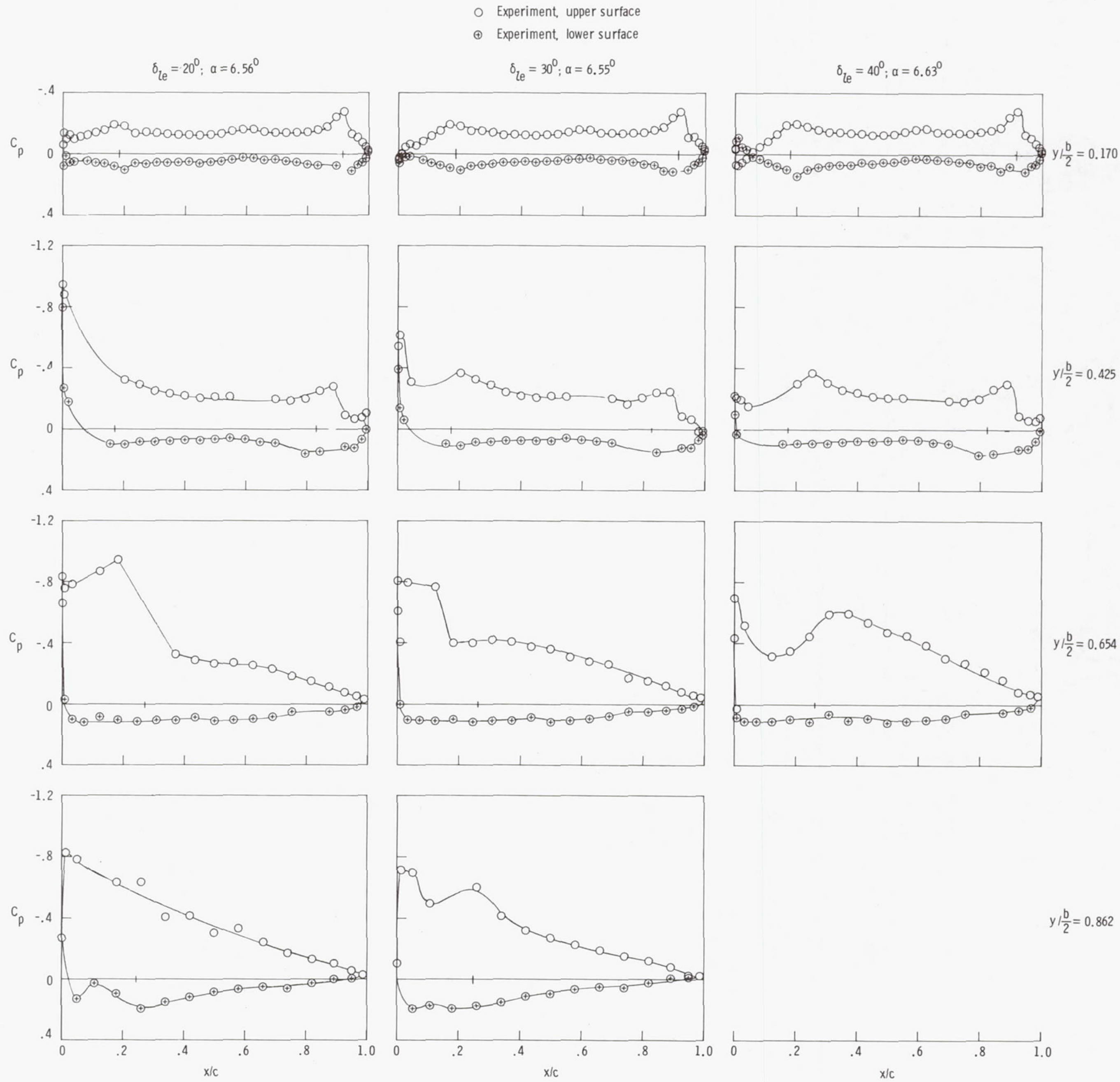

(c) $\alpha = 6.5°$.

Figure 17.- Continued.

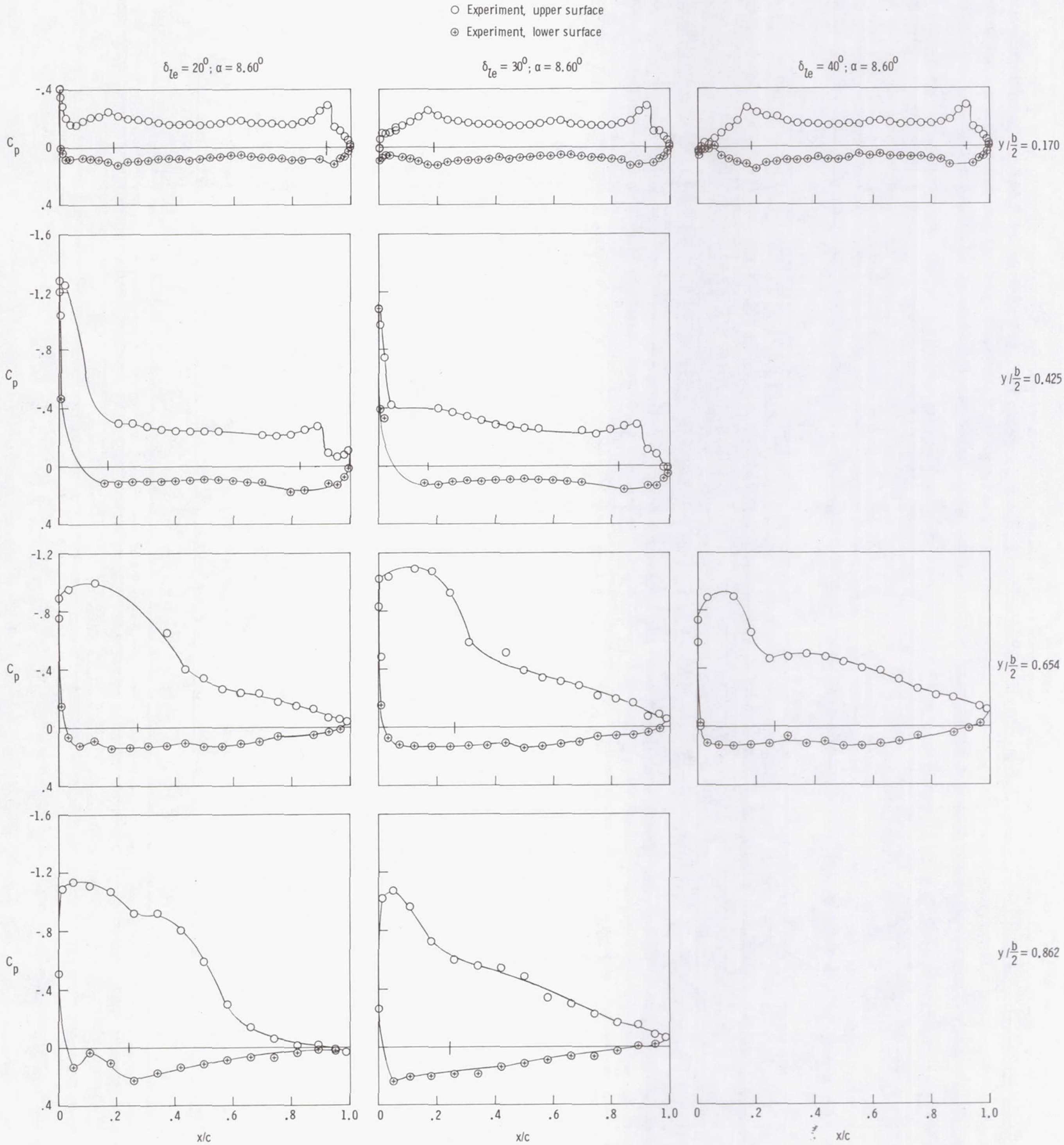

(d) $\alpha = 8.6°$.

Figure 17.- Continued.

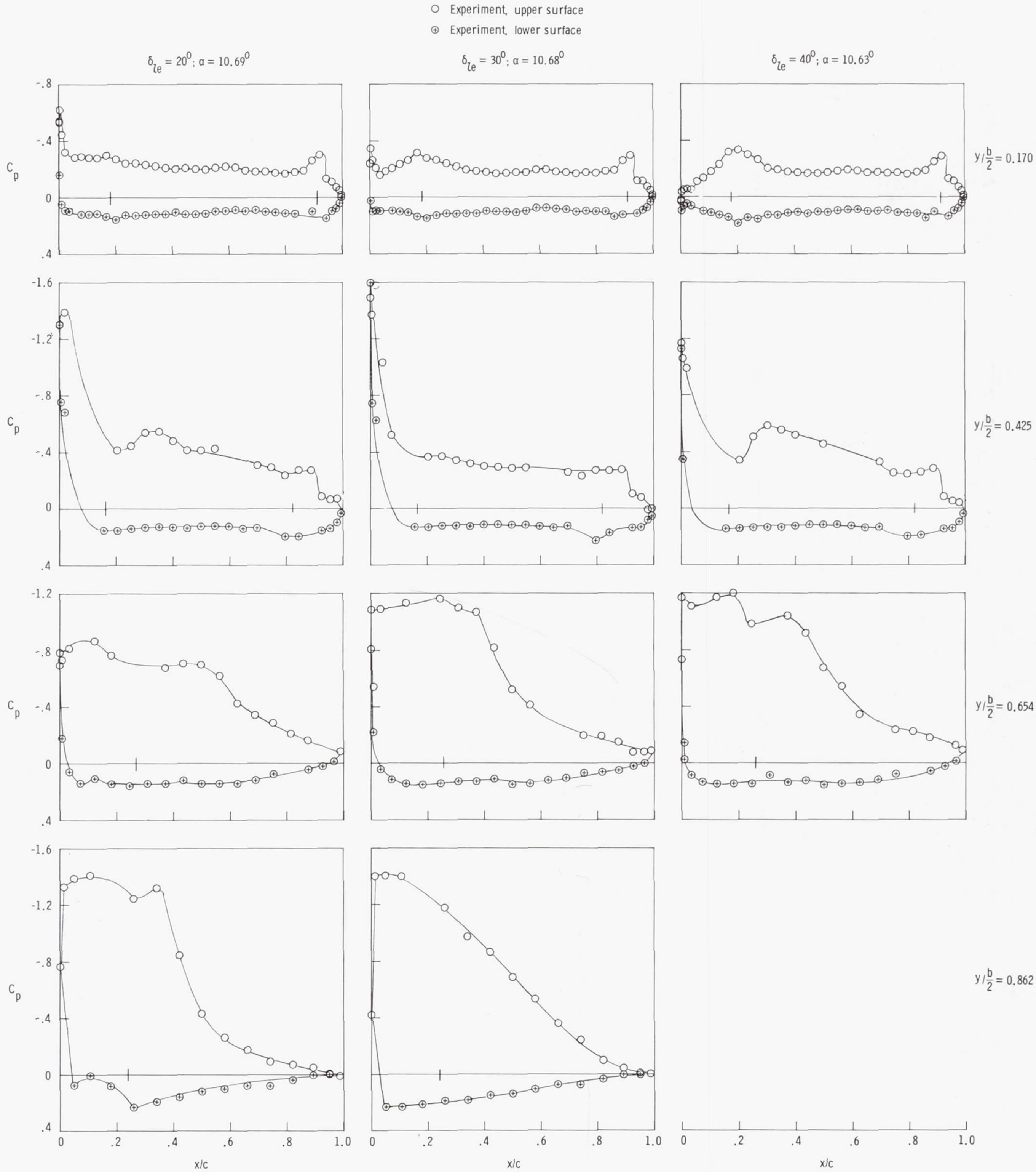

(e) $\alpha = 10.6°$.

Figure 17.- Continued.

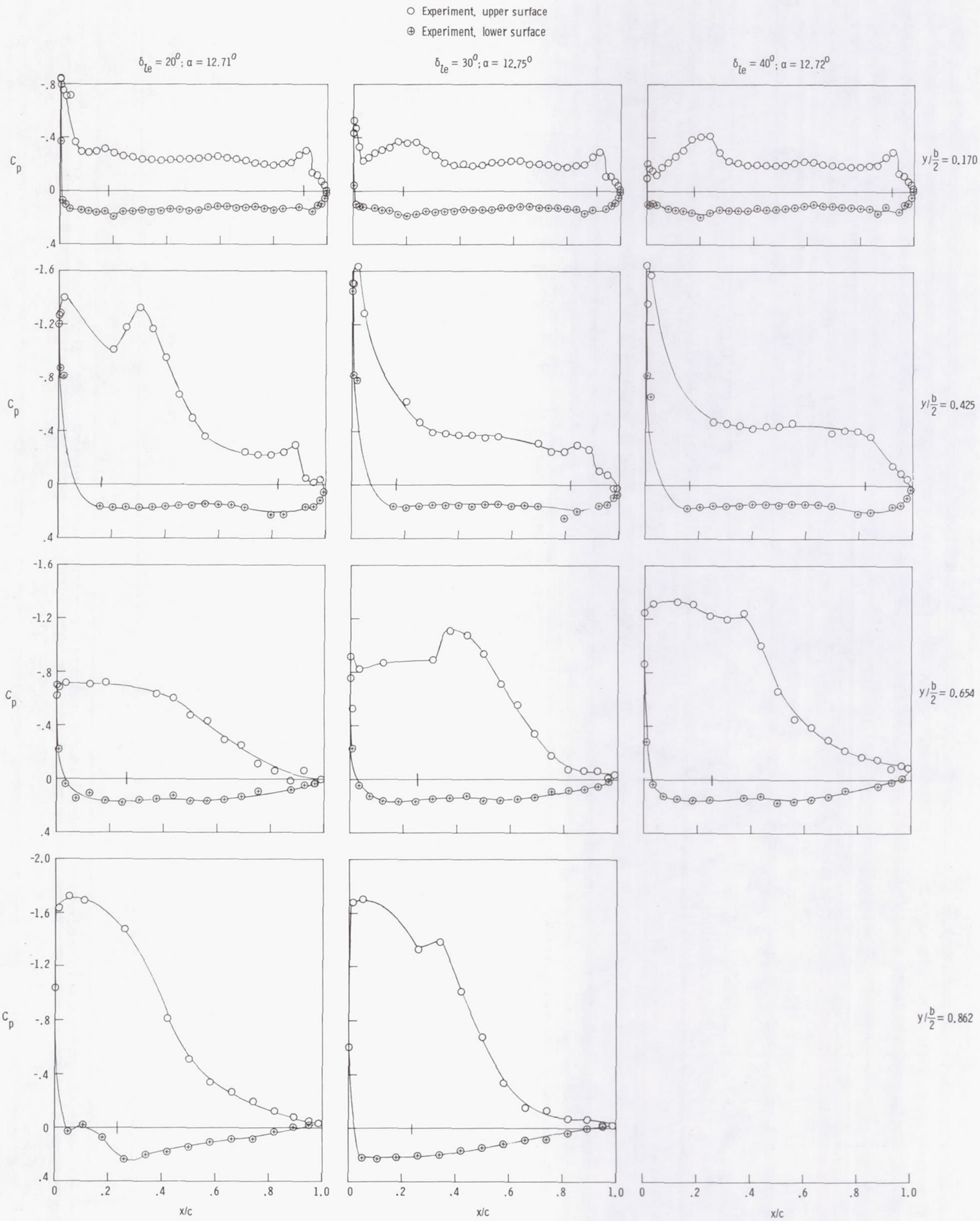

(f) $\alpha = 12.7°$.

Figure 17.- Concluded.

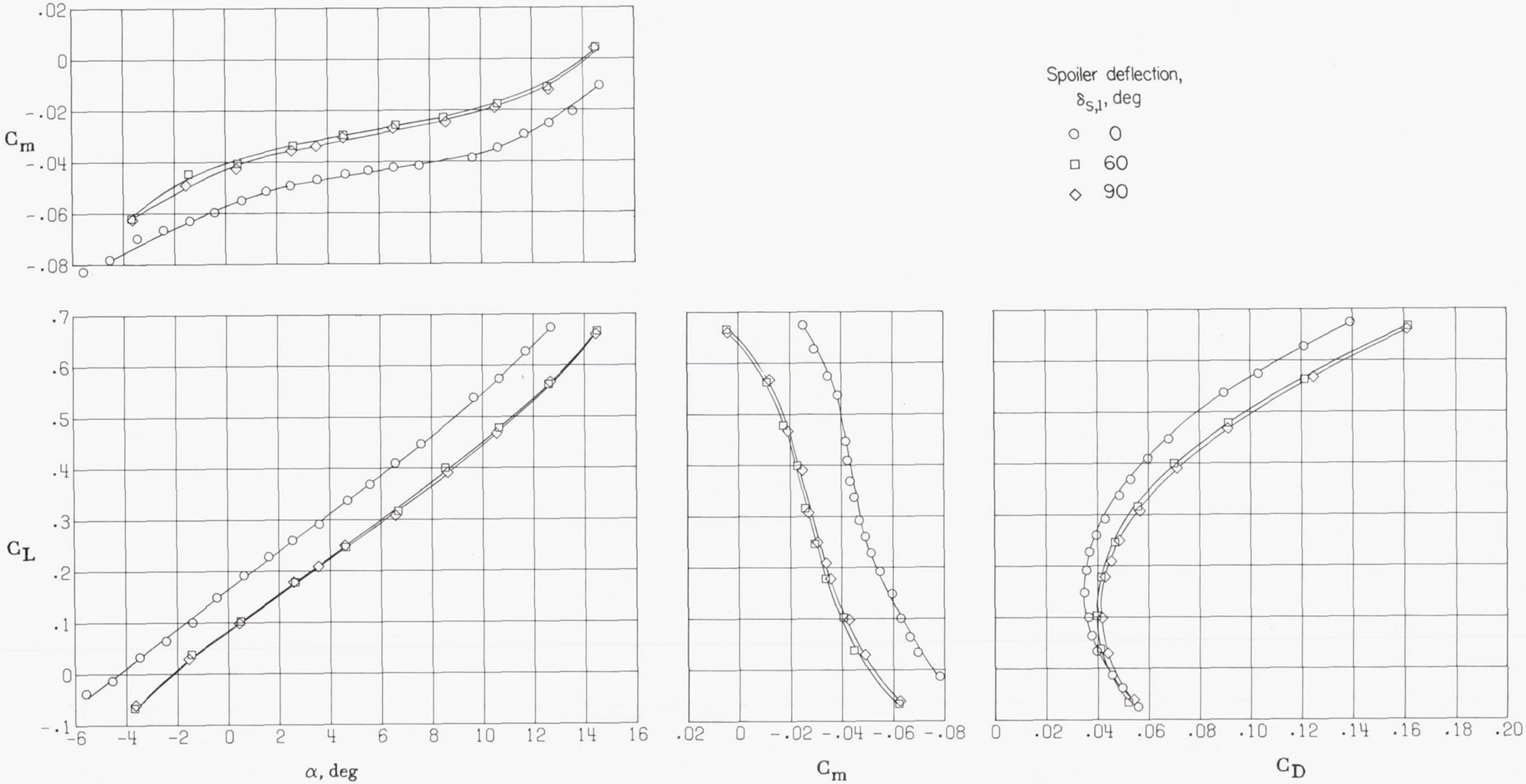

(a) Spoiler element s_1.

Figure 18.- Effect of spoiler deflection on longitudinal aerodynamic characteristics. $\delta_{le} = 30°$; $\delta_f = 30°$.

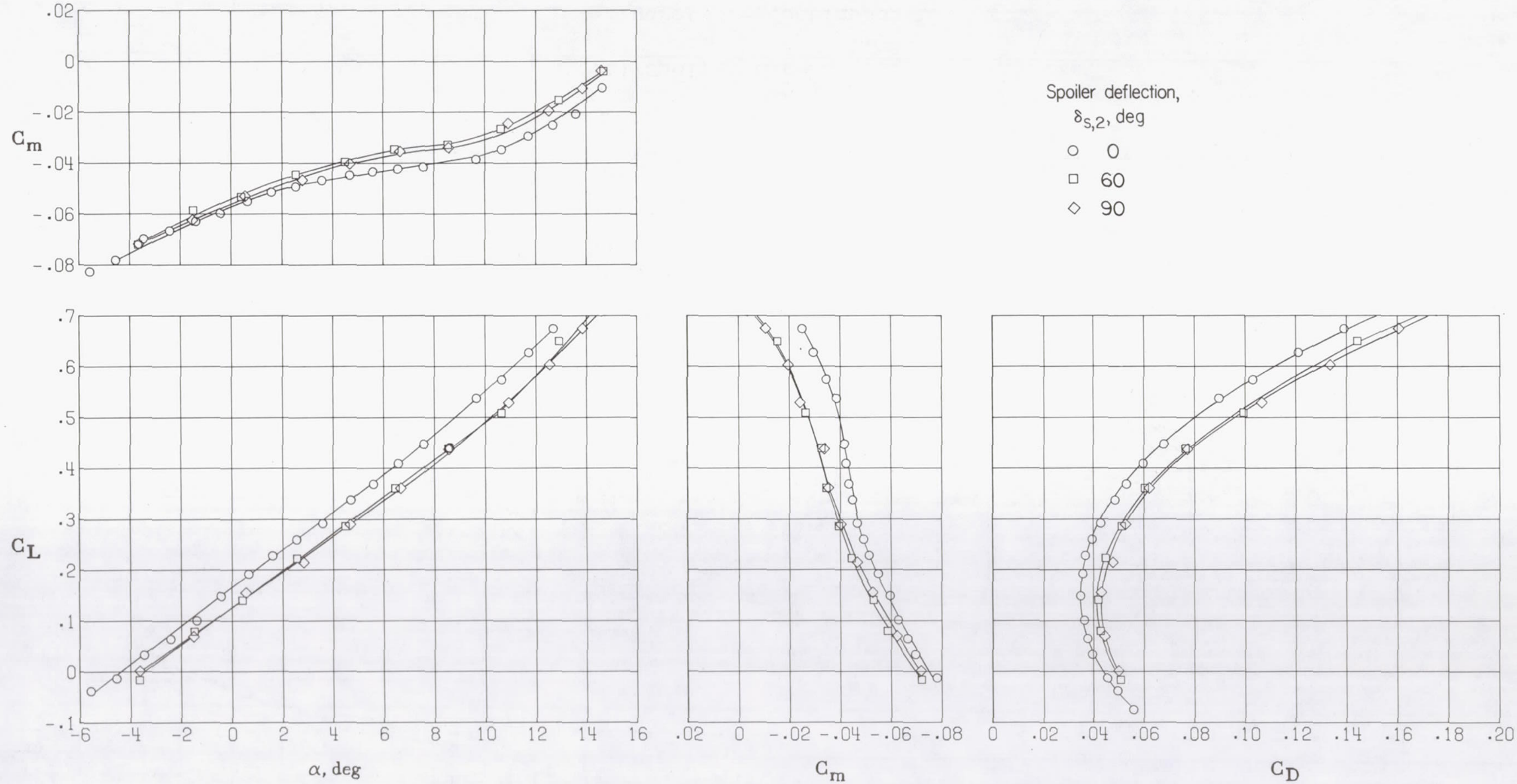

(b) Spoiler element s_2.

Figure 18.- Continued.

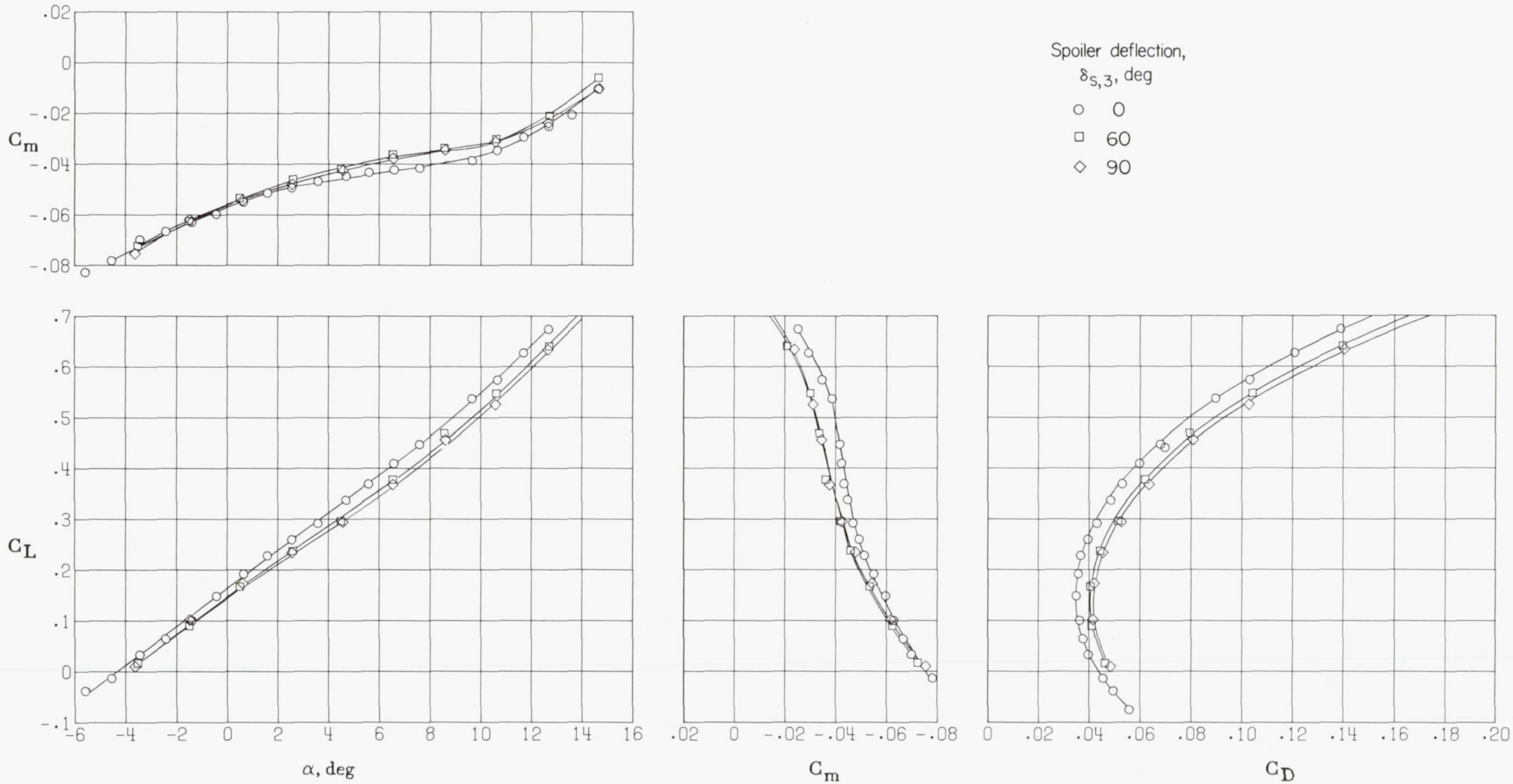

(c) Spoiler element s_3.

Figure 18.- Continued.

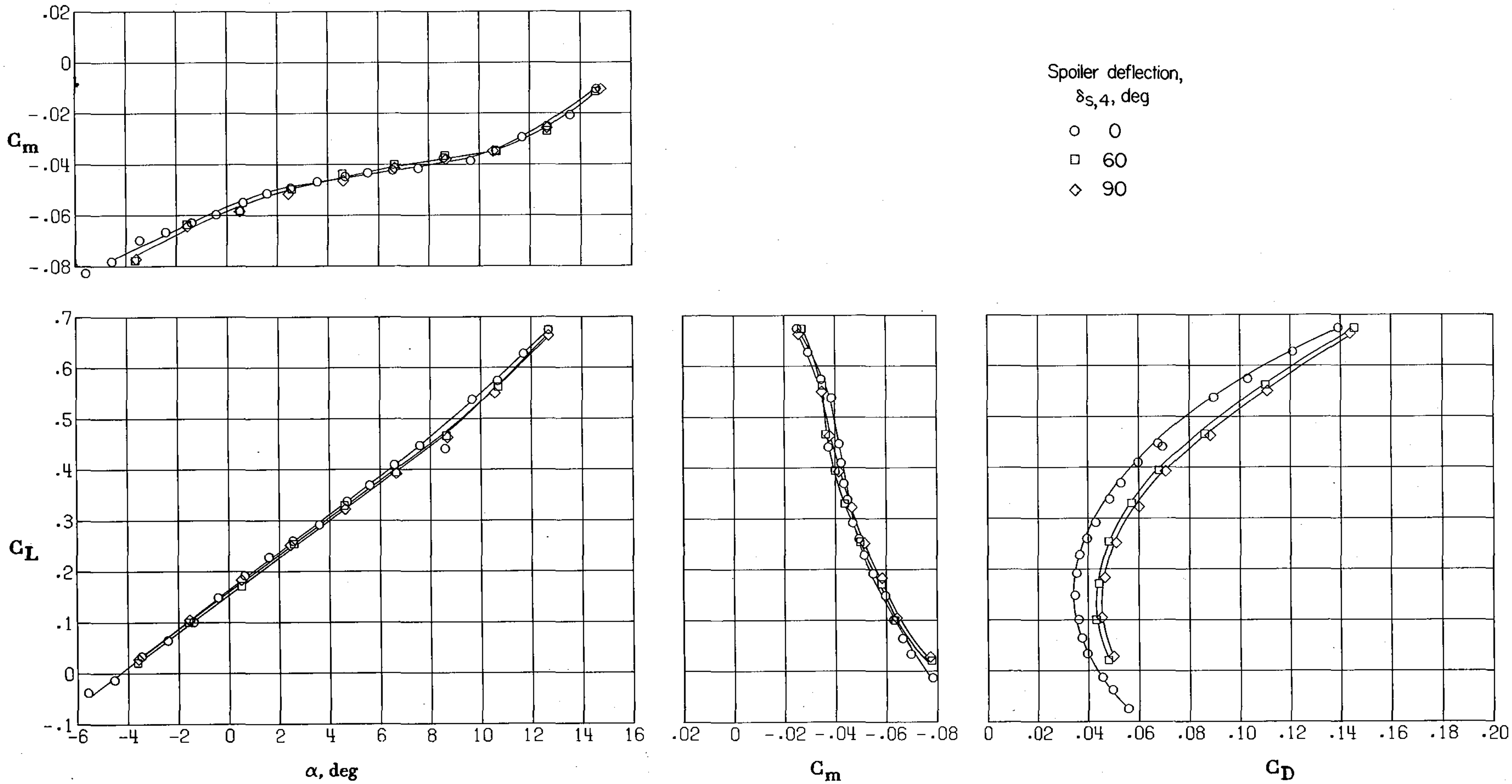

(d) Spoiler element s_4.

Figure 18.- Concluded.

1. Report No.	2. Government Accession No.	3. Recipient's Catalog No.
NASA TP-2176		

4. Title and Subtitle	
LOW-SPEED AERODYNAMIC CHARACTERISTICS OF A HIGHLY SWEPT, UNTWISTED, UNCAMBERED ARROW WING	5. Report Date October 1983
	6. Performing Organization Code 505-45-43-02
7. Author(s) Paul L. Coe, Jr., Scott O. Kjelgaard, and Garl L. Gentry, Jr.	8. Performing Organization Report No. L-15240
9. Performing Organization Name and Address NASA Langley Research Center Hampton, VA 23665	10. Work Unit No.
	11. Contract or Grant No.
12. Sponsoring Agency Name and Address National Aeronautics and Space Administration Washington, DC 20546	13. Type of Report and Period Covered Technical Paper
	14. Sponsoring Agency Code

15. Supplementary Notes

16. Abstract

An investigation was conducted in the Langley 4- by 7-Meter Tunnel to provide a detailed study of wing pressure distributions and forces and moments acting on a highly swept arrow-wing model at low Mach numbers (0.25). A limited investigation of the effect of spoilers at several locations was also conducted. Analysis of the pressure data shows that for the configuration with undeflected leading edges, vortex separation occurs on the outboard wing panel for angles of attack on the order of only 3°, whereas conventional leading-edge separation occurs at a nondimensional semispan station of 0.654 for the same incidence angle. The pressure data further show that vortex separation exists at wing stations more inboard for angles of attack on the order of 7° and that these vortices move inboard and forward with increasing angle of attack. The force and moment data show the expected nonlinear increments in lift and pitching moment and the increased drag associated with the vortex separation. The pressure data and corresponding force and moment data confirm that deflecting the entire wing leading edge uniformly to 30° is effective in forestalling the onset of flow separation to angles of attack greater than 8.6°; however, the inboard portion of the leading edge is overdeflected. The investigation further identifies the contribution of the trailing-edge flap deflection to the leading-edge upwash field.

17. Key Words (Suggested by Author(s))	18. Distribution Statement
Arrow wings Highly swept wings Leading-edge devices	Unclassified - Unlimited Subject Category 02

19. Security Classif. (of this report)	20. Security Classif. (of this page)	21. No. of Pages	22. Price
Unclassified	Unclassified	68	A04

For sale by the National Technical Information Service, Springfield, Virginia 22161

NASA-Langley, 1983